Crystal structure of Agaricus bisporus tyrosinase

Ismaya, Wangsa Tirta

Crystal Structure of *Agaricus bisporus* Tyrosinase

Cover: wall on the grass
By: Wangsa Tirta Ismaya (2009)

The research was carried out at the Protein X-ray crystallography group, Laboratory of Biophysical Chemistry, Groningen Biomolecular Science and Biotechnology Institute, Faculty of Mathematics and Natural Sciences, University of Groningen, The Netherlands

The research project was in collaboration with Agriculture and Food Innovation BV, Wageningen University and Research Center, and funded by Senter IOP (Industrial Onderzoek Project, IEE0002).

RIJKSUNIVERSITEIT GRONINGEN

Crystal structure of *Agaricus bisporus* tyrosinase

Proefschrift

ter verkrijging van het doctoraat in de
Wiskunde en Natuurwetenschappen
aan de Rijksuniversiteit Groningen
op gezag van de
Rector Magnificus, dr. E. Sterken,
in het openbaar te verdedigen op
vrijdag 24 juni 2011
om 14.45 uur

door

Wangsa Tirta Ismaya
geboren op 12 januari 1975
te Jakarta, Indonesië

Promotores	:	Prof. dr. B. W. Dijkstra Prof. dr. H. J. Wichers
Beoordelingcommissie	:	Prof. dr. ir. M. W. Fraaije Prof. dr. E. Boekema Prof. dr. L. Dijkhuizen

ISBN : 978-90-367-4904-6 (electronic version)
ISBN : 978-90-367-4905-3 (printed version)

For papi, mami, Lia, and Hery
and all my teachers
and all my friends

Contents

Chapter 1

An introduction to mushroom *Agaricus bisporus* tyrosinase

Wangsa T. Ismaya, Harry J. Wichers, Bauke W. Dijkstra

1. Tyrosinase and melanin

Tyrosinases (also called monophenol monooxygenases, EC 1.14.18.1) catalyze the *o*-hydroxylation of phenols and the subsequent oxidation of the formed *o*-diphenols to the corresponding *o*-quinones (Figure 1). Tyrosinase is the only copper-containing enzyme known to perform these two subsequent reactions; the related catechol oxidases only catalyze the second reaction, using *o*-diphenols as substrates (Abolmaali, Taylor *et al.* 1998). Tyrosinases recruit molecular oxygen as a co-substrate for the first reaction. One of the oxygen atoms is incorporated in the phenolic ring while the other oxygen atom is reduced to a water molecule. This catalytic cycle requires a reducing agent to provide two electrons to carry out the first step. These two electrons originate from the second step of the reaction (Lind, Siegbahn *et al.* 1999).

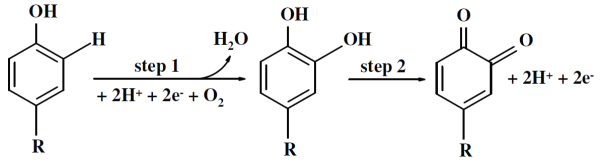

Figure 1. Reaction catalyzed by tyrosinase (Lind, Siegbahn *et al.* 1999).

Starting from tyrosine, the final product of the tyrosinase-catalyzed reaction is dopaquinone. Dopaquinone can undergo subsequent chemical and enzymatic reactions to result in either dopachrome or 5-cysteinyl dopaquinone derivatives, which in turn can be further converted to melanin. The melanin biosynthesis via dopachrome intermediate results in eumelanin, while the latter pathway results in phaeomelanin and trichochrome (Figure 2). Melanins are pigments that can be found in living organisms ranging from bacteria, plants, to mammals. Since tyrosinase catalyzes the initial steps of this conversion, it is regarded as the key enzyme in the melanin biosynthesis pathway (Sanchez-Ferrer, Rodriguez-Lopez *et al.* 1995).

o-Quinones and their derivatives such as melanin play important roles in the survival of organisms. In mammals, melanin is mostly found in the skin, where it functions in the photoprotection against UV radiation. In insects, *o*-quinones are components of the protection system against pathogenic microorganisms and they are involved in the

hardening of cuticle, while in cephalopods *o*-quinones are the major components of the defensive ink spray. Plants employ *o*-quinones in modifying and hardening the protective exterior layer of, for instance, seed envelopes and as an agent against invasive organisms. The latter function also occurs in fruits and potato, and in the fruit bodies of fungi. These examples address the function of tyrosinase to be associated with stress responses to the environment (Land, Ramsden *et al.* 2004).

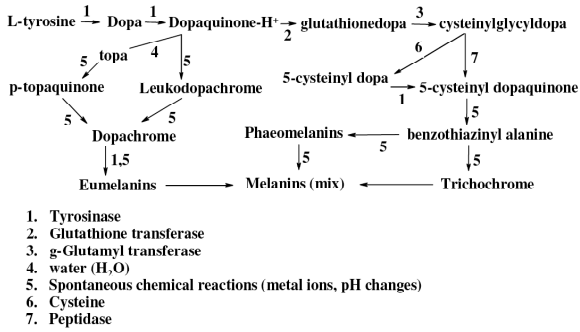

Figure 2. Melanin biosynthesis pathway adapted from Sanchez-Ferrer *et al*. (1995).

2. Mushroom tyrosinase

The first report on tyrosinase activity was the observation by Schönbein in 1856 of the occurrence of aerobic oxidation in mushroom (Whitaker 1993). However, attempts to isolate and purify mushroom tyrosinase were only started decades later (Keilin and Mann 1938). To date, purification of the enzyme directly from mushroom fruit bodies remains a difficult task because of contamination by endogenous phenolic substrates and the presence of many tyrosinase isoforms (Jolivet, Arpin *et al.* 1998). Even in recent years, partially purified enzyme is still employed for biochemical studies (Gouzi and Benmansour 2007), which presents considerable limitations as to the interpretation of findings (Flurkey, Cooksey *et al.* 2008). Therefore, the use of commercially available mushroom tyrosinase, with known enzyme activity, is often preferred.

Commercial mushroom tyrosinase is often employed in the search for inhibitors that can be used for the treatment of skin disorders associated with melanin, or as additives in cosmetics for skin whitening effects (Seo, Sharma *et al.* 2003; Chang

2009). It is also routinely employed in studying the application of the enzyme as a food additive or as an element in detection systems of phenolic compounds in wastewater (Solna, Sapelnikova *et al.* 2005; de Faria, Moure *et al.* 2007). The commercial enzyme is however usually used without any auxiliary purification, although it has been reported that impurities might have effects on enzyme activity and inhibition (Rescigno, Zucca *et al.* 2007; Flurkey, Cooksey *et al.* 2008). The unpurified commercial enzyme has even been used to study changes in secondary structure content of the enzyme upon treatment with SDS (Karbassi, Haghbeen *et al.* 2003). The results of such latter studies should clearly be taken with considerable reservation.

2.1 Molecular characteristics of mushroom tyrosinase

2.1.1 Size and quaternary structure assembly

Detailed molecular studies require purified enzyme material. Starting from commercially available mushroom powder, a heterotetrameric tyrosinase species with a molecular mass of 120 kDa could be obtained after a single gel filtration purification step (Schurink, van Berkel *et al.* 2007). This reported molecular mass of the purified tyrosinase was in agreement with that reported by others, be it determined by moving boundary electrophoresis (Mallette and Dawson 1949), analytical centrifugation (Mallette and Dawson 1949; Yasunobu, Peterson *et al.* 1959) , light scattering (Kertesz and Zito 1962), sedimentation equilibration (Kertesz and Zito 1957; Bouchilloux, McMahill *et al.* 1963) , or gel filtration chromatography (Sharma and Ali 1981). However, the species obtained from the single gel filtration purification step may still contain various tyrosinase isoforms (see further below).

While the molecular masses of the enzyme obtained by the different techniques and investigators were consistent, views as to the quaternary organization of the enzyme has been evolving. In 1957, upon determination of the enzyme molecular mass by means of sedimentation equilibration, the presence of a 26-32 kDa species was detected (Kertesz and Zito 1957). Since Bouchilloux (Bouchilloux, McMahill *et al.* 1963) had shown the presence of four copper ions in the 120-kDa enzyme, and since it was suggested that active tyrosinase (from other species) contained one copper in the active site (Lerch and Ettlinger 1972), it was assumed that the enzyme from

mushroom was composed of four identical ~ 30 kDa subunits. However, taking advantage of the development of the denaturing polyacrylamide gel electrophoresis (SDS PAGE) technique in 1970 and the finding by the group of Mason (Schoot-Uiterkamp and Mason 1973) that the active site of tyrosinase contains actually a pair of copper ions, Strothkamp (Strothkamp, Jolley *et al.* 1976) revised the tetrameric organization and suggested that the enzyme is composed of two heavy subunits of 43 kDa (H-chain) and two light subunits of 13-14 kDa (L-chain) with a total molecular mass of 120 kDa (H_2L_2 configuration). Further, It was suggested that a single H or L subunit had no enzyme activity, suggesting that both the H and L chain needed to be present for active enzyme (Strothkamp, Jolley *et al.* 1976; Eicken, Zippel *et al.* 1998; Jolivet, Arpin *et al.* 1998).

2.1.2 Heterogeneity

Despite the consistent molecular mass of the enzyme obtained by gel filtration chromatography, subsequent purification by ion exchange chromatography resulted in several fractions that all demonstrated tyrosinase activity. Hence, the presence of tyrosinase in mushroom appears to be heterogeneous. This heterogeneity had already been reported during the purification of the enzyme by hydroxylapatite chromatography (Smith and Krüger 1962; Bouchilloux, McMahill *et al.* 1963). Purification attempts that combined gel filtration and ion exchange chromatography also showed heterogeneity (Nelson and Mason 1970; Robb 1979; Menon, Fleck *et al.* 1990). The presence of charge heterogeneity was also shown by Flurkey, who reported two groups of mushroom tyrosinases with a lower pI (4.0-4.3) and a higher pI (4.5-4.8) upon an isoelectric focusing experiment (Flurkey 1991). Later on, the presence of two other mushroom tyrosinases with a pI of 5.1 and 5.2 was reported (Wichers, Gerritsen *et al.* 1996), which showed that the enzyme obtained from the purification varies. Jolivet (Jolivet, Arpin *et al.* 1998) suggested that the variation in the purification results could be caused by the polymerization of proteins by quinones present in the isolates (Loomis 1974), defects in the purification procedure (Bouchilloux, McMahill *et al.* 1963; Vanneste and Zuberbühler 1974; Robb and Gutteridge 1981; Smith and Montgomery 1985), diverse sources of enzyme material

(Ingebrigtsen, Kang *et al.* 1989) or posttranslational modifications (Jimenez, Maloy *et al.* 1989).

2.2 Genetics

The attempts to elucidate the DNA coding for tyrosinase expression in mushroom were initiated in Wageningen by Wichers and coworkers. His group successfully cloned two different polyphenol oxidases/tyrosinases, called PPO1 and PPO2, from the *Agaricus bisporus* strain U1. The size of the corresponding *Abppo1* and *Abppo2* genes suggested the occurrence of two proteins with a similar molecular mass of 64 kDa. Interestingly, alignment of their amino acid sequences showed that the two proteins share only 34% sequence identity (52% similarity) and suggested that the two proteins are rather distant (Figure 3) (Wichers, Recourt *et al.* 2003). Northern blot analysis revealed that PPO1 is expressed by all *Agaricus* strains tested and in all tissues (Wichers, van den Bosch *et al.* 1995), but that PPO2 expression was only detected upon bacterial challenge (Soler-Rivas, Moller *et al.* 2001). These results suggested that PPO1 is constitutively expressed, while PPO2 expression is induced (Wichers, Recourt *et al.* 2003). Moreover, this finding suggested that the variation in purification results could also be due to the differential expression of the tyrosinase encoding genes in mushroom. This hypothesis is supported by the finding of two more genes that also encode the expression of tyrosinase in *A. bisporus*, called *ppo3* and *ppo4* (Wu, Chen et al. 2010).

2.3 Expression forms

Upon isolation of tyrosinase directly from mushroom fruit bodies to prepare antibodies against the enzyme for molecular studies, Wichers (Wichers, Gerritsen *et al.* 1996) detected the presence of two active, monomeric 43 kDa tyrosinase isoforms. This finding suggested that the finding of Strothkamp *et al.* (1976) that the single H subunit was not active needed revision. Instead, this result suggested a similarity to the monomeric and active 46 kDa tyrosinase that is formed upon proteolytic processing of a 75 kDa precursor in *Neurospora crassa*, another fungus.

This similarity was supported by the 64 kDa size of the gene products of the *A. bisporus* tyrosinase and suggested that such posttranslational processing also occurs in *A. bisporus* (Wichers, van den Bosch et al. 1995; Wichers, Recourt et al. 2003). Indeed, the presence of immunological cross-reacting 67 kDa, 58 kDa, 43 kDa, and 35 kDa proteins in mushroom extracts, demonstrated by a Western blot experiment, suggested that the 67 kDa protein was the pro-form of tyrosinase (Wichers, Recourt *et al.* 2003). The difference in molecular mass of the 67 kDa pro-form from the SDS PAGE experiment and the predicted 64 kDa *Abppo1* and *Abppo2* gene products could originate from uncertainties in the molecular mass determination by SDS PAGE (Espin and Wichers 2000). Therefore, in the following we refer to the pro-form as the 64 kDa form of tyrosinase.

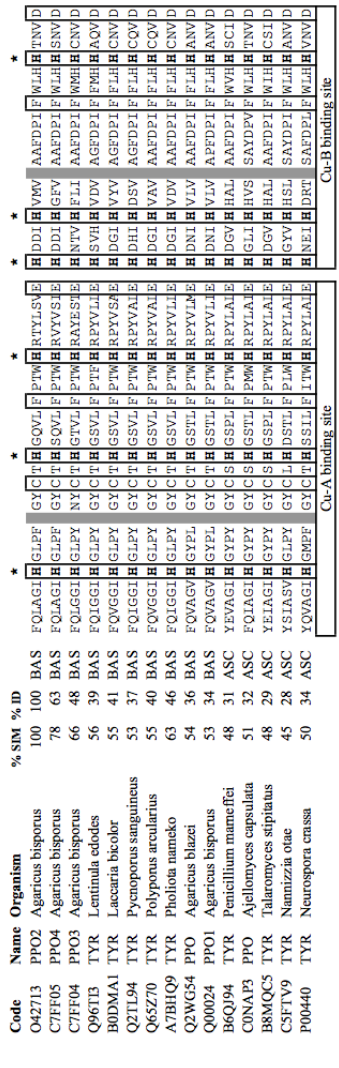

Figure 3. Amino acid sequence conservation of the copper-binding regions of fungal tyrosinases obtained with the program BLAST (Altschul, Gish *et al.* 1990). The asterisks (*) indicate the copper-coordinating histidine residues. The strictly conserved residues in the active site are boxed; the grey box represents an amino acid insertion region. BAS and ASC stand for the fungal phyla basidiomycetes and ascomycetes, respectively.

2.3.1 Latent form

The 64 kDa pro-form of tyrosinase could only be obtained when healthy and undamaged mushroom fruit bodies were employed for preparing the mushroom extracts. This pro-form was found to be inactive (Espin and Wichers 2000). Upon maturation of the

mushroom fruit bodies the amount of inactive pro-enzyme decreased dramatically with a concomitant increase in tyrosinase activity. Therefore, the inactive pro-form is also called the latent form since it can be converted into active, mature enzyme (Espin and Wichers 2000).

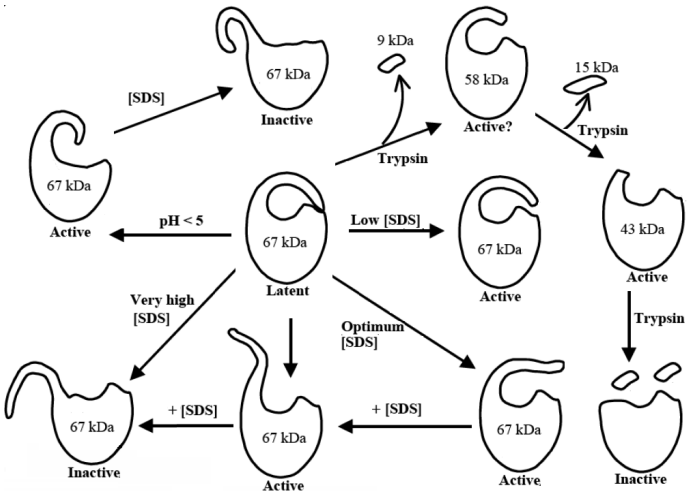

Figure 4. Scheme showing the putative maturation and activation process of mushroom tyrosinase (Espin and Wichers 2000).

The presence of the latent form was first reported by Yamaguchi *et al.* (Yamaguchi, Hwang *et al.* 1970) who observed an increase in tyrosinase activity upon treatment with detergents or protease during preparation of mushroom extracts. Later, Espin and Wichers (Espin and Wichers 2000) confirmed the results of Yamaguchi *et al.* (1970) and further demonstrated that the latent form could be activated by non-covalent modifications such as ultrasonication at low energy level (~ 25 W), addition of the detergent SDS or benzyl alcohol, which is an endogenous compound in mushroom, and by proteolytic cleavage. *In vitro* proteolytic activation resulted in the time-dependent formation of active 58 kDa and 43 kDa fragments, which could be detected by antibodies raised against the 43 kDa tyrosinase. These fragments were strikingly similar in molecular mass to fragments obtained from mushroom extracts.

Based on these results, a maturation and activation scheme for mushroom tyrosinase has been proposed (Figure 4) (Espin and Wichers 2000).

2.3.2 Mature form

The proposed maturation scheme comprises the previously proposed domain organization of fungal tyrosinase based on a comparison of sequence and proteolytic digestion patterns of tyrosinases from higher eukaryotes, plants, fungi, and bacteria (van Gelder, Flurkey *et al.* 1997) Van Gelder *et al.* (1997) proposed that tyrosinases from these species contained a copper-binding domain and a (smaller) C-terminal domain, with a proteolytic cleavage site in between. Accordingly, mushroom tyrosinase was also expected to undergo proteolytic processing resulting in the two domains with sizes in agreement to those of the H and L chains, respectively (van Gelder, Flurkey *et al.* 1997). This led to the assumption that the large H chain is the N-terminal part of the tyrosinase gene product with the copper-binding histidine residues.

Recently, a 120 kDa tyrosinase isoform from a commercially available tyrosinase preparation, purified by a single gel filtration chromatography step, was subjected to mass spectrometry. The mass spectrometry analysis combined with subsequent N-terminal sequencing of the obtained fragments showed that the H subunit contained a peptide fragment with the sequence LNIVDFVKNEKFFTLYVR, which is identical to residues 17-34 of the PPO2 sequence. The N-terminus of the identified L subunit sequence was ATNSGTLIIFDQ, which, however, did not match any known mushroom tyrosinase sequences (Schurink, van Berkel *et al.* 2007). This result showed that the purified enzyme material could contain PPO2 but that the nature of the L subunit in the commercial tyrosinase preparation is not firmly established.

3. Tyrosinase is a type-3 copper protein

Until 2006, no three-dimensional structural information on tyrosinases was available, and therefore early investigators employed the 3D-structures of the related proteins hemocyanin from mollusks and catechol oxidase from plants. This situation changed with the elucidation of the crystal structure of a tyrosinase from *Streptomyces*

castaneoglobisporus (*Sc*TYR) (Matoba, Kumagai *et al.* 2006). The structure of this bacterial tyrosinase provided more direct insight into the general architecture of the enzyme and its active site, but also left open questions on the function of a highly conserved thioether bond (see below), the substrate binding mode, and the precise reaction mechanism (Decker, Schweikardt *et al.* 2006).

Tyrosinase and its homologues share similar active center, which contains two copper ions that are coordinated by six histidine residues (Abolmaali, Taylor *et al.* 1998). This arrangement characterizes tyrosinase, hemocyanin, and catechol oxidase as type-3 copper proteins.

3.1. Early investigations and similarity to hemocyanin

The first structural studies on tyrosinase exploited the presence of copper in the active site of the enzyme. As early as 1938, Kubowitz had already realized the similarity of tyrosinase and hemocyanin, which both are copper proteins, and which both bind one carbon monoxide molecule per two copper ions, suggesting the presence of a pair of copper ions in both proteins (Robb 1984). The similarity in the spectroscopic properties of tyrosinase and hemocyanin was observed by Mason's group (1973-1974), who reported the appearance of intense and weak spectral absorption maxima at ~345 and ~600 nm, respectively, upon treatment of *deoxy*-tyrosinase with hydrogen peroxide, which results in the *oxy*-state of the enzyme. Despite the lack of a blue color, the absorption profile of *oxy*-tyrosinase resembles that of hemocyanin (Makino and Mason 1973; Jolley, Evans *et al.* 1974). The absorbances at ~345 and ~600 nm correspond to O_2^{2-} (π_u^x) → Cu(II) and O_2^{2-} (π_v^x) → Cu(II) charge-transfer transitions, respectively (Eicken, Zippel *et al.* 1998). Further, Resonance Raman spectroscopy showed that the dioxygen is bound to tyrosinase as a peroxide (Eickman, Solomon *et al.* 1978). Interaction of a peroxide (which is a strong σ-donor) and a copper ion pair (which is a strong π-acceptor) results in a strong peroxide-binuclear copper bond, which stabilizes the bound dioxygen and prevents the copper binding site from loosing the dioxygen molecule as a reactive peroxide (Holm, Kennepohl *et al.* 1996). These early spectroscopic studies indicated that the copper in tyrosinase occurs in three forms similar to the three copper forms of hemocyanin, which are the *deoxy*-form (Cu(I) state), the *met*-form (Cu(II) state), and

the *oxy*-form (Cu(II) state with an oxygen molecule bound). More recent spectroscopic studies by X-ray absorption spectroscopy (XAS) confirmed the similarity of the copper sites in tyrosinase and hemocyanin, as well as the occurrence of the *deoxy*-, *met*-, and *oxy*-forms of the copper in the enzyme (Della-Longa, Ascone *et al.* 1996). These spectroscopic studies further classified tyrosinase and hemocyanin as type-3 copper proteins, which are proteins containing a binuclear copper center with antiferromagnetically coupled copper ions (Abolmaali, Taylor *et al.* 1998). Ultimately, the crystal structures of bacterial tyrosinase (Matoba, Kumagai *et al.* 2006) and hemocyanins (Gaykema, Hol *et al.* 1984; Hazes, Magnus *et al.* 1993; Cuff, Miller *et al.* 1998) provided undisputed proof of the similarity of the copper-binding sites of the two proteins.

3.2 Catechol oxidases

Catechol oxidases form the third member of the class of type-3 copper proteins; they catalyze the oxidation of *o*-diphenols to the corresponding *o*-quinones, which is the second step of the reaction catalyzed by tyrosinases. They do however not catalyze the *o*-hydroxylation of monophenols. The spectroscopic properties of catechol oxidase are also very similar to those of hemocyanins and tyrosinases. The crystal structure of sweet potato catechol oxidase confirms the structural similarity, especially in the copper binding site, to hemocyanins and tyrosinases (Klabunde, Eicken *et al.* 1998).

3.3. The binuclear copper center

The two copper ions in the type-3 copper proteins are coordinated by six histidine residues, which are absolutely conserved, not only in tyrosinases but also in hemocyanins and catechol oxidases. These six histidine residues form two clusters of three histidine residues each in the amino acid sequence, which are called the Cu-A and Cu-B regions, respectively. The Cu-A and Cu-B regions are characterized by distinct conserved sequence motifs (see Figure 3) (van Gelder, Flurkey *et al.* 1997).
Both the Cu-A and Cu-B regions consist of a sequence motif F-x-x-x-H, which was first found upon the elucidation of the crystal structure of arthropod hemocyanin (Hazes, Magnus *et al.* 1993). This motif was extended with a negatively charged

residue located in a helix that faces the active site. The negatively charged residue is involved in a hydrogen bonding network with strictly conserved arginine residues (see below for a detailed discussion) (van Holde and Miller 1995; Cuff, Miller *et al.* 1998). In the Cu-A site of mushroom tyrosinase, as well as in catechol oxidase and in molluskan hemocyanin, this negatively charged residue is located three helix turns after the histidine residue of the F-x-x-x-H motif, while in the Cu-B site it is located only two helix turns after the F-x-x-x-H motif (Figure 3). In contrast, the Cu-A site of arthropod hemocyanins resembles the Cu-B site, in the sense that the acidic residue is located two helix turns after the F-x-x-x-H motif. In this way molluscan and arthropod hemocyanins can easily be distinguished. Moreover, based on these sequence motifs, the copper center in type-3 copper proteins can be classified as either a molluscan or an arthropod hemocyanin-like copper center (Abolmaali, Taylor *et al.* 1998). Bacterial, fungal, plant, and mammalian tyrosinases are similar to molluscan hemocyanins, while insect tyrosinase is similar to arthropod hemocyanins (van Gelder, Flurkey *et al.* 1997; Decker, Schweikardt *et al.* 2007). The organization of the copper binding site in *Ipomoea batatas* catechol oxidase (*Ib*COX) also resembles more that of molluscan hemocyanin (Eicken, Krebs *et al.* 1999) (Figure 5). The overall structure of this latter enzyme is also similar to that of the bacterial tyrosinase from *S. castaneoglobisporus* (*Sc*TYR) and the molluscan hemocyanin from *Octopus dofleini* (*Od*HCY) (Figure 6a). Therefore, these three proteins are included in our discussion on the structural studies of mushroom tyrosinase.

Figure 5 (overleaf). Sequence comparison of the tyrosinase domain of PPO1, PPO2, PPO3, PPO4, *Od*HCY, *Sc*TYR, and *Ib*COX. The signs indicate the conserved residues: copper coordinating histidine residues (★), the cysteine involved in the thioether bond (●), the interacting N-terminal arginine and C-terminal tyrosine residues (■), and other highly conserved residues (▲). The secondary structure elements are based on the crystal structure of *Od*HCY (Protein Data Bank (PDB) accession code 1JS8), *Sc*TYR (PDB code 1WX2), and *Ib*COX (PDB code 1BT1). The box in the secondary structure line for *Od*HCY indicates part of the structure that was not visible in the electron density maps.

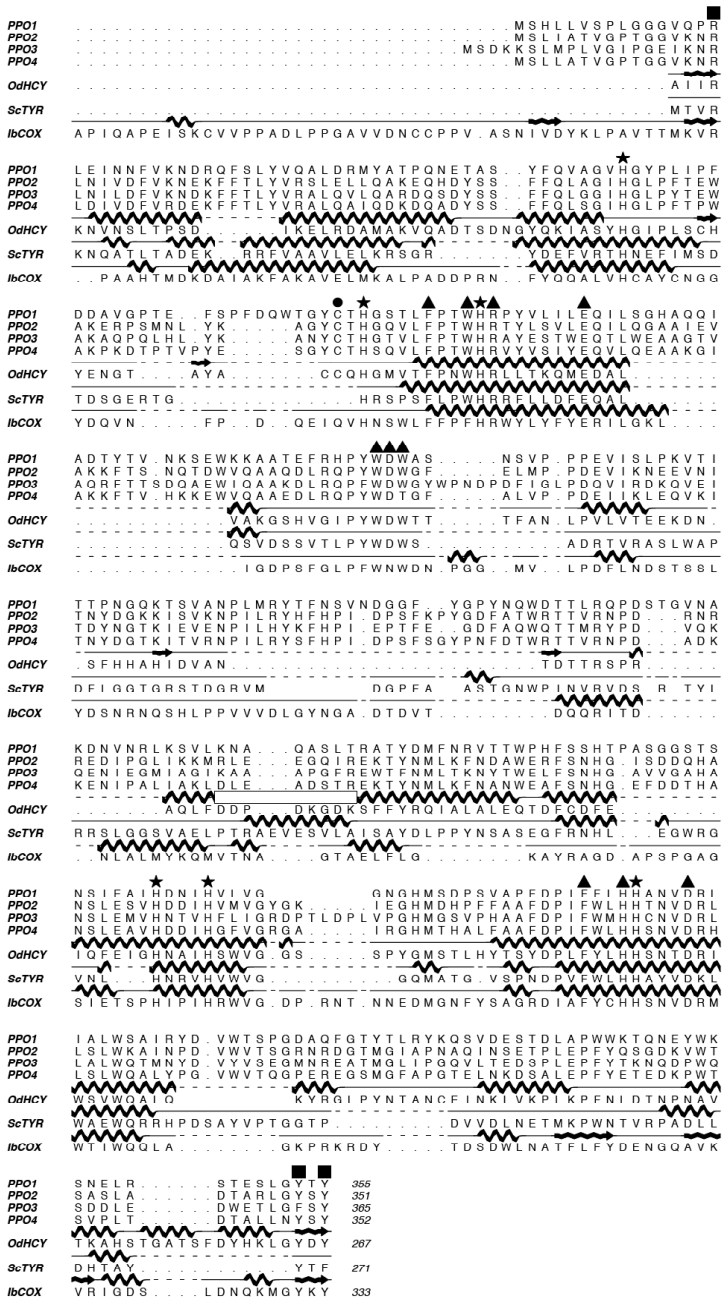
PPO1 MSHLLVSPLGGGVQPR 16
PPO2 MSLIATVGPTGGVKNR 16
PPO3 MSDKKSLMPLVGIPGEIKNR 20
PPO4 MSLLATVGPTGGVKNR 16
OdHCY AIIR 4
ScTYR MTVR 4
IbCOX APIQAPEISKCVVPPADLPPGAVVDNCCPPV.ASNIVDYKLPAVTTMKVR 49
PPO1 LEINNFVKNDRQFSLYVQALDRMYATPQNETAS..YFQVAGVHGYPLIPF 64
PPO2 LNIVDFVKNEKFFTLYVRSLELLQAKEQHDYSS..FFQLAGIHGLPFTEW 64
PPO3 LNILDFVKNDKFFTLYVRALQVLQARDQSDYSS..FFQLGGIHGLPYTEW 68
PPO4 LDIVDFVRDEKFFTLYVRALQAIQDKDQADYSS..FFQLSGIHGLPFTPW 64
OdHCY KNVNSLTPSD..IKELRDAMAKVQADTSDNGYQKIASYHGIPLSCH 48
ScTYR KNQATLTADEK..RRFVAAVLELKRSGR.....YDEFVRTHNEFIMSD 45
IbCOX..PAAHTMDKDAIAKFAKAVELMKALPADDPRN..FYQQALVHCAYCNGG 95
PPO1 DDAVGPTE..FSPFDQWTGYCTHGSTLFPTWHRPYVLILEQILSGHAQQI 112
PPO2 AKERPSMNL.YK.....AGYCTHGQVLFPTWHRTYLSVLEQILQGAAIEV 108
PPO3 AKAQPQLHL.YK.....ANYCTHGTVLFPTWHRAYESTWEQTLWEAAGTV 112
PPO4 AKPKDTPTVPYE.....SGYCTHSQVLFPTWHRVYVSIYEQVLQEAAKGI 109
OdHCY YENGT....AYA.....CCQHGMVTFPNWHRLLTKQMEDAL..... 80
ScTYR TDSGERTG.....HRSPSFLPWHRFFIDFEGAL..... 74
IbCOX YDQVN.....FP..D..QEIQVHNSWLFFPFHRWYLYFYERILGKL.... 132
PPO1 ADTYTV.NKSEWKKAATEFRHPYWDWAS.....NSVP.PPEVISLPKVTI 155
PPO2 AKKFTS.NQTDWVQAAQDLRQPYWDWGF.....ELMP.PDEVIKNEEVNI 151
PPO3 AQRFTTSDQAEWIQAAKDLRQPFWDWGYWPNDPDFIGLPDQVIRDKQVEI 162
PPO4 AKKFTV.HKKEWVQAAEDLRQPYWDTGF.....ALVP.PDEIKLEQVKI 152
OdHCY VAKGSHVGIPYWDWTT.....TFAN.LPVLVTEEKDN. 111
ScTYR QSVDSSVTLPYWDWS.....ADRTVRASLWAP 101
IbCOX IGDPSFGLPFWNWDN.PGG..MV..LPDFLNDSTSSL 164
PPO1 TTPNGQKTSVANPLMRYTFNSVNDGGF..YGPYNQWDTTLRQPDSTGVNA 203
PPO2 TNYDGKKISVKNPILRYHFHPI.DPSFKPYGDFATWRTTVRNPD...RNR 197
PPO3 TDYNGTKIEVENPILHYKFHPI.EPTFE..GDFAQWQTTMRYPD...VQK 206
PPO4 TNYDGTKITVRNPILRYSFHPI.DPSFSGYPNFDTWRTTVRNPD...ADK 198
OdHCY .SFHHAHIDVAN.....TDTTRSPR..... 130
ScTYR DFIGGTGRSTDGRVM.....DGPFA..ASTGNWPINVRVDS.R.TYI 139
IbCOX YDSNRNQSHLPPVVVDLGYNGA.DTDVT.....DQQRITD..... 198
PPO1 KDNVNRLKSVLKNA...QASLTRATYDMFNRVTTWPHFSSHTPASGGSTS 250
PPO2 REDIPGLIKKMRLE...EGQIREKTYNMLKFNDAWERFSNHG.ISDDQHA 243
PPO3 QENIEGMIAGIKAA...APGFREWTFNMLTKNYTWELFSNHG.AVVGAHA 252
PPO4 KENIPALIAKLDLE...ADSTREKTYNMLKFNANWEAFSNHG.EFDDTHA 244
OdHCY .....AQLFDDP.....DKGDKSFFYRQIALALEQTDFCDFE..... 162
ScTYR RRSLGGSVAELPTRAEVESVLAISAYDLPPYNSASEGFRNHL...EGWRG 186
IbCOX..NLALMYKQMVTNA....GTAELFLG.....KAYRAGD.APSPGAG 233
PPO1 NSIFAIHDNIHVIVG.....GNGHMSDPSVAPFDPIFFIHHANVDRI 292
PPO2 NSLESVHDDIHVMVGYGK.....IEGHMDHPFFAAFDPIFWLHHTNVDRL 288
PPO3 NSLEMVHNTVHFLIGRDPTLDPLVPGHMGSVPHAAFDPIFWMHHCNVDRL 302
PPO4 NSLEAVHDDIHGFYGRGA.....IRGHMTHALFAAFDPIFWIHHSNVDRH 289
OdHCY IQFEIGHNAIHSWVG.GS.....SPYGMSTLHYTSYDPLFYLHHSNTDRI 206
ScTYR VNL...HNRVHVWVG.....GQMATG.VSPNDPVFWLHHAYVDKL 222
IbCOX SIETSPHIPIHRWVG.DP.RNT.NNEDMGNFYSAGRDIAFYCHHSNVDRM 280
PPO1 IALWSAIRYD.VWTSPGDAQFGTYTLRYKQSVDESTDLAPWWKTQNEYWK 341
PPO2 LSLWKAINPD.VWVTSGRNRDGTMGIAPNAQINSETPLEPFYQSGDKVWT 337
PPO3 LALWQTMNYD.VYVSEGMNREATMGLIPGQVLTEDSPLEPFYTKNQDPWQ 351
PPO4 LSLWQALYPG.VWVTQGPEREGSMGFAPGTELNKDSALEPFYETEDKPWT 338
OdHCY WSVWQAIQ.....KYRGIPYNTANCFINKIVKPIKPFNIDTNPNAV 247
ScTYR WAEWQRRHPDSAYVPTGGTP.....DVVDLNETMKPWNTVRPADLL 263
IbCOX WTIWQQLA.....GKPRKRDY.....TDSDWLNATFLFYDENGQAVK 317
PPO1 SNELR.....STESLGYTY 355
PPO2 SASLA.....DTARLGYSY 351
PPO3 SDDLE.....DWETLGFSY 365
PPO4 SVPLT.....DTALLNYSY 352
OdHCY TKAHSTGATSFDYHKLGYDY 267
ScTYR DHTAY.....YTF 271
IbCOX VRIGDS....LDNQKMGYKY 333

4. The crystal structure of *Streptomyces castaneoglobisporus* tyrosinase

4.1. The overall structure

The structure of *Sc*TYR (Figure 6a) consists of a central core of two pairs of long antiparallel α-helices, which host the copper-binding sites. The two pairs of α-helices are tilted with respect to each other by about 45°. This helical central core of *Sc*TYR superimposes very well on that of *Ib*COX and *Od*HCY with r.m.s.d. (root mean square deviation) values on Cα atoms of 0.94 Å and 1.34 Å (Figure 6a), respectively (Matoba, Kumagai *et al.* 2006). However, tyrosinases and catechol oxidases are small in comparison to hemocyanins, which are very large protein complexes and consist of three structural domains: an N-terminal α-helical domain, a copper-containing α-helical core domain, and a C-terminal β-barrel domain (Cuff, Miller *et al.* 1998). The structure of *Sc*TYR contains only the copper-containing α-helical core domain of molluscan hemocyanins. This core domain is sealed with two short β-strands from the N- and C-termini, respectively, that form a parallel β-sheet structure (Matoba, Kumagai *et al.* 2006).

4.2. The copper binding site

The copper-binding histidine residues reside in the middle of helices α2 and α3 (for Cu-A), and in the middle of helices α6 and α7 (for Cu-B) (Matoba, Kumagai *et al.* 2006). They are located at the bottom of a large cavity formed by hydrophobic residues similar to the environment of the copper-binding residues in hemocyanin. However, in *Sc*TYR, this cavity is open to the solvent, in contrast to *Od*HCY (Cuff, Miller *et al.* 1998) and the arthropodan hemocyanin from *Limulus polyphemus* (Hazes, Magnus et al. 1993), in which the cavities are shielded by the C- and N-terminal domains, respectively. The presence of the terminal domains is proposed to prevent organic molecules to enter the active site and interact with the copper ions. Interestingly, it has been shown that hemocyanins can be converted to a polyphenol oxidase, both *in vitro* and *in vivo*, upon removal or reorganization of these terminal domains (Decker and Rimke 1998). These results support the role of the terminal

domains of hemocyanins in confining their function to the transport of oxygen (Decker, Schweikardt *et al.* 2007).

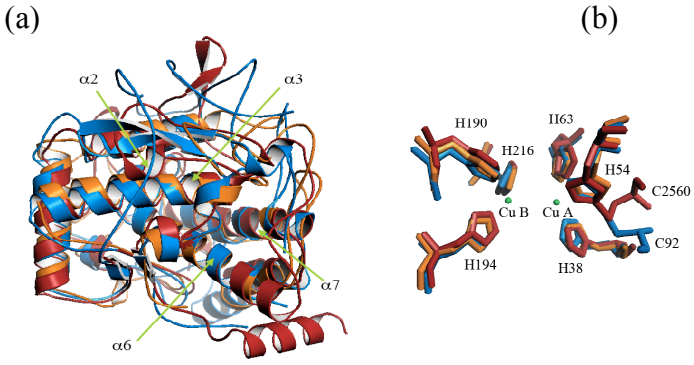

Figure 6. (a) Superimposition of *Sc*TYR (orange), *Ib*COX (blue), and *Od*HCY (red) showing the four-helix architecture of the core of the proteins. (b) Comparison of the copper-binding sites of *Sc*TYR, *Ib*COX, and *Od*HCY showing the conserved residues, colored as in (a). The numbering of *Sc*TYR is used, except for the cysteine residue that participates in the thioether bond; it is numbered according to *Ib*COX and *Od*HCY. The Sγ of the cysteine in both *Ib*COX and *Od*HCY is covalently bound to the Cε1 atom of H54. The copper ions are presented as green spheres.

The Cu-A copper-binding site in *Sc*TYR comprises H38, H54, and H63, and the Cu-B copper-binding site is made up of H190, H194, and H216 (Matoba, Kumagai *et al.* 2006). The histidine residues coordinate the pair of copper ions in the active site. F59 and E71 are also part of the Cu-A sequence motif, while F212 and D220 are part of the Cu-B motif. The histidine residues that coordinate the copper ions are located in α-helices, except for H54, which resides in a flexible loop.

The phenylalanine side chains of the Cu-A and Cu-B motifs, F59 and F212, respectively, are located perpendicular to the Cu – Cu axis, similar to F2567 and F2698 in *Od*HCY. Moreover, being located one helix turn away from the adjacent copper-coordinating histidines (H63 and H216), their side chains also point to the same direction as the histidine side chains, providing tight steric interactions to control the histidine side chain conformations. These phenylalanine residues are conserved in hemocyanins, tyrosinases, and catechol oxidases and they participate in supporting the integrity of the copper binding sites (Hazes, Magnus *et al.* 1993).

5. Tyrosinase core domain

In the *Sc*TYR structure, residues E71 and D220 (the carboxylate parts of the Cu-A and Cu-B motifs, respectively) form hydrogen bonds with R4 and Y269, respectively. This hydrogen bonding network is identical to that which is present in hemocyanin (Cuff, Miller *et al.* 1998). R4 and Y269 belong to a conspicuous structural motif consisting of two parallel β-strands at the N- and C-terminus, respectively, which form a β-sheet. R4 is a strictly conserved residue at the N-terminus. This arginine residue interacts with Y269, which is a strictly conserved aromatic residue at the C-terminus and is part of the highly conserved Y/F-x-Y/F motif. Flurkey and Inlow (Flurkey and Inlow 2008) have proposed that this β-sheet structure forms the beginning and the end of the "tyrosinase core domain" structure, connecting the N- and C-termini of the core-domain to form a compact globular protein. The hydrogen bonding interaction between R4 and Y269 keeps the N- and C-termini together, thus contributing to the overall stability of the structure. The absence of this R-Y interaction would make the protein prone to unfolding and destabilize other regions of the core domain, and could result in loss of enzyme activity.

6. The thioether bond

The *Sc*TYR structure does not give information on the thioether bond that has been found in fungal tyrosinases and mollusk hemocyanins. This thioether bond is found in a C-X-H sequence motif (Figure 5), which was demonstrated in *N. crassa* tyrosinase (Lerch 1982). It was suggested that this covalent bond is the result of a post-translational modification of the enzyme. Later, Gielens *et al.* (Gielens, Geest *et al.* 1997) confirmed the presence as well as the location of this bond in molluscan hemocyanins. On the basis of the conservation of the motif, Gielens *et al.* (Gielens, Geest et al. 1997) proposed the hypothesis that molluscan hemocyanin evolved from a tyrosinase, and further speculated that the absence of this thioether bond in arthropod hemocyanin suggests that the latter has evolved differently. Interestingly, this thioether bond is also absent in insect, mouse, human, and bacterial tyrosinases (Decker, Schweikardt *et al.* 2007).

The thioether bond occurs between the Sγ atom of the cysteine and the $C\varepsilon_1$ atom of the adjacent histidine residue that is responsible for binding the copper in the Cu-A binding site (Cuff, Miller *et al.* 1998) thereby fixes the position of the histidine. In *Sc*TYR, this particular histidine residue is disordered in the absence of copper, indicating inherent flexibility of this residue. Although in the presence of copper the side chain conformation of the residue becomes better defined, it was still less rigid than the other five copper-ligating histidines, as evidenced by its higher atomic *B*-factor. Based on this observation, Matoba *et al.* (2006) speculated that the presence of the thioether bond may enhance the rigidity of the Cu-A binding site (Matoba, Kumagai *et al.* 2006). Additional evidence for the plasticity of the Cu-A binding site is provided by the structure of the tyrosinase from *Bacillus megaterium*, where the thioether bond is also absent (Sendovski, Kanteev *et al.* 2011). This speculation is to be resolved when the structure of a fungal tyrosinase containing the thioether bond is elucidated (this thesis).

Interestingly, this thioether bond also occurs in *Ib*COX, despite the absence of the C-x-H motif. In *Ib*COX, the thioether bond is formed between the Sγ atom of C92 and the Cε1 of H109, which latter residue is equivalent to the copper-binding H54 of *Sc*TYR. The Sγ of the cysteine and Cε1 of the histidine that form the thioether bond in *Ib*COX reside at exactly the same position as in *Od*HCY (Figure 6b) (Klabunde, Eicken *et al.* 1998). Moreover, this alternative thioether bond forming cysteine residue is highly conserved in plant catechol oxidases (Marusek, Trobaugh *et al.* 2006). The *Ib*COX structure shows that this bond not only fixes the position of H109 but also causes additional structural restraints on the ligand sphere of the Cu-A binding site. These restraints could help to impose Cu(I) geometry on Cu(II) and thereby may optimize the redox potential of the copper for the reaction, as well as allowing rapid electron transfer in the redox process (Klabunde, Eicken *et al.* 1998). The conservation of this structural motif emphasizes the functional importance of the presence of the thioether bond in fungal tyrosinases, catechol oxidases, and molluscan hemocyanins.

7. Current perspective on the reaction mechanism

7.1. Changes in the copper states during the reaction

Based on the active site under copper-free, *met*-, *deoxy*-, and *oxy*-conditions, Matoba *et al.*(Matoba, Kumagai et al. 2006) described changes in the active site upon the binding of dioxygen and further proposed a substrate-binding mode for tyrosinase. Additionally, two *met*-forms, called *met*-I and *met*-II, which differ only in the copper-copper distance, were obtained upon soaking the protein in copper sulfate solutions during different times; the *met*-I was obtained after 18 hours soaking, while ~60 hours soaking time resulted in the *met*-II form. The two forms may represent intermediate states between the *met*- and the *oxy*-forms. The copper-copper distance of the *deoxy*-form was ~ 4.1 Å and gradually decreased to 3.9 and 3.3 Å in the *met*-I and *met*-II forms, respectively. The copper-copper distance in the presence of hydrogen peroxide (H_2O_2), which mimics the *oxy*-form with a bound dioxygen molecule, was 3.4 Å, similar to the distance in the *met*-II form. However, the H54 becomes less ordered in the H_2O_2-bound state, which indicates that this *oxy*-form is less stable than the *met*-II state. Matoba *et al.* proposed that the instability of this *oxy*-state might be related to high reactivity of this state for catalysis (Matoba, Kumagai *et al.* 2006).

7.2. The binding of oxygen

The H_2O_2 molecule is bound to the copper ions in a bridging, side on, μ-η^2:η^2 binding mode (Matoba, Kumagai *et al.* 2006), which is similar to the oxygen binding mode in hemocyanin (Holm, Kennepohl *et al.* 1996). Nevertheless, the oxygen-binding mode in tyrosinase still needs to be firmly established, because the two currently standing oxygen-binding modes, i.e. side-on (Karlin and Gultneh 1987) and end-on (Kitajima 1992) are still possible (Reedijk 2005). Furthermore, in tyrosinase, the oxygen molecule needs to be activated prior to the hydroxylation of the monophenolic substrate (Reedijk 2005), whereas in hemocyanin such activation should be prevented.

Matoba *et al.* (2006) proposed that the oxygen molecule, which is bound as a peroxide, serves as the catalytic base that abstracts the proton from the hydroxyl

group of a monophenolic substrate. The deprotonated hydroxyl group then binds to the Cu-B copper ion. This binding permits the carbon atom at the *ortho*-position of the substrate to come near the peroxide ion. The proton at the *ortho*-position is abstracted by H54 and the oxygen ion can be attached to the phenolic ring. Finally, the product and a water molecule are released, and the copper ions have returned to the Cu(I) state (Figure 7a) (Matoba, Kumagai *et al.* 2006).

7.3. Substrate binding disagreement and the present reaction mechanism

A tyrosine residue from a so-called caddie protein, of which the 3D-structure was co-elucidated with that of *Sc*TYR, occupies a similar position as the phenylthiourea, an inhibitor, in the *Ib*COX structure. Therefore, similar to *Ib*COX, Cu-B was proposed as the substrate binding site in tyrosinase (Matoba, Kumagai *et al.* 2006). However, Decker *et al.* (2006) disagreed with that proposal and suggested that the binding of the substrate could also take place at the Cu-A site. In *Ib*COX, a phenylalanine residue (F261) resides above the Cu-A site, whereas in the *Sc*TYR structure, an isoleucine occupies this position. Decker *et al.* argue that the presence of large bulky residue at the Cu-A site of *Ib*COX prevents the Cu-A from substrate binding, which is not the case in *Sc*TYR. Furthermore, Decker *et al.* proposed that this F261 makes the difference in the functionality of tyrosinase and catechol oxidase (Decker, Schweikardt *et al.* 2006). Therefore, they have proposed an alternative mechanism for the hydroxylation of tyrosine (Figure 7b) (Decker, Schweikardt *et al.* 2006).

According to this mechanism, the monophenolic substrate is first pre-oriented by a $\pi\pi$-interaction with the H194 side chain near Cu-B binding site. As a result, the hydroxyl group becomes oriented towards the Cu-A site. The substrate then binds to Cu-A. The O-O axis of the peroxide ion rotates to allow electrophilic attack of the Cu_2O_2 moiety on the *ortho*-carbon atom of the monophenolic substrate, which is followed by cleavage of the O-O bond. The diphenol intermediate probably binds to Cu-A as well, forming a phenoxo-bridge to Cu-B, in a bidentate binding mode. Finally, the diphenol intermediate is oxidized and leaves the active site as a quinone, while the copper ions are reduced to Cu(I). This proposed mechanism predicts that no diphenol is released during the reaction, which is different from the reaction

catalyzed by catechol oxidase. For the second part of the tyrosinase reaction, the diphenol intermediate only needs to approach Cu-B without the need for any further interactions (Decker, Schweikardt *et al.* 2006).

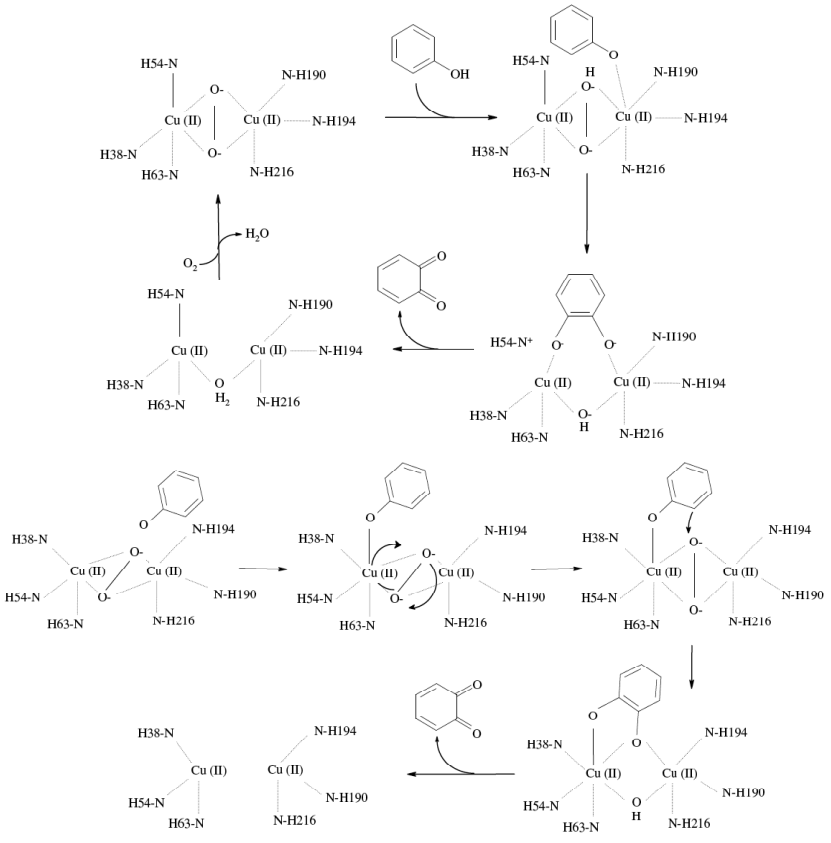

Figure 7. Scheme showing the catalytic mechanism of tyrosinase according to (a) Matoba *et al.* (2006) and (b) Decker *et al.* (2006).

8. Working hypothesis

Until very recently, the structure of *Sc*TYR was the only published structure of a tyrosinase. Only this year, in 2011, the structure of a second tyrosinase, the tyrosinase from *Bacillus megaterium*, was published (Sendovski, Kanteev *et al.* 2011). Still, the substrate binding mode and exact mechanism of the reaction catalyzed by tyrosinase

remains uncertain. Mushroom tyrosinase has been the subject of many investigations, because of its importance as a 'role model' for browning reactions in food. The enzyme is larger than its bacterial counterparts and incorporates a covalent thioether bond in its active site. The elucidation of the structure of mushroom tyrosinase could show the importance of this structural feature. Furthermore, a bound substrate analogue or inhibitor in the structure could provide more insight into the mechanism.

9. Scope and content of this thesis

Elucidation of an enzyme's structure requires pure enzyme material. Obtaining pure tyrosinase from mushroom fruiting bodies is difficult because of the frequent contamination with melanin and the heterogeneity of the enzyme. Therefore, we attempted to overproduce the mushroom tyrosinase isoform PPO2 in *Escherichia coli* (**Chapter 2**). Unfortunately, the enzyme was found in inclusion bodies. Although it was possible to refold the enzyme, the activity of the refolded enzyme was very low in comparison to that of commercial mushroom tyrosinase. Moreover, no protein crystals could be obtained with this recombinantly produced protein.

During our work on recombinant mushroom tyrosinase, a procedure was reported to obtain relatively pure enzyme from commercially available mushroom tyrosinase. Using that approach, we succeeded in obtaining protein crystals for structure elucidation by X-ray crystallography (**Chapter 3**). However, crystallization remained difficult, because the mushroom tyrosinase crystals grew in competition with aggregation and suffered from aging. It appeared to be important to have calcium ions present during sample preparation. In the end, diffracting crystals with sufficient quality for X-ray diffraction analysis were obtained in the presence of holmium, a calcium analogue. Analysis of the crystal content indicated that the crystals contained both the heavy and light tyrosinase subunits (H and L chains).

Elucidating the structure proved to be another great challenge (**Chapter 4**). On the basis of the information available at the time, we attempted to solve the mushroom tyrosinase structure using the PPO2 amino acid sequence and an initial model generated from the conserved parts in the structures of its homologs. During the model building, we found that the PPO2 sequence did not fit the electron density map very well, and several insertions and deletions, as well as amino acid substitutions

had to be introduced into the PPO2 sequence. This modified amino acid sequence matched with the recently published PPO3 sequence, which was then used to complete the model of the H chain. The amino acid sequence of PPO3 did however not fit the L chain, and therefore an initial amino acid sequence was guessed from the electron density map. This sequence did not match any amino acid sequences in the public databases. Fortunately, it matched with the amino acid sequence of ORF239342 of the as yet unpublished mushroom *Agaricus bisporus* genome database. Using the sequence of ORF239342, the structural model of the L chain could be completed. Thus, we have not only successfully elucidated the structure of mushroom tyrosinase, but also revealed the identity of the enzyme's subunits. The structure of PPO3 (this thesis) also provides the evidence of the highly conserved thioether bond in the active site. The structure in the presence of tropolone suggests that the inhibitor is not bound specifically and provides evidence that the enzyme was crystallized in the *deoxy*- state. It also proposes several amino acid residues that may be involved in the binding of substrate.

The structure of mushroom tyrosinase (PPO3) can now serve as a solid base for obtaining further insights into the enzyme's mechanism and the development of specific tyrosinase inhibitors. Furthermore, detailed structure-function studies of the L subunit are now possible, which may reveal the biological function of this protein.

Chapter 2

Overproduction, purification and refolding of recombinant mushroom tyrosinase

Wangsa T. Ismaya, Carmen G. Boeriu, Harry J. Wichers, Bauke W. Dijkstra

Abstract

A tyrosinase isoform from *Agaricus bisporus* was overexpressed in *Escherichia coli* as a C-terminally histidine$_6$-tagged protein and found in inclusion bodies. The inclusion bodies were solubilized in the presence of a high concentration of guanidinium chloride and β-mercaptoethanol. The enzyme was successfully purified from the solubilized inclusion bodies using a Ni-NTA affinity column. Subsequently, the protein was refolded while still bound to the column, by lowering the guanidinium chloride concentration in the presence of salt and glycerol under reducing conditions. The refolded enzyme was activated by the introduction of copper and recovered from the column by applying a high concentration of imidazole. Gel filtration analysis suggested that the molecular mass of the refolded enzyme was 64 kDa. A circular dichroism analysis indicated a secondary structure content of 30 % α-helix, 24 % β-strand, 19 % turns, and 27 % coil, respectively. Furthermore, an X-ray absorption analysis showed the presence of a binuclear copper center in the enzyme. The activity of the refolded enzyme was much lower than that of enzyme isolated directly from mushroom reported in the literature. The possible causes for the low enzyme activity are discussed.

Introduction

Tyrosinase is a copper containing monooxygenase that catalyses the *o*-hydroxylation of phenolic compounds (monophenolase activity) and the subsequent oxidation of the formed *o*-diphenols to the corresponding *o*-quinones (diphenolase activity). *o*-Quinones are the main precursors in the biosynthesis of melanin, one of the most widely distributed pigments in living organisms (Sanchez-Ferrer, Rodriguez-Lopez *et al.* 1995).

In plants and fungi, melanin is the cause of the brown discoloration as a result of ageing, damage, or infection. For instance, in the common mushroom, *Agaricus bisporus*, a constitutively expressed tyrosinase (PPO1) is present that is responsible for the browning of the mushroom during maturation (Van Leeuwen and Wichers 1999). Break down of cellular compartments upon ageing or injury brings the melanogenous substrate (phenols and oxygen) into contact with tyrosinase, which triggers the browning by means of the synthesis of *o*-quinones, which can polymerise into melanins (Jolivet, Arpin *et al.* 1998). In addition, a second tyrosinase isoform (PPO2) is present in mushroom that is induced upon microbial infection. Since *o*-quinones can cross-link proteins, and thereby inactivate them, this isoform has been proposed to have a function in the defence of the mushroom against pathogens (Soler-Rivas, Moller *et al.* 2001).

Mushroom tyrosinase appears to be heterogeneous. The predominant form was described as a heterotetramer composed of two H subunits of 43-48 kDa and two L subunits of 13-14 kDa (H_2L_2 configuration) (Strothkamp, Jolley *et al.* 1976). In more recent investigations, a model was proposed in which tyrosinase is initially formed as a monomeric 64 kDa latent precursor, which can be activated by non-covalent or covalent (proteolytic) modifications. The non-covalent modifications result in a 64 kDa active form, while the proteolytic ones result in 58, 43, and 35 kDa forms than can be detected by western blotting, while only the 43 kDa-form was proven to be active until now (Wichers, Gerritsen *et al.* 1996; Espin, Soler-Rivas *et al.* 2000). Recently, Flurkey *et al.* confirmed this model and alluded that the L subunit reported by Strothkamp (1976) is either the C-terminal domain of the 64 kDa latent precursor or even another, perhaps unrelated, protein that co-purified with the H-chain (Flurkey and Inlow 2008). Moreover, Wichers *et al.* found that the 43 kDa tyrosinase consists

of two isoforms that differ in isoelectric point (Wichers, Gerritsen *et al.* 1996). This suggests that mushroom tyrosinase is not only heterogeneous in molecular mass, but also in charge. Moreover, the amounts of the different tyrosinase variants may vary according to the mushroom strain or age (Wichers, van den Bosch *et al.* 1995; Van Leeuwen and Wichers 1999). The existence of several tyrosinase variants in mushroom with different molecular properties (Jolivet, Arpin *et al.* 1998; Soler-Rivas, Jolivet *et al.* 1999) is not conducive for the large-scale purification of the enzyme for 3D-structure determination purposes.

To overcome the expected difficulties of obtaining pure enzyme from natural sources we decided to work with recombinant mushroom tyrosinase. Wichers *et al.* successfully cloned two genes from mushroom cDNA that encoded two 64 kDa tyrosinases, and their gene products could be overexpressed in *Escherichia coli* as His_6-tagged or GST-tagged proteins (Wichers, Recourt *et al.* 2003). As part of our attempts to solve the structure of mushroom tyrosinase, we describe here our efforts to obtain a sufficient amount of pure and active PPO2 from tyrosinase inclusion bodies produced by *E. coli* by means of refolding and we give a preliminary characterization of the refolded enzyme.

Materials and methods

Materials

All chemicals were purchased from Merck, Sigma Aldrich, or Calbiochem. The Ni-NTA agarose affinity matrix was purchased from Qiagen.

Overproduction of tyrosinase in E. coli M15

The *ppo2* gene with a C-terminal His_6-tag was inserted into the pQE60 expression vector (Qiagen Benelux B.V., Venlo, The Netherlands) and was overexpressed in *E. coli* M15 [pREP4] as a host (Wichers, Recourt *et al*. 2003). The bacteria were grown overnight at 37 ^{o}C on an agar plate containing LB medium (5 g/L yeast extract, 10 g/L sodium chloride, 10 g/L tryptone, supplemented with 25 μg/ml kanamycin and 100 μg/ml ampicillin). A single colony was transferred to 100 ml LB medium in an Erlenmeyer flask and was grown overnight at 30 ^{o}C with an agitation speed of 200

rpm. This overnight culture was transferred to 1 L LB medium and the cells were grown at 35 ^{o}C until an OD_{600} of 0.6 – 0.75 was reached. Enzyme production was induced by the addition of IPTG to a final concentration of 1 mM. The *E. coli* cells were harvested approximately 5 hours after the IPTG induction by centrifugation at 6000 *g* during 30 minutes.

Isolation and solubilization of inclusion bodies

The *E. coli* cell pellet was washed 3 times with buffer 1 (Table 1) and was resuspended in this buffer. The cell suspension was sonicated on ice by applying ten 10-second bursts (130 W, 20 kHz) with 10-second cooling intervals. After centrifugation at 6000 *g* for 30 minutes, the pellet was collected and resuspended in buffer 2. The suspension was sonicated on ice for another ten 10-second bursts with 10-second cooling intervals. Finally, the pellet of inclusion bodies was collected by centrifugation at 6000 *g* for 30 minutes. The pellet was washed 3 times with buffer 1, and stored at -80 ^{o}C.

The inclusion bodies were solubilized overnight in buffer 3 (10 mg inclusion bodies pellet per ml buffer, *w/v*), with constant stirring at room temperature. The insoluble contaminants were removed by centrifugation at 10000 *g* for 30 minutes and by subsequent filtration through a 0.45 μm micro-filter. Finally, the β-mercaptoethanol containing buffer 3 was exchanged for the β-mercaptoethanol-free buffer 4 over a 10-kDa cut-off filter (Macrosep centrifugal devices, Pall Life Sciences, Ann Arbor MI, USA).

Purification and refolding of tyrosinase

The solubilized inclusion bodies were loaded onto a Ni-NTA column, which had been equilibrated with buffer 4 in the cold room (8 ^{o}C). After sample application, the column was eluted with 5 column volumes of buffer 4, after which the imidazole in the column was removed by elution with 5 column volumes of buffer 5 at a constant flow rate of 0.5 ml/min.

Refolding was started by elution with 10 column volumes of buffer 6 and was completed with a copper-charging step by elution with 10 column volumes of buffer 7 at a constant flow rate of 0.1 ml/min. Subsequently, the excess of copper present in

the Ni-NTA column was removed by an overnight washing step with 75 column volumes of buffer 8. The column was then transferred to an FPLC system (GE Healthcare, Uppsala, Sweden) and the enzyme was recovered from the Ni-NTA column by elution with 2 column volumes of buffer 9 at a flow rate of 0.5 ml/min.

Protein concentration and activity assay

The protein concentration was determined with the Bradford method (Biorad Protein Assay, Bio-Rad Laboratories, Hercules CA, USA) using bovine serum albumin as a standard or by measuring the protein absorption at 280 nm, using a theoretical molar extinction coefficient of 98,780 $M^{-1}.cm^{-1}$.

Enzyme activity was measured at 25 ^{o}C by a colorimetric method essentially as described by (Espin, Morales *et al*. 1997) using 3,4-dihydroxyphenylalanine (L-dopa) as the substrate. Briefly, in a 1 ml cuvette, 100 µl of a 5 mM 3-methyl-2-benzothiazolinone hydrazone (MBTH) solution in water was mixed with 800 µl of L-dopa solution (18 mM in 50 mM sodium phosphate buffer, pH 6.5). The reaction was started with the addition of 100 µl enzyme solution to the reaction mixture. The increase in the absorbance at 484 nm was followed during the first three minutes. The measurements were carried out in an Ultrospec 4300 Pro spectrometer equipped with a temperature control unit (GE Healthcare, Uppsala, Sweden), on-line interfaced to a computer. The spectra were recorded and processed with the time-drive measurement module (SWIFT II program, version 2.01, GE Healthcare, Uppsala, Sweden).

Characterization of the refolded enzyme

The molecular mass and monodispersity of the refolded enzyme was analyzed on a gel filtration column (Smart-FPLC, GE Healthcare, Uppsala, Sweden) and dynamic light scattering (Dynapro, Protein Solutions, Charlottesville VA, USA), respectively. The secondary structure content of the refolded enzyme was determined by CD spectrometry (AVIV 62 DS, Lakewood NJ, USA) using the CDPro software (Sreerama and Woody 2000). The EXAFS (Extended X-ray Absorption Fine Structure) and XANES (X-ray Absorption Near Edge Structure) measurements were kindly performed by the beam line scientist at DESY (Deutsches Elektronen Synchrotron), Hamburg.

Results

Overexpression of the enzyme

Mushroom tyrosinase was satisfactorily expressed in *E. coli* M15. The SDS-PAGE analysis suggested a protein with a molecular mass of 64 kDa (Figure 1), as expected for the protein encoded by the *ppo2* gene (Wichers, Recourt *et al*. 2003). The enzyme expression increased during the first 3-4 hours after IPTG induction and became constant after 5 hours.

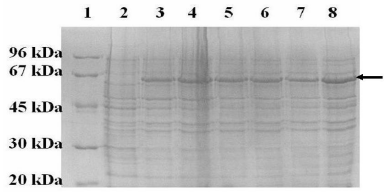

Figure 1. SDS-PAGE analysis of the overexpression of mushroom tyrosinase in *E. coli* M15. Lane 1, molecular mass markers; Lane 2, proteins expressed by non-induced *E. coli* M15 cells; Lanes 3-8, protein expression profiles taken 1, 2, 3, 4, 5, and 6 hours after IPTG induction, respectively. The arrow marks the position of the 64 kDa tyrosinase band.

The enzyme was found in the insoluble fraction upon isolation. Prolonged sonication and/or cell wall digestion with lysozyme were insufficient to release the enzyme from the pellet. This result suggested that the enzyme was produced as insoluble inclusion bodies. Modification of the overproduction conditions by means of lowering the temperature, varying the IPTG concentration, the introduction of copper at 0.1 mM as well as 3% ethanol, was not able to prevent the formation of inclusion bodies.

Isolation and solubilization of inclusion bodies

The inclusion bodies precipitated together with the cell debris after cell disruption. The cell debris could be removed by washing with buffer containing detergent. After the washing step, the inclusion bodies were successfully solubilized in a high concentration of GdmCl in the presence of β-mercaptoethanol. Residual contaminants from the cell debris, appearing as a dark precipitate, could be removed by ultracentrifugation. SDS gel electrophoresis of the solubilized inclusion bodies (Figure 2a) showed that most of contaminants from the *E. coli* cells were successfully removed.

Purification and refolding of recombinant mushroom tyrosinase

SDS gel electrophoresis of the solubilized inclusion bodies (Figure 2a) showed the presence of two other protein bands of lower molecular mass (approximately 35 and 38 kDa). As shown in Figure 2b, a single Ni-NTA affinity column chromatography step was able to remove the two proteins, yielding pure protein. This allowed us to attempt the refolding directly, while the enzyme was still bound to the affinity matrix.

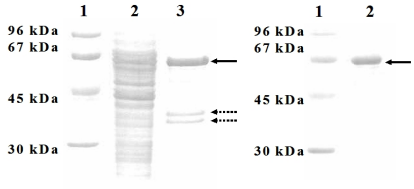

Figure 2. (a) SDS-PAGE analysis of solubilized inclusion bodies. Lane 1, molecular mass markers; Lane 2, supernatant after the cell disruption step; Lane 3, solubilized inclusion bodies. The solid arrow marks the position of the tyrosinase band, while the dashed arrows mark contaminants. (b) SDS-PAGE analysis of purified tyrosinase. Lane 1, molecular mass markers; Lane 2, purified tyrosinase after Nickel-NTA affinity chromatography. The solid arrow marks the position of the tyrosinase.

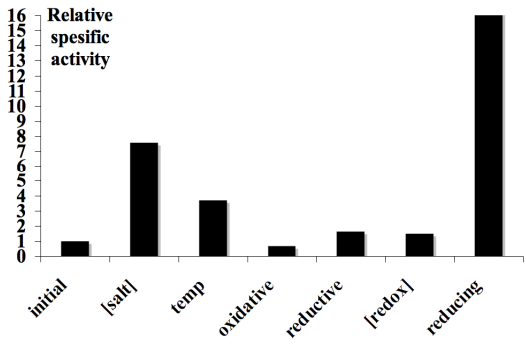

Figure 3. Specific activity of the refolded enzyme from various refolding conditions. The initial condition for the refolding was 0.25 M GdmCl, 0.5 M NaCl, 10% Glycerol, GSH:GSSG (5:1), 50 mM Tris HCl, pH 8.0, at 8 ºC. The specific activity at the initial condition was 2 nano-Katals/mg protein, which is represented as unity. Notation: [salt] is for refolding with 0.25 M NaCl; temp for room temperature (25 ºC), oxidative and reductive for a GSH:GSSG redox ratio of 1:1 and 10:1, respectively; [redox] for a redox concentration of one-tenth of the initial condition at a 5:1 redox ratio; and reducing for a fully reducing condition (only GSH employed).

Recombinant tyrosinase was refolded by lowering the GdmCl concentration in the presence of glycerol, sodium chloride, and a redox system. Optimization of the refolding buffer composition suggested that a lower salt concentration as well as the introduction of reduced glutathione improved the refolding yield (Figure 3).

The temperature at which the refolding takes place also affects the refolding yield. A higher yield was observed when the temperature was increased from 8 ^{o}C to 25 ^{o}C. However, the aggregation rate upon refolding at higher temperatures is also higher, and therefore the refolding was kept at 8 ^{o}C.

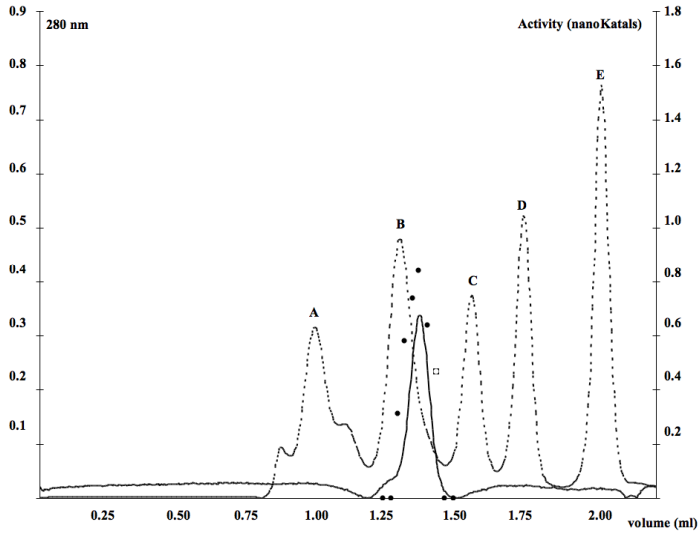

Figure 4. Superdex-200 gel filtration profile of refolded enzyme eluted from a HR30/10 column at 8 ^{o}C. The elution buffer was 50 mM Tris-HCl, pH 8.0, containing 0.25 M NaCl and 10% glycerol at a flow rate of 40 µl/min. The absorption at 280 nm (solid line) nm with a peak at an elution volume of 1.45 ml originates from the refolded tyrosinase, with the enzyme activity given by the dotted line. The protein molecular weight markers (dashed lines) are bovine thyroglobulin (670 kDa, A), bovine γ-globulin (158 kDa, B), chicken ovalbumin (44 kDa, C), horse myoglobulin (17 kDa, D), and vitamin B12 (1.35 kDa, E).

Characterization of the refolded enzyme

The refolded enzyme was monomeric in solution. The gel filtration profile of the refolded enzyme (Figure 4) suggested a protein with a molecular mass of approximately 64 kDa, which is in agreement with the molecular mass derived from

the gene sequence and the molecular mass obtained from the SDS-PAGE analysis. A dynamic light scattering experiment showed that the refolded protein was monodisperse with a predicted molecular mass of 60-70 kDa, which was similar to that suggested by the gel filtration analysis. The amount of refolded enzyme recovered from the purification and refolding steps was ~50%.

The structural features of the refolded enzyme were studied by means of circular dichroism and X-ray absorption spectroscopy. The circular dichroism profile of the refolded enzyme (Figure 5) suggested α-helix, β-strand, turn and coil contents of 30 %, 24 %, 19 %, and 27 %, respectively. A XANES spectrum (Figure 6a) indicated the presence of copper (II) in the protein (Borghi, Solari *et al.* 2002). Furthermore, an EXAFS spectrum (Figure 6b) of the refolded enzyme was comparable to that of the binuclear copper site of *Octopus vulgaris* hemocyanin in the Cu (II) state (Borghi, Solari *et al.* 2002), suggesting the presence of a binuclear copper site in mushroom tyrosinase. The results indicated that the refolded enzyme contained secondary structure and that copper ions were present in the enzyme.

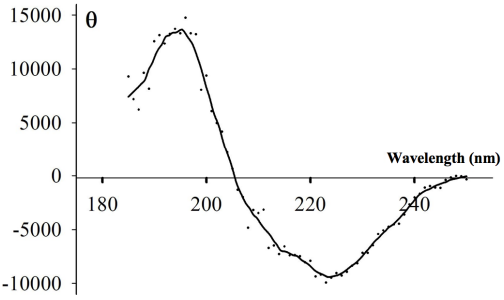

Figure 5. Circular dichroism spectrum of 0.7 mg/ml refolded tyrosinase in 20 mM potassium phosphate buffer, pH 6.8, containing 50 mM potassium fluoride. The measurement was carried out at room temperature. The spectrum was recorded from 280 to 185 nm with a bandwidth of 1 nm and an averaging time of 5 seconds. The final spectrum presented is the average result of 10 scans.

The success of the refolding was also evaluated by determining the enzyme activity after refolding. The activity of the refolded enzyme was ~ 40 nanoKatals per milligram of protein, which is ~ 0.2 % of the reported 18 μKatals (the activity of the probably proteolytically activated 43 kDa enzymes) (Wichers, Gerritsen *et al*. 1996).

The refolded enzyme activity was not affected by the SDS addition. On the other hand, addition of tyrosinase inhibitors, such as EDTA, tropolone, and kojic acid, showed a characteristic inhibition profile of tyrosinase (Figure 7). These results suggested that the refolded enzyme had low but nevertheless true tyrosinase activity.

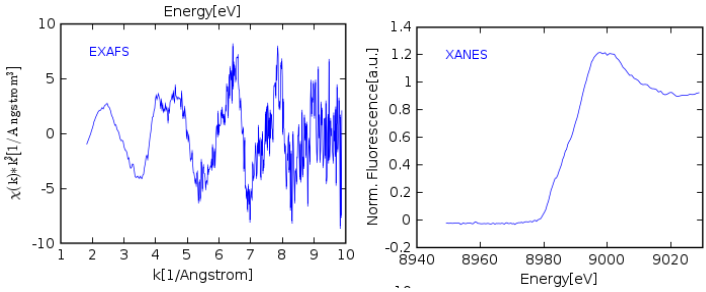

Figure 6. (A) XANES and (B) EXAFS spectra of refolded tyrosinase recorded at the DESY, Hamburg. The sample was diluted in 20 mM Tris HCl, pH 8.0, containing 50 mM sodium chloride.

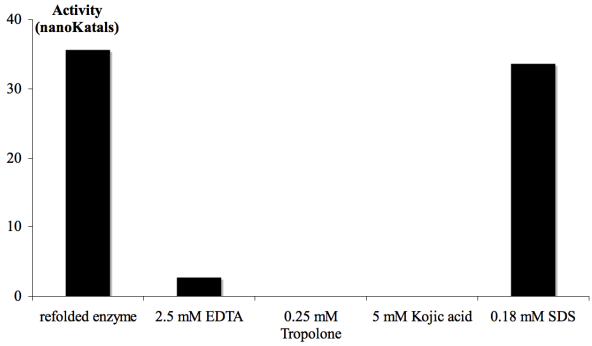

Figure 7. Activity of the refolded enzyme in the presence of SDS and inhibitors. The concentration indicated is the final concentration in the enzyme solution.

Discussion

At the start of our research, we considered that the use of a bacterial expression system for the production of pure mushroom tyrosinase might circumvent the anticipated difficulties with obtaining pure tyrosinase directly from mushroom due to heterogeneity. Our results show that this approach is not straightforward because the

enzyme is not overexpressed as active enzyme, but as inclusion bodies, which require a refolding step to recover the active enzyme.

Nevertheless, the results from our refolding procedure suggest that properly folded protein was obtained. The elution profile from the gel filtration column showed a single band eluting at a molecular mass of ~ 64 kDa, showing that the refolded protein did not suffer from aggregation. Aggregation is the usual indication of the presence of incorrectly folded species (Clark 1998). A dynamic light scattering experiment confirmed the result of the gel filtration that there is no aggregation, and CD spectra of the refolded protein clearly indicated the presence of secondary structure. Moreover, EXAFS and XANES spectra of the refolded tyrosinase resembled that of the homologous molluscan hemocyanin, which suggests that an intact binuclear copper centre was present. Although the refolded enzyme demonstrated only low activity, the activity inhibition profile suggests that the detected activity was true tyrosinase activity, and not aspecific conversion of L-dopa.

A plausible explanation for the enzyme's low activity could be that copper was not fully or not productively incorporated during the refolding process. In this respect, it should be noted that overexpression of recombinant *Streptomyces castaneoglobisporus* tyrosinase required the co-expression of a "caddie protein" that functions to deliver copper into the active site (Matoba, Kumagai *et al.* 2006). The absence of this caddie protein in the *S. castaneoglobisporus* tyrosinase overexpression system resulted also in the formation of inclusion bodies (Kohashi, Kumagai *et al.* 2004). A defective copper-charging step could be the cause that only a small portion of the refolded enzyme became active. Indeed, when performing the X-ray absorption measurements, the beam line scientist found that the copper content in the sample was lower than expected (W. Meyer-Klaucke, personal communication). Recently, upon the expression of mature PPO3 and PPO4 in *E. coli*, soluble tyrosinases that demonstrated no enzyme activity were obtained (Wu, Chen *et al.* 2010). This finding suggests that although bacterial expression system could produce soluble tyrosinases, the active site of the enzyme could not be properly formed.

Another plausible explanation for the lack of activity could be the absence of the thioether bond between Cys79 and His81 in the refolded enzyme. This thioether bond

fixes the orientation of the His81 side chain, which is involved in the binding of copper. This feature is highly conserved among fungal tyrosinases, and occurs also in the tyrosinase homologs hemocyanin from molluscs and catechol oxidase. Although the structure of *S. castaneoglobisporus* tyrosinase suggests no clear relationship between this bond and tyrosinase activity (Decker, Schweikardt *et al.* 2007), the thioether bond may be essential for activity of mushroom tyrosinase.

Finally, the presence of sodium chloride could also be a cause for the low enzyme activity. Park *et al.* demonstrated that sodium chloride concentrations above 50 mM resulted in more than 50% enzyme inhibition and that increasing salt concentrations give a linear increase in the inhibition. Furthermore, they showed that this phenomenon also applied to potassium and ammonium chloride salts (Park, Kim et al. 2005). We have observed the same salt-induced inhibition pattern, using purified commercial mushroom tyrosinase preparations. Therefore, the salt concentration in the final reaction mixture for the enzyme activity measurements was kept below 50 mM. Nevertheless, the enzyme activity remained at maximally ~ 40 nanoKatals per milligram of protein.

Expression of recombinant proteins in bacteria often results in the accumulation of the protein product as inclusion bodies. In most cases, the formation of inclusion bodies is a consequence of the high expression rate of a protein, regardless of the system or protein used (Lilie, Schwarz *et al.* 1998). Our experiments show that manipulation of the overexpression procedure could not prevent the formation of inclusion bodies. Moreover, our refolding procedure has so far remained unsuccessful to obtain fully active enzyme. The use of another (fungal) expression system that can efficiently incorporate copper into the expressed protein, co-expression of the protein that functions in delivering the copper, or modification of the construct to make the expressed protein better soluble, could provide future routes to obtain recombinant mushroom tyrosinase as soluble and active protein.

Acknowledgements

We thank Frank Hoeberichts at Wageningen University and Research Centre, for preparing the *E. coli* M15 strain, and Prof. Rainer Rudolph, Martin Luther – Universität Halle-Wittenberg, Germany, for advice and discussion on the refolding.

We also thank Dr. Wolfram Meyer-Klaucke for the measurement and analysis of the EXAFS and XANES spectra. The work was funded by the Innovation-driven Research Program for Industrial Proteins (IIE00022) and was supported by DMV-International, DSM, Cargill, and NIVE.

Appendix

Table 1. Buffers used for the purification and refolding of recombinant mushroom tyrosinase. All buffers contain 50 mM Tris-HCl, pH 8.0. Buffers 2-9 were freshly prepared, filtered and degassed prior to use. Buffer 6 was saturated with nitrogen gas prior to use to lower the presence of molecular oxygen.

Buffer No.	GdmCl (M)	NaCl (M)	Glycerol %	Imidazole (mM)	Addition
1	0	0	0	0	-
2	0	0	0	0	2% Triton X-100
3	6	0	0	10	10 mM β-mercaptoethanol
4	6	0	0	10	-
5	6	0.25	10	0	-
6	0.25	0.25	10	0	2 mM GSH
7	0	0.25	10	0	0.1 mM CuCl
8	0	0.25	10	0	
9	0	0.25	10	250	

Chapter 3

Crystallization and preliminary X-ray crystallographic analysis of mushroom *Agaricus bisporus* tyrosinase

Wangsa T. Ismaya, Henriëtte J. Rozeboom, Marloes Schurink, Carmen G. Boeriu, Harry J. Wichers, Bauke W. Dijkstra

Published in Acta Crystallographica **F67**, 575-578

Abstract

Tyrosinase catalyzes the conversion of tyrosine into dihydroxyphenylalanine quinone, which is the main precursor for the biosynthesis of melanin. The enzyme from *Agaricus bisporus*, the common button mushroom, was purified and crystallized in two different space groups. Crystals with space group $P2_1$ (a = 104.2 Å, b = 105.0 Å, c = 119.1 Å, and $\beta = 110.6^{o}$, four molecules per asymmetric unit) diffracted to 3.0 Å resolution. Crystals with space group $P2_12_12$ (a = 104.0 Å, b = 104.5 Å, and c = 108.4 Å, two molecules per asymmetric unit) diffracted to 2.6 Å resolution. It was essential to include 5 mM $HoCl_3$ in all crystallization conditions to obtain well-diffracting crystals.

1. Introduction

Tyrosinase (E.C.1.14.18.1) is a copper-containing monooxygenase that is widely distributed in nature, occurring in organisms from all phyla. It catalyzes the *o*-hydroxylation of monophenols (monophenolase activity) and the subsequent oxidation of the formed *o*-diphenols to the corresponding *o*-quinones (diphenolase activity) (van Gelder, Flurkey *et al.* 1997), which are precursors for the biosynthesis of melanins. The precise physiological function of the enzyme is not well understood. In mammals, including humans, the enzyme is mainly found in melanocytes, which are pigment-producing cells. The mammalian enzyme has been implicated in pigmentary diseases such as albinism, vitiligo, and other melanin-related syndromes (Cesarini 1996).

In *Agaricus bisporus* mushroom, tyrosinase has been proposed to be involved in defense mechanisms against pathogens, because of the bacteriostatic properties of *o*-quinones and melanins, and because of the inducibility of at least one tyrosinase isoform upon microbial challenge (Soler-Rivas, Jolivet *et al.* 1999). The enzyme is also an important factor for the browning of the mushroom upon aging and microbial infection (Soler-Rivas, Jolivet *et al.* 1999), and consequently there is substantial interest in its catalytic properties (Sanchez-Ferrer, Rodriguez-Lopez *et al.* 1995; Espin, Varon *et al.* 2000; Fenoll, Rodriguez-Lopez *et al.* 2002) and its inhibition (Kubo, Kinst-Hori *et al.* 2000; Ley and Bertram 2001; Zhang, Chen *et al.* 2006).

So far, four genes coding for *A. bisporus* tyrosinase have been described. These genes, *Abppo1* (UniProt protein sequence data base entry Q00024) and *Abppo2* (O42713) (Wichers, Recourt *et al.* 2003), and *Abppo3* (C7FF04) and *Abppo4* (C7FF05) (Wu, Chen *et al.* 2010), code for proteins with a molecular mass of 64 – 67 kDa. However, isolation of the enzyme directly from mushroom fruit bodies, yields a heterotetramer composed of two subunits of 43 - 48 kDa (H chain) and two subunits of 13 – 14 kDa (L chain) (H_2L_2 configuration) (Strothkamp, Jolley *et al.* 1976). This information led to the hypothesis that tyrosinase is initially formed as a monomeric 64 kDa latent precursor, which can be proteolytically activated, resulting in ~43 kDa active forms (Espin, Soler-Rivas *et al.* 2000). The nature of the L chain is not known. Although the L chain may represent the C-terminal fragment resulting from the proteolytic cleavage of the latent precursor, it may also be an unrelated protein that is

co-purified with active tyrosinase and that is difficult to remove (Flurkey and Inlow 2008).

X-ray absorption studies have indicated that *A. bisporus* tyrosinase contains two copper ions in its active site with spectroscopic properties resembling those of the two copper ions found in molluscan hemocyanin, a copper-containing oxygen carrier protein (Della-Longa, Ascone *et al.* 1996). The presence of two copper ions in tyrosinase was also shown in the crystal structure of the *Streptomyces castaneoglobisporus* tyrosinase (Matoba, Kumagai *et al.* 2006), with each of the two copper ions coordinated by three histidine side chains. However, in *A. bisporus* tyrosinase, the side chain of one of these copper-coordinating histidine residues is covalently linked *via* a thioether bond to the side chain of the preceding cysteine residue in the C-x-H sequence motif (van Gelder, Flurkey *et al.* 1997). The role of this thioether bond is still elusive. Here, we report the purification and crystallization of commercially available mushroom tyrosinase and the preliminary X-ray diffraction data analysis as an initial step toward the elucidation of the 3D-structure of the enzyme.

2. Material and Methods

2.1. Sample preparation

Mushroom tyrosinase powder was purchased from Sigma (Sigma-Aldrich, T3824-250KU) and was purified at 277 K essentially as previously described (Schurink, van Berkel *et al.* 2007). The mushroom powder was dissolved in 50 mM sodium phosphate buffer, pH 6.5, to a concentration of 10 $mg.ml^{-1}$ ($w.v^{-1}$). The insoluble material was removed by centrifugation at 277 K, 12,000 *g* for 15 minutes. The supernatant was carefully recovered and was loaded onto a 10/30 Superdex S-200 column (Amersham Biosciences) equilibrated with 100 mM HEPES buffer, pH 7.5, containing 10 mM calcium chloride. Elution from the gel filtration column was carried out with the same buffer, with a constant flow rate of 0.25 $ml.min^{-1}$. Fractions with tyrosinase activity were pooled and concentrated with a concomitant buffer exchange to 10 mM HEPES, pH 7.5, over a 10 kDa cut-off Amicon membrane (Millipore) to a final protein concentration of approximately 6 $mg.ml^{-1}$. The

concentrated protein was either directly subjected to crystallization experiments or was frozen at 253 K for storage.

2.2. Determination of protein concentration and enzyme activity

The protein concentration was estimated from the absorption at 280 nm using the experimentally determined ε value of 132,000 $M^{-1}.cm^{-1}$. Absorbance measurements were done with a Nanodrop ND-1000 spectrometer (Nanodrop Technologies Inc., Wilmington USA).

Enzyme activity was measured at 298 K by a colorimetric method essentially as previously described (Espin, Morales *et al.* 1997) using 3,4-dihydroxyphenylalanine (L-dopa) as substrate. One unit of tyrosinase activity is defined as the formation of one μmol L-dopaquinone per minute. Briefly, in a 1 ml cuvette, 100 μl of a 5 mM 3-methyl-2-benzothiazolinone hydrazone (MBTH) solution in water was mixed with 800 μl of L-dopa solution (18 mM in 50 mM sodium phosphate buffer, pH 6.5). The reaction was started with the addition of 100 μl enzyme solution to the reaction mixture. The increase in the absorbance at 484 nm was followed during the first three minutes. The measurements were carried out in an Ultrospec 4300 Pro spectrometer equipped with a temperature control unit (Amersham Biosciences), on-line interfaced to a computer. The spectra were recorded and processed with the time-drive measurement module (SWIFT II program, version 2.01, Amersham Biosciences).

2.3. Characterization of protein samples

The purity of the enzyme was routinely checked with sodium dodecyl sulphate polyacrylamide gel electrophoresis (SDS-PAGE), using a PhastGel System (Amersham Biosciences) with pre-cast SDS gels and electrode strips. The staining was conducted in the same system using silver nitrate as the staining solution.

The temperature stability of the protein in solution was analyzed by the thermal-shift assay (Ericsson, Hallberg *et al.* 2006). Briefly, in a 96-well thin-wall PCR plate (BioRad), 5 μl of 200 times diluted Sypro-orange solution (Invitrogen, Breda, The Netherlands) as molecular probe, 5 μl of 4.5 $mg.ml^{-1}$ enzyme solution in water, 2.5 μl of 1 M buffer stock solution, and 2.5 - 5 μl of additive stock solution were mixed.

The final reaction volume was adjusted to 25 μl by adding an appropriate volume of filtered and degassed milli-Q water. The plate was sealed with optical quality sealing tape (BioRad Laboratories B.V., Veenendaal, The Netherlands). The sealed plate was inserted into a real-time PCR machine (iCycler, BioRad Laboratories B.V., Veenendaal, The Netherlands) and was heated from 293 to 363 K with a 0.5 K increment per 20 seconds. The changes in fluorescence of the Sypro-orange probe were monitored with a fluorescence detector (MyIQ^{TM} single color RT-PCR detection system, BioRad) at excitation and emission wavelengths of 490 and 575 nm, respectively.

The monodispersity of the enzyme was analyzed by dynamic light scattering, using a Dynapro Dynamic Light Scattering instrument (Wyatt Technologies, Santa Barbara, U.S.A.). The protein sample (1 mg.ml^{-1}) was centrifuged at 12,000 *g* for 15 minutes at 277 K, and the supernatant was carefully transferred to a DLS cuvette. Measurements were performed at both 298 K and 277 K.

2.4. Crystallization procedures

The initial screening for crystallization conditions was carried out at 298 K with the sitting drop vapor diffusion method, employing an Oryx-6 crystallization robot (Douglas Instruments, Hungerford, U.K.), equipped with an anti-evaporation shielding plate. The following commercial screens were used in 96-wells CrystalClear strips for sitting drop set ups (Hampton Research): Structure Screens I and II (Molecular Dimensions, Apopka, U.S.A.), Cryoscreens I and II (Emerald Biosystems, Bainbridge Island, U.S.A.), and the JCSG+ Suite (Qiagen, Venlo, the Netherlands). The starting volume of the drop was 0.3 μl consisting of 0.12 μl protein solution and 0.18 μl reservoir solution. Optimization of promising crystallization conditions was done with the hanging drop vapor diffusion method, varying the precipitant type and concentration, the temperature, pH, and additives.

2.5. Data collection and processing

Prior to the X-ray diffraction analysis, crystals were transferred to a cryo-protectant solution containing 15% PEG 4000, 20% PEG 400, 1 mM $HoCl_3$, and 100 mM sodium acetate buffer, pH 4.6, before flash-freezing in liquid nitrogen. X-ray

diffraction experiments were carried out at beam lines BM16, ID23-2, and ID14-4 at the ESRF (Grenoble, France). Diffraction data were recorded at 100 K with a CCD detector available at the beam line, with 0.5^{o}-1.0^{o} oscillations. The data sets were processed using either the program *XDS* (Kabsch 1993) or *MOSFLM* (Leslie 2006). Scaling and merging was done with the program *SCALA* (Evans 2006), which is part of the *CCP*4 program suite (Collaborative Computational Project Number 4 1994).

3. Results and Discussion

Commercially available mushroom tyrosinase was successfully purified using a single gel filtration step. In the elution profile, the tyrosinase activity was detected in a peak with a retention time corresponding to a molecular mass of ~120 kDa, as expected for the mass of the H_2L_2 form of mushroom tyrosinase (Strothkamp, Jolley *et al.* 1976). Further, an SDS PAGE analysis of this peak confirmed the presence of the heavy (H) and light (L) chains, with molecular masses of 45 and 14 kDa, respectively, in agreement with previous reports (Schurink, van Berkel *et al.* 2007). Analysis of the protein content and specific activity indicated that approximately 50% of the total protein in the mushroom powder consisted of tyrosinase. The purification scheme recovered up to 90% of the enzyme activity.

The thermostability of tyrosinase was investigated by following the unfolding of the protein as a function of temperature under various conditions (Ericsson, Hallberg *et al.* 2006). The shift in the melting temperature (T_m) of the protein to higher values indicates an increase in thermostability. Figure 1a shows that the enzyme demonstrated the highest T_m value in 100 mM HEPES buffer, pH 7.5, 10 mM $CaCl_2$. In the absence of calcium or when the calcium was replaced by sodium the T_m value shifted to lower temperatures. Based on this observation, 100 mM HEPES buffer, pH 7.5, with 10 mM $CaCl_2$, was chosen for the purification.

To assess the aggregation behaviour of tyrosinase, a dynamic light scattering experiment was done. The regularization fit on mass showed one main peak with a mean R_H of 4.4 nm and 6% polydispersity, indicating a monodisperse solution at 298 K (Figure 1b). The calculated mass of this peak was 110 kDa, in agreement with size exclusion chromatography, and confirming the presence of a H_2L_2 tetramer in solution (Strothkamp, Jolley *et al.* 1976). Although some noise was observed owing

to protein aggregation, it resulted from less than 0.1% of the mass in the sample. Because at 277 K the monodispersity of the enzyme solution was reduced (data not shown), the subsequent crystallization experiments were carried out at 298 K.

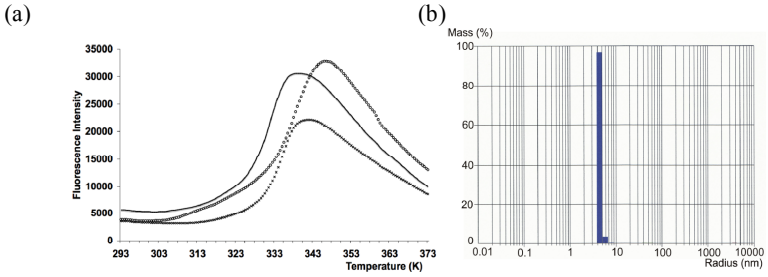

Figure 1. Stability and monodispersity of tyrosinase in solution. (a) Thermal unfolding of tyrosinase in 100 mM HEPES buffer, pH 7.5 (black line), in 100 mM HEPES buffer with additional 10 mM calcium chloride (○), or in 100 mM HEPES buffer with additional 10 mM sodium chloride (×). (b) Monodispersity of tyrosinase in 100 mM HEPES buffer, pH 7.5, containing 10 mM $CaCl_2$ at 298 K.

The first crystals were obtained with the JCSG+ screen after 48 hours at 298 K, using a reservoir solution composed of 8% PEG 4000 in 100 mM sodium acetate buffer, pH 4.6. However, these crystals diffracted to ~8 Å resolution only (BM16, ESRF, Grenoble). Optimization using the hanging-drop vapor diffusion method, followed by an extensive additive screen, revealed that 5 mM $HoCl_3$ improved the diffraction quality of the crystals. After this discovery, plate-shaped crystals suitable for X-ray data collection (Figure 2) were routinely obtained from drops of 2 µl protein solution (~6 $mg.ml^{-1}$) and 2 µl reservoir solution, which were suspended over 800 µl reservoir solution containing 10% PEG 4000 ($w.v^{-1}$), 100 mM sodium acetate buffer, pH 4.6, and 5 mM $HoCl_3$. Crystals with reasonable size (200 x 200 x 50 µm) could be obtained within 4-5 days. They diffracted to 2.6 Å resolution using synchrotron radiation (ESRF, Grenoble). Finally, it appeared necessary to include 1 mM $HoCl_3$ in the cryo-protectant solution for reproducible diffraction by the crystals.

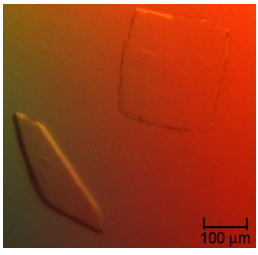

Figure 2. Plate-shaped crystals of mushroom tyrosinase.

The obtained crystals were analyzed by X-ray diffraction (Table 1). They belong to either space group $P2_1$ or

space group $P2_12_12$. Crystals with space group $P2_1$ had cell dimensions of a = 104.2 Å, b = 105.0 Å, c = 119.1 Å, and β = 110.6°, and diffracted to 3.0 Å resolution. Crystals with space group $P2_12_12$ had cell dimensions of a = 104.0 Å, b = 104.5 Å, and c = 108.4 Å, and diffracted to 2.6 Å resolution. Assuming the presence of four 60 kDa HL heterodimers per asymmetric unit in the $P2_1$ crystals, and two HL heterodimers per asymmetric unit in the $P2_12_12$ crystals, gave similar values for the Matthews coefficient and solvent content of ~2.4 $Å^3.Da^{-1}$ and 49 %, respectively. Data collection statistics are summarized in Table 1.

An SDS-PAGE analysis of a tyrosinase crystal showed the presence of both the 45 and 14 kDa polypeptides, indicating that both the H and L chains are present in the crystal. Furthermore, an X-ray fluorescence scan of a tyrosinase crystal grown in the absence of $HoCl_3$ showed the presence of copper in the protein crystal (Figure 3).

Finally, significant tyrosinase activity was observed after dissolving a crystal that had been exposed to X-rays. Since the activity of the enzyme relies on the presence of the copper in the active site, this result did not only confirm the presence of copper, but it also indicates that the copper is still functional. Thus, we have crystallized active mushroom tyrosinase. Currently, we are trying to solve the structure of the enzyme by molecular replacement with multiple crystal averaging, using the structures of the core domain of *Octopus dofleini* hemocyanin (PDB entry 1js8) (Cuff, Miller *et al.* 1998) and *S. castaneoglobisporus* tyrosinase (PDB entry 1wx2) (Matoba, Kumagai *et al.* 2006), which have sequence identities of 19% and 20% for 274 and 275 aligned amino acids, respectively, as search models.

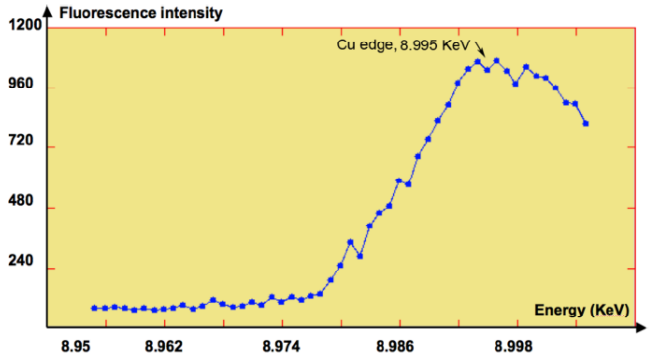

Figure 3. Energy scan of a tyrosinase crystal. The peak occurs at an energy of ~8995 eV, which is specific for copper in tyrosinase (Della Longa, Ascone et al. 1996).

Acknowledgements

We thank the beam line scientists at BM16, ID23-2, and ID14-4 (ESRF, Grenoble, France) for their support during data collection. This work was funded by the Innovation-driven Research Program for Industrial Proteins (project number IIE00022). Data collection at the ESRF was supported by the ESRF and by the European Molecular Biology Laboratory (EMBL) under the European Community's Seventh Framework Program (FP7/2007-2013, grant agreement No. 226716).

Appendix

Table 1. Summary of crystallographic data collection and processing.

	Native $P2_1$	Native $P2_12_12$
Beam line	ESRF ID23-2	ESRF ID14-4
Wavelength (in Å)	0.8726	0.9395
Resolution (in Å)	50.0 – 3.0	54.2 – 2.60
Cell parameters		
a (in Å)	104.2	104.0
b (in Å)	105.0	104.5
c (in Å)	119.1	108.4
β (°)	110.6	90
R_{merge} [§]	0.16 (0.34)	0.12 (0.45)
R_{pim} [#]	0.11 (0.24)	0.07 (0.28)
Mean I/σI	7.3 (2.3)	8.2 (2.3)
Completeness (%)	88.9 (90.5)	94.8 (81.8)
Multiplicity	2.8 (2.9)	4.0 (2.7)

[§]$R_{merge} = \sum_{hkl}\sum_i|I_i(hkl) - \langle I(hkl)\rangle| / \sum_{hkl}\sum_i(hkl)$ and the [#]$R_{pim} = \sum_{hkl}[1/(N-1)]^{1/2}\sum_i|I_i(hkl) - \langle I(hkl)\rangle| / \sum_{hkl}\sum_i(hkl)$, where $I_i(hkl)$ is the integrated intensity of a reflection, $\langle I(hkl)\rangle$ is the mean intensity of multiple corresponding symmetry-related reflections, and N is the multiplicity of the given reflections. (Values in parentheses are for the highest resolution shell).

Chapter 4

Crystal structure of *Agaricus bisporus* mushroom tyrosinase – Identity of the tetramer subunits and interaction with tropolone

Wangsa T. Ismaya, Henriëtte J. Rozeboom, Amrah Weijn, Jurriaan J. Mes, Fabrizia Fusetti, Harry J. Wichers, Bauke W. Dijkstra

Submitted to Biochemistry

Abstract

Tyrosinase catalyzes the conversion of phenolic compounds into their quinone derivatives, which are precursors for the formation of melanin, a ubiquitous pigment in living organisms. Because of its importance for browning reactions in the food industry, the tetrameric tyrosinase from the mushroom *Agaricus bisporus* has been investigated in depth, but the identity of its subunits and the molecular basis of its activity have remained unknown. Its 2.3 Å resolution crystal structure presented here is the first structure of a fungal tyrosinase. The enzyme possesses two H subunits of about 400 residues originating from the *ppo3* gene, which have a fold similar to other tyrosinases, and two L subunits of about 150 residues, which are the product of *orf239342* and have a lectin-like fold. The tyrosinase subunit contains a binuclear copper-binding site in the *deoxy*-state, in which three histidine residues coordinate each copper ion. The side chains of these histidines have their orientation fixed by hydrogen bonds or, in the case of His85, a thioether bridge with the side chain of Cys83. The specific tyrosinase inhibitor tropolone forms a pre-Michaelis complex with the enzyme. It binds near the binuclear copper site without directly coordinating the copper ions. The function of the ORF239342 subunits is not clear. Carbohydrate binding sites identified in other lectins are not conserved in ORF239342, and the subunits are over 25 Å away from the active site, making a role in activity unlikely. The structures explain how calcium ions stabilize the tetrameric state of the enzyme.

Introduction

Tyrosinase (EC 1.14.18.1) is a binuclear copper-containing enzyme that catalyzes the conversion of a monophenol (tyrosine) and/or *o*-diphenol (L-dopa) into its corresponding *o*-quinone derivative (L-dopaquinone), which is further converted into melanin. Melanin is a pigment that is ubiquitously present in living organisms from all phyla. Since tyrosinase is the key enzyme in the first step of melanin biosynthesis, the enzyme is frequently associated with pigmentation (Sanchez-Ferrer, Rodriguez-Lopez *et al.* 1995).

So far, four tyrosinase genes of the common button mushroom, *Agaricus bisporus*, have been described. Wichers and coworkers have found two genes that encode two 64 kDa tyrosinases, *ppo1* (Genebank accession number X85113) and *ppo2* (AJ223816) (Wichers, Recourt *et al.* 2003). Recently, two other genes encoding a 66 kDa and a 68 kDa tyrosinase were reported, *ppo3* (GQ354801) and *ppo4* (GQ354802), respectively (Wu, Chen *et al.* 2010).

The enzyme is commonly found as a tetrameric protein with a molecular mass of 120 kDa, composed of two subunits of ~43 kDa (H subunit) and two subunits of ~14 kDa (L subunit) (Strothkamp, Jolley *et al.* 1976). The discovery of an active monomeric 43-kDa tyrosinase isolated from mushroom fruit bodies (Wichers, Gerritsen *et al.* 1996) suggests that the H subunit is tyrosinase. The identity, function and origin of the L subunit are as yet unknown (Schurink, van Berkel *et al.* 2007; Flurkey and Inlow 2008).

Insight into the structure of the mushroom tyrosinases is, so far, based on the structures of a plant catechol oxidase from *Ipomoea batatas* (*Ib*COX) (Klabunde, Eicken *et al.* 1998) and a bacterial tyrosinase from *Streptomyces castaneoglobisporus* (*Sc*TYR) (Matoba, Kumagai *et al.* 2006), which have 17-21% sequence identity to ~380 N-terminal residues of the *A. bisporus* tyrosinases. Structures of *Ib*COX showed the various oxidation states of the two copper ions in the active site and the binding mode of the inhibitor phenylthiourea. The *Sc*TYR structure also provided information on the various oxidation states of the copper ions. Although the two structures show a strong structural similarity of tyrosinase and catechol oxidase, the mechanism of the reaction is still under dispute because of disagreement on the substrate-binding mode (Decker, Schweikardt *et al.* 2006).

A highly conserved Cys-X-His sequence motif is present in the mushroom tyrosinases (van Gelder, Flurkey *et al.* 1997). In the fungal *Neurospora crassa* tyrosinase the cysteine and histidine side chains of this motif are connected by a covalent thioether bond (Lerch and Ettlinger 1972), with the histidine residue also functioning as one of the Cu-A coordinating ligands. Interestingly, this thioether bond is also conserved in mollusc hemocyanin and, with a different sequence motif, in catechol oxidase (Decker, Schweikardt *et al.* 2006), which may indicate its importance. However, the thioether bond is absent in the bacterial tyrosinase (Matoba, Kumagai *et al.* 2006), and therefore its function remains unclear.

In the present study, we have successfully crystallized a commercially available tyrosinase from *A. bisporus* (*Ab*TYR) and elucidated the structure by means of X-ray crystallography. The structure allowed us to establishing the identity of the two different subunits in the tetramer, and explaining the role of calcium in the tetramerization. A structure of the enzyme with the bound inhibitor tropolone shows that this inhibitor forms a pre-Michaelis complex with *deoxy*-tyrosinase. These structures are of particular interest because commercial mushroom tyrosinase has been employed extensively in various studies for agricultural, industrial, pharmaceutical and medical purposes.

Experimental procedures

Protein purification, crystallization and X-ray data collection

A. bisporus tyrosinase, *Ab*TYR, was purchased from Sigma-Aldrich (St. Louis MO, USA). Purification and crystallization of the enzyme were done as described elsewhere (Ismaya, Rozeboom *et al.* 2011). Briefly, tyrosinase crystals were obtained at room temperature using the hanging-drop vapor diffusion technique with drops made of a 1:1 mixture of protein solution (~6 mg/ml) in 10 mM HEPES buffer, pH 7.5, and reservoir solution, containing 10% (*w/v*) PEG4000 in 100 mM sodium acetate buffer, pH 4.6, with 5 mM holmium chloride as additive. After 4-5 days two different crystal forms appeared in the drops, belonging to space groups $P2_12_12$ or $P2_1$. Diffraction data were collected at the European Synchrotron Radiation Facility (ESRF) in Grenoble, France, and processed with the programs *XDS* (Kabsch 1993) or *MOSFLM* (Leslie 2006) (For details, see Table 1). Scaling and merging of the data

sets processed with MOSFLM was done with the program *SCALA* (Evans 2006) using the *CCP4* interface (Collaborative Computational Project Number 4 1994). The Matthews coefficient, V_M (Matthews 1968) and self rotation maps from the program *MOLREP* (Vagin and Teplyakov 1997) suggested that the crystals contained one ($P2_12_12$) or two ($P2_1$) H_2L_2 tetramers of 120 kDa per asymmetric unit. For substrate binding studies diffraction data were collected from a crystal belonging to space group $P2_1$, which had been soaked in reservoir solution containing 5 mM of the inhibitor tropolone (2-hydroxy-2,4,6-cycloheptatrien-1-one) (Table 1).

Peptide mass fingerprinting

A tyrosinase crystal was dissolved in water and subjected to SDS-PAGE analysis. After staining with Coomassie Brilliant Blue R25, the bands corresponding to the H and L subunits were excised from the gel. After destaining the gel pieces, the proteins were digested with trypsin and identified by tandem mass spectrometry searching against the UniProtKB/Swiss-Prot protein sequence database (The UniProt Consortium 2007). For a detailed description of the procedure see (Saller, Fusetti *et al.* 2009).

Rapid amplification of cDNA ends (RACE)

RNA was isolated from 40 mg grinded epidermis tissue of *A. bisporus* (strain Les Miz 36) according to the protocol of total RNA purification from filamentous fungi from Qiagen. DNase treatment of the purified RNA was performed on column with the RNase free DNase set of Qiagen according to the manufacturer's instructions. cDNA synthesis was performed using random primers and SuperScript III RT according to the manufacturer's instructions. The 3' and 5' RACE analysis was performed according to the manufacturer's protocol of the GeneRacer kit (Invitrogen) with slight modifications. The GeneRacer 3' nested primer CGCTACGTAACGGCATGACAGTG and forward L-subunit specific primer GAGGCAACACAGTCCTTGGT were used for the 3' RACE. For the 5' RACE the GeneRacer 5' primer CGACTGGAGCACGAGGACACTGA and reversed L-subunit primer AGTCCAGACAGCACCTCCAC were used. The amplified fragments were separated by 2% agarose gel elecrophoresis and the fragment with the desired length

was extracted from the gel and purified with the QIAquick gel extraction kit from Qiagen according to protocol. The purified PCR product was cloned into the pCR4-TOPO vector according to the protocol of Invitrogen. Transformation into the competent TOP10 *Escherichia coli* cells was done according to the one shot TOP10 chemically competent *E. coli* protocol from Invitrogen, followed by DNA sequencing of 10 individual clones.

Starting model and phasing by molecular replacement

On the basis of previous mass spectrometry studies (Schurink, van Berkel *et al.* 2007) the PPO2 sequence was selected to search the Protein Data Bank (PDB) for homologous structures, using the FFAS03 server (Jaroszewski, Rychlewski *et al.* 2005). Four structures were obtained, with highest identity to the N-terminal part of *A. bisporus* PPO2 ((Wichers, Recourt *et al.* 2003), putative H subunit, ~43 kDa), *i.e. Octopus dofleini* hemocyanin (PDB code 1js8, 17% sequence identity (Cuff, Miller *et al.* 1998)), *Rapana thaliana* hemocyanin (PDB code 1lnl, 17% sequence identity (Perbandt, Guthöhrlein *et al.* 2003)), *I. batata* catechol oxidase (PDB code 1bt1, 17% sequence identity (Klabunde, Eicken *et al.* 1998)), and *S. castaneoglobisporus* tyrosinase (PDB code 1wx2, 21% sequence identity (Matoba, Kumagai *et al.* 2006)). No homology model could be obtained for the C-terminal part of PPO2 (putative L subunit, ~14 kDa), because of lack of sequence homology. Using these four structures as templates, homology models were generated with the SCWRL server (Canutescu, Shelenkov *et al.* 2003). Molecular replacement was performed with the program *PHASER* (McCoy, Grosse-Kunstleve et al. 2005) at 2.6 Å resolution using an ensemble of the four H-subunit homology models, which resulted in a solution with two H-subunit molecules in the $P2_12_12$ asymmetric unit, consistent with the V_M and self-rotation map.

Model building

The molecular replacement solution was subjected to the automatic model-building program *RESOLVE* (Terwilliger 2003), with non-crystallographic symmetry (NCS) restraints applied. The resulting model covered 580 residues of the two H subunits in the asymmetric unit, with only 180 side chains assigned. It was manually rebuilt with

the program *COOT* (Emsley, Lohkamp et al. 2010) against a 2.6 Å NCS-averaged composite omit map, refined with the program *REFMAC5* (Murshudov, Vagin et al. 1997), further improved against a new NCS-averaged omit map and resubmitted to *RESOLVE*. This procedure was iterated until the model did not further improve. Visual inspection of the electron density map obtained from each iterative cycle was used to monitor the progress in the model building. Regularly, the model was transferred to space group $P2_1$ (3.0 Å resolution) to exploit the averaging power of four molecules in the asymmetric unit to extend the main chain of the working model. Moreover, this approach also reduced model bias because of the independency of the data sets. The extended model was then transferred back to space group $P2_12_12$ to continue the iterative model building and refinement procedure. Nevertheless, the refinement stalled at an R_{factor} of 42% and only an incomplete model was obtained. Next, when a new data set with higher completeness and resolution (2.3 Å) became available, the program *ARP/warp* (Lamzin, Perrakis et al. 2001) was used to extend the model, also using NCS restraints. Various substitutions and insertions in the H subunit had to be introduced, which were in full agreement with the recently published *A. bisporus* PPO3 sequence (Wu, Chen *et al.* 2010). Consequently, the model building of the H subunit was completed using the PPO3 sequence.

The electron density for the L subunit generated by *ARP/wARP* was not compatible with the amino acid sequence of the C-terminal part of PPO2, or with that of PPO3. Therefore, all residues were set to alanines, and when interpretable side chain density became visible by model building and refinement, changed to amino acids corresponding to the electron density. A BLAST search (Altschul, Gish *et al.* 1990) with the partial amino acid sequence derived from the electron density maps against public sequence databases did not reveal any homologous proteins. However, comparison of this amino acid sequence with sequences derived from open reading frames in the *A. bisporus* genome database gave one clear hit, which allowed completing the model building of the L subunit. The complete genome sequence of *A. bisporus* is still in preparation, and the sequence of the L subunit was kindly provided by the *A. bisporus* genome consortium (Dr. M. Challen, personal communication).

Refinement with *REFMAC* including TLS optimization (Winn, Isupov *et al.* 2001) finalized the model building, converging to a conventional R_{factor} of 18.1% and an R_{free} of 23.7% (space group $P2_12_12$), and 23.6% and 28.9% (space group $P2_1$) (Table 2). The models were validated with the program MolProbity (Lovell, Davis *et al.* 2003). A Ramachandran analysis of the HL protomer in space group $P2_12_12$ showed no outliers, with 509 and 14 residues being in the favored and allowed regions, respectively. All ligands, cations, and inhibitor molecules were added after inspection of *Fo – Fc* difference Fourier maps. A dictionary for the inhibitor tropolone was generated with the PRODRG server (Schüttelkopf and van Aalten 2004) and bond lengths and angles were obtained from the crystal structure of tropolone (Shimanouchi and Sasada 1973).

The atomic coordinates and structure factors have been deposited with the PDB with accession codes 2y9w and 2y9x for native and tropolone-bound *A. bisporus* tyrosinase, respectively. The sequence alignment and the structure figures presented in this article were prepared using the programs *ALINE* (Bond and Schüttelkopf 2009) and PyMol (DeLano 2008), respectively.

Results and discussion

Identity of the crystallized protein material

The *A. bisporus* tyrosinase crystals contain both the H and L subunits. Using an ensemble of four structures with sequence homology to PPO2 gave a molecular replacement solution for the H subunit (see Experimental Procedures). However, at various positions the PPO2 sequence did not match the electron density, and insertions and substitutions had to be introduced. In contrast, the recently reported PPO3 sequence (53.6% identity to PPO2 in the 392 N-terminal residues (Wu, Chen *et al.* 2010) fitted the electron density without the need for insertions and deletions. A tandem mass spectrometry analysis of the H subunit isolated from a dissolved crystal confirmed its identity as PPO3 (94% coverage, data not shown). Therefore, the model building of the H subunit was completed with the PPO3 sequence, and henceforth the enzyme will be referred to as PPO3 (Fig. 1a).

The identity of the L subunit has so far remained unknown (Schurink, van Berkel *et al.* 2007; Flurkey, Cooksey *et al.* 2008; Flurkey and Inlow 2008). It was obvious that

the electron density maps did not correspond to any of the C-terminal PPO sequences or the sequences of an *A. bisporus* lectin or putative mannanase suggested previously (Schurink, van Berkel *et al.* 2007; Flurkey, Cooksey *et al.* 2008; Flurkey and Inlow 2008). While a BLAST (Altschul, Gish *et al.* 1990) search with a partial amino acid sequence of the L subunit derived from the electron density maps against public sequence databases did not reveal any homologous proteins, a BLAST search in the very recently generated *A. bisporus* genome sequence (Schurink, van Berkel *et al.* 2007) resulted in the identification of a single ORF (protein ID 239342), which contained a previously identified sequence from the L subunit (ATNSGTLIIFDQ; (Schurink, van Berkel *et al.* 2007)). 3' and 5' RACE, cloning and sequence analysis using white button mushroom cap tissue yielded four almost identical full sequences, very likely allelic variations of the same gene. The mature L subunit comprised 150 amino acids (~16.5 kDa; Fig. 1b), which showed no significant sequence identity to other proteins. With this sequence the model building of the L subunit was completed. To further confirm the amino acid sequence of the L subunit, protein crystals were dissolved, subjected to SDS-PAGE analysis, and analyzed by tandem mass spectrometry against the *A. bisporus* genome sequence. This analysis confirmed the identity of the crystallized L subunit as the product of *orf239342* (83% coverage; data not shown).

Figure 1 (overleaf). (a) Amino acid sequence alignment of the translated N-terminal sequences of mushroom genes *ppo1*, *ppo2*, *ppo3*, and *ppo4* (up to PPO3 residue 392). The circles indicate the copper-coordinating histidine residues, and the stars show Arg20, Cys83, and the Tyr/Phe-X-Tyr and Tyr-Gly motifs discussed in the text. (b) Amino acid sequence of the L subunit. The stars indicate the residues previously identified as belonging to the L subunit (Schurink, van Berkel *et al.* 2007). The dashes indicate residues not visible in the electron density. The secondary structure assignments are based on the *Ab*TYR structure.

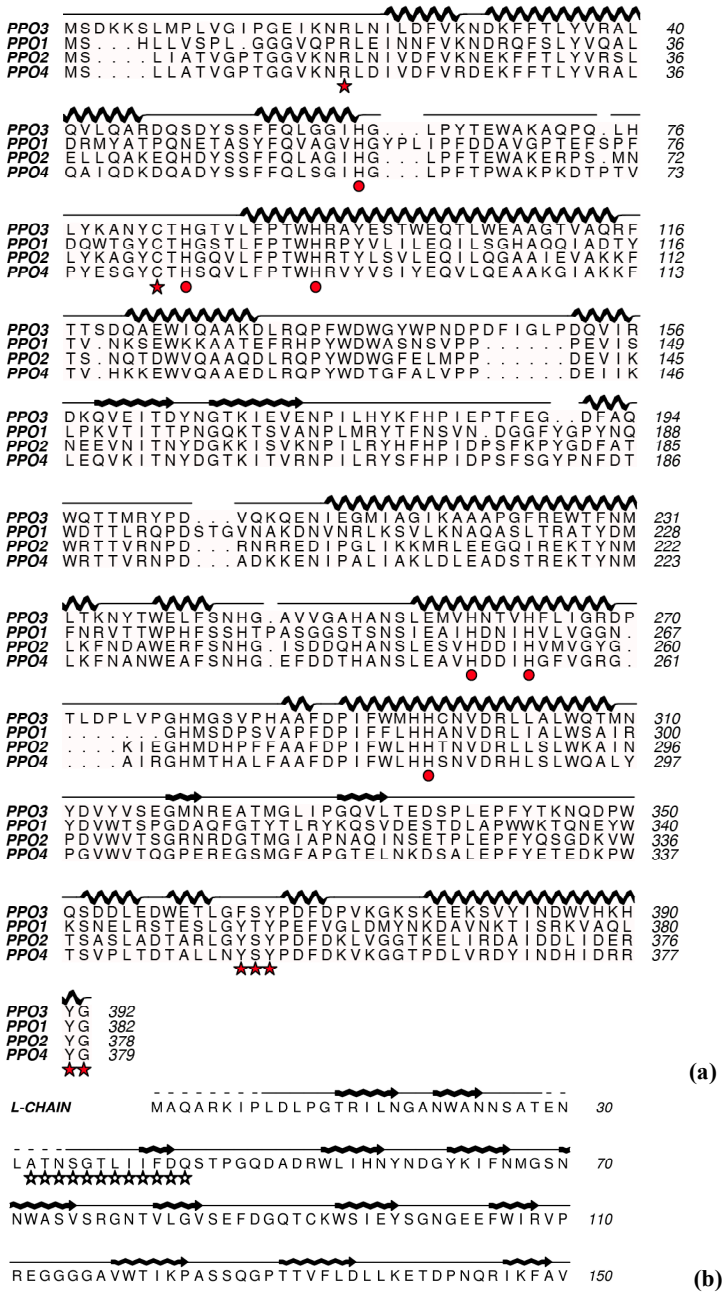
PPO3 MSDKKSLMPLVGIPGEIKNRLNILDFVKNDKFFTLYVRAL 40
PPO1 MS...HLLVSPL.GGGVQPRLEINNFVKNDRQFSLYVQAL 36
PPO2 MS....LIATVGPTGGVKNRLNIVDFVKNEKFFTLYVRSL 36
PPO4 MS....LLATVGPTGGVKNRLDIVDFVRDEKFFTLYVRAL 36
PPO3 QVLQARDQSDYSSFFQLGGIHG...LPYTEWAKAQPQ.LH 76
PPO1 DRMYATPQNETASYFQVAGVHGYPLIPFDDAVGPTEFSPF 76
PPO2 ELLQAKEQHDYSSFFQLAGIHG...LPFTEWAKERPS.MN 72
PPO4 QAIQDKDQADYSSFFQLSGIHG...LPFTPWAKPKDTPTV 73
PPO3 LYKANYCTHGTVLFPTWHRAYESTWEQTLWEAAGTVAQRF 116
PPO1 DQWTGYCTHGSTLFPTWHRPYVLILEQILSGHAQQIADTY 116
PPO2 LYKAGYCTHGQVLFPTWHRTYLSVLEQILQGAAIEVAKKF 112
PPO4 PYESGYCTHSQVLFPTWHRVYVSIYEQVLQEAAKGIAKKF 113
PPO3 TTSDQAEWIQAAKDLRQPFWDWGYWPNDPDFIGLPDQVIR 156
PPO1 TV.NKSEWKKAATEFRHPYWDWASNSVPP.....PEVIS 149
PPO2 TS.NQTDWVQAAQDLRQPYWDWGFELMPP.....DEVIK 145
PPO4 TV.HKKEWVQAAEDLRQPYWDTGFALVPP.....DEIIK 146
PPO3 DKQVEITDYNGTKIEVENPILHYKFHPIEPTFEG..DFAQ 194
PPO1 LPKVTITTPNGQKTSVANPLMRYTFNSVN.DGGFYGPYNQ 188
PPO2 NEEVNITNYDGKKISVKNPILRYHFHPIDPSFKPYGDFAT 185
PPO4 LEQVKITNYDGTKITVRNPILRYSFHPIDPSFSGYPNFDT 186
PPO3 WQTTMRYPD...VQKQENIEGMIAGIKAAAPGFREWTFNM 231
PPO1 WDTTLRQPDSTGVNAKDNVNRLKSVLKNAQASLTRATYDM 228
PPO2 WRTTVRNPD...RNRREDIPGLIKKMRLEEGQIREKTYNM 222
PPO4 WRTTVRNPD...ADKKENIPALIAKLDLEADSTREKTYNM 223
PPO3 LTKNYTWELFSNHG.AVVGAHANSLEMVHNTVHFLIGRDP 270
PPO1 FNRVTTWPHFSSHTPASGGSTSNSIEAIHDNIHVLVGGN. 267
PPO2 LKFNDAWERFSNHG.ISDDQHANSLESVHDDIHVMVGYG. 260
PPO4 LKFNANWEAFSNHG.EFDDTHANSLEAVHDDIHGFVGRG. 261
PPO3 TLDPLVPGHMGSVPHAAFDPIFWMHHCNVDRLLALWQTMN 310
PPO1 .....GHMSDPSVAPFDPIFFLHHANVDRLIALWSAIR 300
PPO2 ....KIEGHMDHPFFAAFDPIFWLHHTNVDRLLSLWKAIN 296
PPO4 ....AIRGHMTHALFAAFDPIFWLHHSNVDRHLSLWQALY 297
PPO3 YDVYVSEGMNREATMGLIPGQVLTEDSPLEPFYTKNQDPW 350
PPO1 YDVWTSPGDAQFGTYTLRYKQSVDESTDLAPWWKTQNEYW 340
PPO2 PDVWVTSGRNRDGTMGIAPNAQINSETPLEPFYQSGDKVW 336
PPO4 PGVWVTQGPEREGSMGFAPGTELNKDSALEPFYETEDKPW 337
PPO3 QSDDLEDWETLGFSYPDFDPVKGKSKEEKSVYINDWVHKH 390
PPO1 KSNELRSTESLGYTYPEFVGLDMYNKDAVNKTISRKVAQL 380
PPO2 TSASLADTARLGYSYPDFDKLVGGTKELIRDAIDDLIDER 376
PPO4 TSVPLTDTALLNYSYPDFDKVKGGTPDLVRDYINDHIDRR 377
PPO3 YG 392
PPO1 YG 382
PPO2 YG 378
PPO4 YG 379
(a)
L-CHAIN MAQARKIPLDLPGTRILNGANWANNSATEN 30
LATNSGTLIIFDQSTPGQDADRWLIHNYNDGYKIFNMGSN 70
NWASVSRGNTVLGVSEFDGQTCKWSIEYSGNGEEFWIRVP 110
REGGGGAVWTIKPASSQGPTTVFLDLLKETDPNQRIKFAV 150
(b)

The H_2L_2 tetramer

Mushroom tyrosinase crystallizes with one (space group $P2_12_12$) or two (space group $P2_1$) H_2L_2 tetramers in the asymmetric unit. To investigate whether these tetramers are also the likely tetramers in solution (Strothkamp, Jolley *et al.* 1976), we analyzed the packing of the molecules in both crystal forms. For space group $P2_12_12$ two alternative tetrameric arrangements of the H and L subunits are possible, which differ by ~10% in the interaction surface between the molecules (2980 $Å^2$ compared to 2680 $Å^2$ buried surface). The tetrameric arrangement with the largest buried surface is also observed in space group $P2_1$, and therefore we propose that this is the tetrameric organization occurring in solution (Fig. 2). It is stabilized by two holmium ions in the H–H interface, each coordinated by the side chains of Asp336, Asp353 and Gln351 from one H subunit and the Asp312 side chain from the other, and by two water molecules. Interestingly, in the $P2_12_12$ crystal form one of the holmium ions occupies two closely related positions, 3.0 Å apart, in a ~70%/30% ratio, indicating that it is not bound very specifically. Holmium is an analogue of calcium, and it was used as an additive in the crystallization experiments. The Ho^{3+} ions possibly diminish the repulsion between the negatively charged residues in the dimer interface, which is in agreement with a previous report that calcium stimulates the association of mushroom tyrosinase into tetramers (Jolley, Robb *et al.* 1969).

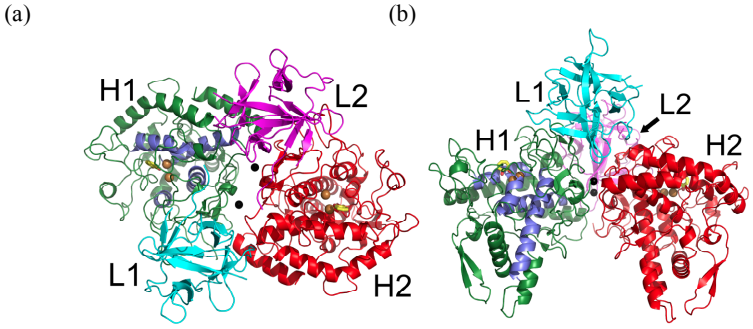

Fig. 2. Top (a) and side (b) views of the *A. bisporus* tyrosinase H_2L_2 tetramer structure. H-L dimer interactions are between H1 (green) and L1 (cyan) and H2 (red) and L2 (magenta). The brown and black spheres indicate the copper and holmium ions, respectively, and the yellow sticks the tropolone molecule in the active site. The four α-helices that make up the active site (α3, α4, α10, α11) are marked in purple.

Two salt bridges, His76 (H) – Glu139 (L) and Glu317 (H) – His56 (L), stabilize the H–L interface, which covers an area of ~800 Å^2. Hydrogen bonds are present between the peptide nitrogen atom of Val332 (H) and the carbonyl oxygen atom of Ile55 (L), and between the Ser337 (H) Oγ and the side chain Oδ1 of Asn57 (L). The side chains of Tyr78 (H) and Tyr98 (L) have an aromatic T-stacking interaction, and Met318 (H) is buried in a hydrophobic environment provided by Leu11, Pro12, and Val150 of the L subunit, as is Ile328 (H), which interacts with Phe105, Phe148 and Ile96 of the L subunit. The association of the H and L subunits is commonly observed; already in 1969 several tryptic peptides of a mushroom tyrosinase preparation were found (Jolley, Nelson *et al.* 1969) that now can be attributed to the L subunit (*e.g.* the amino acid composition of peptide V corresponds to residues 7-15 of the L subunit, that of peptide VI to residues 139-145, and that of peptide VII to the C-terminal residues 148-150 (Jolley, Nelson *et al.* 1969).

The H subunit is the tyrosinase domain

The H subunit comprises residues 2-392 of PPO3. No density is visible for Met1 and most of Ser2, and for any residues beyond 392. It contains 15 α-helices, four β-strands and many loops (Fig. 3a). Its overall structure is similar to the tyrosinase domain of *S. castaneoglobisporus* (*Sc*TYR; rmsd 1.7 Å, 211 matched residues), *Octopus dofleini* hemocyanin (rmsd 1.6 Å, 219 matched residues), and *I. batatas* (*Ib*COX; rmsd 1.6 Å, 189 matched residues). A bundle of four helices (α3, α4, α10, and α11) in the centre of the domain make up the catalytically essential binuclear copper-binding site (Fig. 3a). The H subunit comprises the tyrosinase core region as defined by Flurkey & Inlow (Flurkey and Inlow 2008), which starts at Arg20 and ends with Tyr365. The first residue of the core region, Arg20, is part of a short peptide stretch (residues 18-20), which lies parallel to residues 363-365. Arg20 stacks *via* a π-cation interaction with the Phe363 side chain in this latter stretch, and is hydrogen-bonded to Glu102 (part of the Cu-A binding motif; see below) and to Asp300 (part of the Cu-B binding motif). Phe363 is the first residue of a Tyr/Phe-x-Tyr conserved sequence motif, of which the tyrosine, Tyr365, is hydrogen-bonded to one of the side chain Nη‘s of Arg20. The equivalents to Arg20, Glu102, Asp300, and the Tyr/Phe-x-Tyr sequence motif are also present in *O. dofleini* hemocyanin,

*Ib*COX, and *Sc*TYR, although in this latter protein the second aromatic residue is a Phe. These residues serve to stabilize the N- and C-terminal regions of the tyrosinase core domain, as well as the Cu-A and Cu-B binding motifs.

The core region is followed by a 27-residue extension, containing α-helices α14 (residues 368-372) and α15 (residues 375-391) (Fig. 1a). The extension ends with residues Tyr391-Gly392, which are conserved in fungal tyrosinases (Marusek, Trobaugh *et al.* 2006; Kawamura-Konishi, Tsuji *et al.* 2007). The hydroxyl group of Tyr391 has hydrogen-bonding interactions with the side chains of the conserved Asp137 and Arg301, ensuring that the C-terminal end of the extension is closely associated with the tyrosinase core domain. No density is visible for Phe393 and beyond. Interestingly, proteolytic maturation of the fungal tyrosinases from *N. crassa* (Kupper, Niedermann et al. 1989) and *Pholiota nameko* (Kawamura-Konishi, Tsuji et al. 2007) occurs at a phenylalanine a few residues after the Tyr-Gly sequence motif. PPO3 also has a Phe after the Tyr-Gly motif, suggesting that maturation could be similar to that of the *N. crassa* and *P. nameko* tyrosinases. However, the *A. bisporus* PPO1, PPO2 and PPO4 tyrosinases do not have a Phe after the Tyr-Gly motif. Based on this observation, we speculate that if they are proteolytically activated, alternative maturation mechanisms must exist.

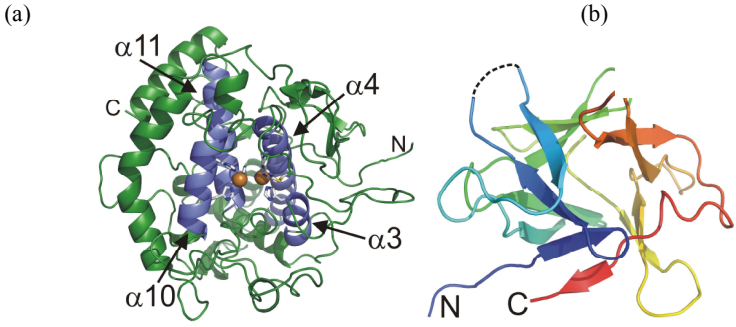

Fig. 3. Cartoon representation of the individual subunits. (a) The tyrosinase subunit, the six histidine ligands and the cysteine are colored to atom type. The brown spheres are the Cu-A (right) and Cu-B (left). Backbone coloring as in Fig. 2. (b) The lectin subunit, in rainbow coloring from N- (blue) to C-terminus (red). The dashed line indicates the residues not visible in the electron density.

The L subunit has a lectin-like fold

The L subunit comprises residues 9-28 and 35-150 of ORF 239342. No density is visible for the first 8 residues and residues 29-34 (Fig. 3b). Likely, proteolytic cleavage has occurred between residues 31 and 32, since previously an N-terminal sequence of the L subunit was determined as ATNSGTLIIFDQ (Schurink, van Berkel et al. 2007), which corresponds to residues 32-43 of ORF 239342. The C-terminal residues Phe148-Ala149-Val150 are in agreement with a previous C-terminal sequence analysis (Jolley, Nelson *et al.* 1969).

The L subunit adopts a β-trefoil fold, consisting of 12 antiparallel β-strands assembled in a cylindrical barrel of six 2-stranded sheets. A structural homologue search using DALI (Holm, Kaariainen *et al.* 2008) revealed several homologues, covering mostly fibroblast growth factors and lectin-like proteins. The closest structural homologue was the hemagglutinating protein HA33 from *Clostridium botulinum* (Arndt, Gu et al. 2005) with a Z-score of 16.7, an rmsd of 1.9 Å and 14% sequence identity for 120 aligned residues. Other DALI matches included the ricin-B-like lectins, which, like HA33, are carbohydrate-binding proteins. Their carbohydrate-binding sites have been characterized, but the carbohydrate-binding residues are not conserved in the L subunit.

The L subunit is about 25 Å away from the active site, and none of its residues hinders access to the active site. Since no allosteric behaviour of mushroom tyrosinase has been observed, a role in catalysis of the L subunit appears unlikely. The absence of conserved carbohydrate binding residues suggests that a role in carbohydrate binding or cell wall attachment is neither obvious. Thus, further research is needed to establish the biological role of the L subunit, if any, as well as its importance for the functioning of the H subunit.

The binuclear copper-binding site

The H subunit of *Ab*TYR contains a binuclear copper site, with each copper ion coordinated by three histidine residues. The site is located at the heart of two pairs of anti-parallel α-helices (α3/α4 and α10/α11, respectively), which make an angle of nearly 90^{o} with each other (Fig. 3a). The ligands of the first copper ion, Cu-A, are the Nε2 atoms of His61 (end of helix α3), His85 (in the loop connecting α3 and α4) and

His94 (beginning of α4). The second copper ion, Cu-B, has as ligands the Nε2 atoms of His259, His263 (α10) and His296 (α11). Viewed along the Cu-A—Cu-B axis the histidine side chains are staggered, although His296 deviates somewhat (Fig. 4a). Four of these histidine residues (61, 94, 259, 263) have hydrogen bonds of their Nδ1 atom with a peptide carbonyl oxygen atom, which restricts their side chain rotational freedom, and may contribute to the affinity for the metal. A covalent thioether bond with Cys83 fixes the orientation of the His85 side chain (Fig. 4a). His296 is the only copper ligand that has no direct interactions with the protein. However, its side chain is kept in position by a hydrogen bond to an internal water molecule, which, in turn, is hydrogen bonded to the carbonyl oxygen atom of His296 and another water molecule hydrogen bonded to Oδ1 of the conserved Asp300 and O of Pro91. Thus, the copper-coordinating histidine residues all have interactions that limit their rotational freedom. In addition, Phe90 is wedged between His94, His259 and His296, while Phe292 is between His61, His263 and His296, thereby also restricting the histidine side chain conformations to maintain the integrity of the copper binding sites (Hazes, Magnus *et al.* 1993). Phe90 and Phe292 are part of the highly conserved Phe90-x_3-His94 and Phe292-x_3-His296 motifs of tyrosinases, catechol oxidase, and hemocyanins, in which His94 and His296 are the most C-terminal histidine ligand of the Cu-A and Cu-B ions, respectively (Hazes, Magnus *et al.* 1993).

The geometry of the binuclear copper-binding site

Both copper binding sites adopt a nearly planar trigonal geometry. In agreement with density functional theory calculations (Yoon, Fujii *et al.* 2009), the copper ions are slightly (0.5 ± 0.1 Å) out of the plane defined by the Nε2 atoms of their ligands. The distance between the Cu-A and Cu-B ions is 4.5 ± 0.2 Å, which is close to the 4.2 Å distance calculated for the *deoxy*-hemocyanin binuclear copper site (Yoon, Fujii *et al.* 2009), and the 4.1 Å, 4.5-4.9 Å, and 4.4 Å distances observed in *deoxy-Sc*TYR (Matoba, Kumagai *et al.* 2006), *Manduca sexta* prophenoloxidase (Li, Wang *et al.* 2009), and *Ib*COX (Klabunde, Eicken *et al.* 1998), respectively. This suggests that the copper centre in our *Ab*TYR structure is in the *deoxy* state.

A water molecule or hydroxyl ion bridges the two copper ions at distances of 2.65 ± 0.2 Å to Cu-A and Cu-B (Fig. 4a). It completes the four-coordinate trigonal

pyramidal coordination sphere for both copper ions. It is nearest to the side chain of His259 (3.1 ± 0.1 Å), but does not make any hydrogen bonding interactions with the protein. A single bridging water molecule has also been observed in the crystal structures of *S. castaneoglobisporus deoxy*-tyrosinase (Matoba, Kumagai *et al.* 2006) and *M. sexta* prophenoloxidase (Li, Wang *et al.* 2009).

Substrate-binding site and tropolone binding

The binuclear copper-binding site is located at the bottom of a spacious cavity in the surface of the H-subunit. This cavity is readily accessible from the solvent, and not occluded by the L subunit or by loops of side chains of the H subunit. The slow-binding, reversible tyrosinase inhibitor tropolone (Kahn and Andrawis 1985; Espin and Wichers 1999) binds in this cavity without the need for conformational changes of the protein (Fig. 4b). It binds in a position somewhat similar to that of the phenylthiourea inhibitor of *Ib*COX (Klabunde, Eicken *et al.* 1998), and of the tyrosine side chain of the caddie protein in the *Sc*TYR structure (Matoba, Kumagai *et al.* 2006). Its 7-membered aromatic ring is at van der Waals distance from the side chains of Val283 and the copper ligand His263, and has edge-to-face aromatic interactions with the side chain of Phe264. Details of the tropolone-protein binding interactions differ for the four molecules in the asymmetric unit, suggesting that tropolone is not bound very specifically. Its oxygen atoms have a shortest distance of about 3.0 to 3.5 Å to either Cu-A or Cu-B, depending on which of the four H subunits is considered. Since in the crystal structure of tropolone with a bound cupric ion the Cu-O distance is about 1.9 Å (Macintyre, Robertson *et al.* 1966), we conclude that the tropolone-binding mode represents a pre-Michaelis complex. This result is in agreement with the finding that tropolone only inhibits *oxy*-tyrosinase (Espin and Wichers 1999) and supports our conclusion that we have crystallized *deoxy*-tyrosinase. A similar unproductive binding mode has been observed for kojic acid bound to *Bacillus megaterium* tyrosinase (Sendovski, Kanteev *et al.* 2011).

The active site is further lined with His244, part of the carboxylate of Glu256, Asn260, the main chain atoms of residues 279-282, and Ala286. Of these residues, His244, Glu256, and Ala286 are all conserved in PPO1, PPO2, PPO3, and PPO4 (Fig. 1). Although they do not interact with the tropolone, they may interact with

productively bound *bona fide* substrates. The space of the active site cavity is large enough to even accommodate phenolic steroids as substrates, as exemplified by the ability of the enzyme to *ortho*-hydroxylate compounds such as 17β-estradiol (Woerdenbag, Pras *et al.* 1990).

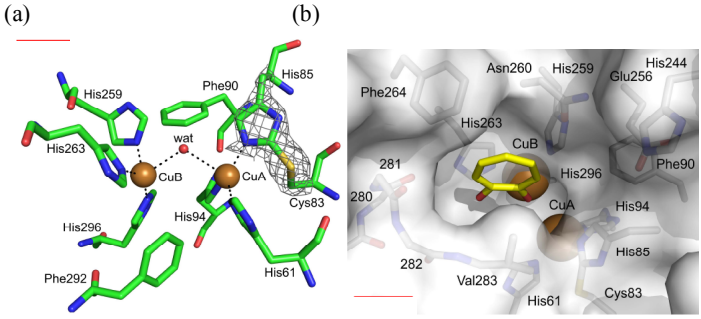

Fig. 4. (a) Geometry of the binuclear copper-binding site in the orthorhombic space group. The ligands are colored according to atom type (green, blue, red, yellow for carbon, nitrogen, oxygen, sulfur, respectively). The brown spheres are the Cu-A and Cu-B copper ions, and the red sphere is a bound water molecule/hydroxyl ion. The electron density for the covalent thioether bond between the Cys83 Sγ and His85 Cε1 atoms is contoured at 2.0 σ and is shown in black mesh. (b) Geometry of the active site as surface representation with tropolone in sticks. Amino acids in the cavity are indicated in stick representation, for residues 280-282 only backbone sticks are shown.

The thioether bond

In mushroom tyrosinase a thioether bond is formed post-translationally between the Cε atom of the Cu-A ligand His85 and the side chain of Cys83. Clear electron density for the covalent bond is present, and both Cys83 and His85 are well defined (Fig. 4a). Binding of tropolone does not affect the residues. The role of the thioether bond in binuclear copper proteins is not clear. An essential, direct role in catalysis (by e.g. stabilizing the tyrosine radical generated during the reaction (Ito, Phillips *et al.* 1991)) can be excluded, because the thioether bond is not conserved (Klabunde, Eicken *et al.* 1998). Instead, it has been proposed that the thioether bond imposes structural restraints on the binuclear copper site to optimize its redox potential and allow rapid electron transfer (Klabunde, Eicken *et al.* 1998) However, in the absence of an *oxy*-tyrosinase structure and supporting quantum chemical evidence such a role remains speculative.

Implications for the enzyme reaction mechanism

The precise reaction mechanism of tyrosinase is unclear. No information is available on the binding modes of the monophenolic substrate for the *o*-hydroxylation reaction and the diphenolic substrate for the oxidation reaction. On the basis of the structures of *Ib*COX and *Sc*TYR it has been hypothesized that the monophenolic substrate is preoriented through a hydrophobic interaction with the Cu-B ligand His263 (PPO3 numbering) (Decker, Schweikardt *et al.* 2006). Our PPO3-tropolone structure fully supports this notion. Next, the hydroxyl group of the substrate is proposed to be deprotonated by the peroxide ion bound between Cu-A and Cu-B at the start of the reaction. Whether the ensuing phenolate oxygen coordinates Cu-A or Cu-B is not clear at this moment (Decker, Schweikardt *et al.* 2006; Matoba, Kumagai *et al.* 2006). Subsequently, an *ortho*-carbon atom of the substrate approaches the peroxide, and the substrate is *ortho*-hydroxylated. Although Matoba *et al.* (2006) suggest that the *ortho*-hydroxylation would require the displacement of His54 (*Sc*TYR numbering), this seems improbable for *Ab*TYR since the equivalent His85 is covalently connected to Cys83 *via* a thioether bond, and is therefore unlikely to move away. Finally, the diphenolic compound adduct undergoes oxidation to result in *ortho*-quinone product (Decker, Schweikardt *et al.* 2007).

Further details of the substrate binding mode and reaction mechanism may be obtained from detailed analysis of *Ab*TYR structures with bound substrates or substrate analogues in conjunction with spectroscopic analysis of crystals. Understanding of the interaction of tyrosinase with inhibitors may be of importance for evidence-based development of novel regulators of the enzyme's activity. Such compounds are actively searched for as a means to reduce the quality decay of food resulting from the action of oxidative enzymes (Kim and Uyama 2005; Chang 2009). The *Ab*TYR crystal structure may take this search from the ad-hoc nature that it has had until now, to a more directed and targeted effort for this commercially important enzyme.

A. bisporus tyrosinase occurs in latent (inactive) and active forms. How the latent form is activated is not unequivocally known, although several hypotheses have been put forward, ranging from removal of active site-covering amino acids to removal of

the entire C-terminal domain (Espin, van Leeuwen *et al.* 1999; Espin, Soler-Rivas *et al.* 2000; Decker, Schweikardt *et al.* 2007). In all cases, improved substrate accessibility of the active site appears to be crucial. The current crystal structure suggests that the L subunit is not involved in the activation mechanism of mushroom tyrosinase, since it is located far away and not in a position to block access to the active site. A crystal structure of full-length mushroom tyrosinase may reveal whether the C-terminal part of the pro-enzyme that is cleaved off upon maturation plays a role in limiting access to the active site.

Conclusions

A commercially available tyrosinase from *A. bisporus* was crystallized and its structure was elucidated. The structure showed that the crystallized enzyme material consisted of PPO3. Six histidine residues coordinate the two copper ions in the active site with their Nε atoms. In turn, these histidine residues are held in place by hydrogen bonds of their Nδ atoms, and by a thioether bond between Cys83 and His85. The ~4.5 Å distance between the two copper ions suggests that the enzyme is in the *deoxy*-state. In the crystals an *A. bisporus* protein with a lectin-like fold was also present, but potential carbohydrate binding sites were not conserved. A complex with the inhibitor tropolone showed that tropolone binds in the active site, but that it does not coordinate the copper ions, suggesting that it forms a pre-Michaelis complex.

Acknowledgements

This work was funded by the Innovation-driven Research Program for Industrial Proteins (project number IIE00022). Data collection at the ESRF was supported by the ESRF and by the European Molecular Biology Laboratory (EMBL) under the European Community's Seventh Framework Program (FP7/2007-2013, grant agreement No. 226716). We thank the Groningen Biomolecular Sciences and Biotechnology Institute (GBB) for providing the funding for the completion of the work. We also thank Prof. J. J. Beintema for his valuable advice and discussion.

Appendix

Table 1. Summary of crystallographic data collection and processing

	Native $P2_1$	Native $P2_12_12$	Tropolone $P2_1$	Native $P2_12_12$
Beam line	ESRF ID23-2	ESRF ID14-4	ESRF ID23-2	ESRF ID14-4
Wavelength (in Å)	0.8726	0.9395	0.8726	0.9395
Resolution (in Å)	50.0 – 3.0	54.2 – 2.60	58.0 – 2.78	61.1 – 2.30
Cell parameters				
a (in Å)	104.2	104.0	103.8	104.1
b (in Å)	105.0	104.5	104.8	104.5
c (in Å)	119.1	108.4	119.4	109.0
β (·)	110.6	90	110.5	90
R_{merge} [§]	0.16 (0.34)	0.12 (0.45)	0.24 (0.62)	0.12 (0.55)
R_{pim} [#]	0.11 (0.24)	0.07 (0.28)	0.17 (0.44)	0.07 (0.34)
Mean I/σI	7.3 (2.3)	8.2 (2.3)	3.5 (1.6)	7.7 (2.3)
Completeness (%)	88.9 (90.5)	94.8 (81.8)	89.6 (89.7)	99.4 (99.6)
Multiplicity	2.8 (2.9)	4.0 (2.7)	2.7 (2.6)	3.7 (3.5)

[§] $R_{merge} = \sum_{hkl}\sum_i |I_i(hkl) - \langle I(hkl)\rangle| / \sum_{hkl}\sum_i (hkl)$

[#] $R_{pim} = \sum_{hkl} [1/(N-1)]^{1/2} \sum_i |I_i(hkl) - \langle I(hkl)\rangle| / \sum_{hkl}\sum_i (hkl)$

$I_i(hkl)$ is the integrated intensity of a reflection, $\langle I(hkl)\rangle$ is the mean intensity of multiple corresponding symmetry-related reflections, and N is the multiplicity of the given reflections. Values in parentheses are for the highest resolution shell.

Table 2. Summary of model refinement

Model	Native $P2_12_12$	Tropolone $P2_1$
R / R_{free} (%)	18.1 / 23.7	23.6 / 28.9
Resolution (Å)	47.1 - 2.30	58.0 - 2.78
HL subunits / asymmetric unit	2	4
No. of atoms		
Protein	8526	17052
Ligands	4 Cu, 6 Ho 3 diethyleneglycol, 1 triethyleneglycol	8 Cu, 4 Ho, 4 tropolone
Water molecules	390	25
B factors (Å^2)		
Main chain H-, L-subunits	31.8, 36.7	55.3,56.7
Cu^{2+} ions	32.8	47.2
Ho^{3+} ions	44.3	70.2
Ligands	40.7	84.5
Rms deviations		
Bond lengths (Å)	0.010	0.006
Bond angles (°)	1.16	0.95
PDB accession code	2y9w	2y9x

References

Abolmaali, B., H. V. Taylor, *et al.* (1998). "Evolutionary aspects of copper binding centers in copper proteins." *Struct. Bond.* **91**: 92-181.

Altschul, S. F., W. Gish, *et al.* (1990). "Basic local alignment search tool." *J. Mol. Biol.* **215**(3): 403-410.

Arndt, J. W., J. Gu, *et al.* (2005). "The structure of the neurotoxin-associated protein HA33/A from *Clostridium botulinum* suggests a reoccurring β-trefoil fold in the progenitor toxin complex." *J. Mol. Biol.* **346**(4): 1083-1093.

Bond, C. S. and A. W. Schüttelkopf (2009). "ALINE: a WYSIWYG protein-sequence alignment editor for publication-quality alignments." *Acta Cryst.* **D65**: 510-512.

Borghi, E., P. L. Solari, *et al.* (2002). "Oxidized Derivatives of Octopus vulgaris and Carcinus aestuarii Hemocyanins at pH 7.5 and Related Models by X-ray Absorption Spectroscopy." *Biophys. J.* **82**(6): 3254-3268.

Bouchilloux, S., P. McMahill, *et al.* (1963). "The multiple forms of mushroom tyrosinase. Purification and molecular properties of the enzymes." *J. Biol. Chem.* **238**(5): 1699-1707.

Canutescu, A. A., A. A. Shelenkov, *et al.* (2003). "A graph theory for protein side-chain prediction." *Prot. Sci.* **12**: 2001-2014.

Cesarini, J. P. (1996). "Melanins and their possible roles through biological evolution." *Adv. Space Res.* **18**(12): 35-40.

Chang, T. S. (2009). "An updated review of tyrosinase inhibitors." *Int. J. Mol. Sci.* **10**: 2440-2475.

Clark, E. D. B. (1998). "Refolding of recombinant proteins." *Curr. Opin. Biotechnol.* **9**(2): 157-163.

Collaborative Computational Project Number 4 (1994). "The CCP4 suite: programs for protein crystallography." *Acta Cryst.* **D50**: 760 -763.

Cuff, M. E., K. I. Miller, *et al.* (1998). "Crystal structure of a functional unit from *Octopus* hemocyanin." *J. Mol. Biol.* **278**: 885-870.

de Faria, R. O., V. R. Moure, *et al.* (2007). "The biotechnological potential of mushroom tyrosinases." *Food Technol. Biotech.* **45**(3): 287-294.

Decker, H. and T. Rimke (1998). "*Tarantula* hemocyanin shows phenoloxidase activity." *J. Biol. Chem.* **273**(40): 25889-25892.

Decker, H., T. Schweikardt, *et al.* (2007). "Similar enzyme activation and catalysis in hemocyanins and tyrosinases." *Gene* **398**: 183-191.

Decker, H., T. Schweikardt, *et al.* (2006). "The first crystal structure of tyrosinase: All questions answered?" *Angew. Chem. Int. Ed.* **45**(28): 4546-4550.

DeLano, W. L. (2008). The PyMOL molecular graphics system, Delano Scientific LLC, Palo Alto, CA - USA.

Della Longa, S., I. Ascone, *et al.* (1996). "The dinuclear copper site structure of *Agaricus bisporus* tyrosinase in solution probed by X-ray absorption spectroscopy." J. Biol. Chem. **271**(35): 21025-21030.

Della-Longa, S., I. Ascone, *et al.* (1996). "The dinuclear copper site structure of *Agaricus bisporus* tyrosinase in solution probed by X-ray absorption spectroscopy." *J. Biol. Chem.* **271**(35): 21025-21030.

Eicken, C., B. Krebs, *et al.* (1999). "Catechol oxidase - structure and activity." *Curr. Opin. Struct. Biol.* **9**(6): 677-683.

Eicken, C., F. Zippel, *et al.* (1998). "Biochemical and spectroscopic characterization of catechol oxidase from sweet potatoes (*Ipomoea batatas*) containing a type-3 dicopper center." *FEBS Lett.* **436**(2): 293-299.

Eickman, N. C., E. I. Solomon, *et al.* (1978). "Ultraviolet resonance raman study of oxytyrosinase. Comparison with oxyhemocyanins." *J. Am. Chem. Soc.* **100**(20): 6529-6531.

Emsley, P., B. Lohkamp, *et al.* (2010). "Features and development of Coot." *Acta Cryst.* **D66**: 486-501.

Ericsson, U. B., B. M. Hallberg, *et al.* (2006). "Thermofluor-based high-throughput stability optimization of proteins for structural studies." *Anal. Biochem.* **357**: 289-298.

Espin, J. C., M. Morales, *et al.* (1997). "Improvement of a continuous spectrophotometric method for determining the monophenolase and diphenolase activities of mushroom polyphenol oxidase." *J. Agric. Food Chem.* **45**: 1084-1090.

Espin, J. C., C. Soler-Rivas, *et al.* (2000). Maturation and activation of latent tyrosinase from *Agaricus bisporus*. Science and cultivation of edible fungi. L. J. L. D. van Griensven. Rotterdam, Balkema**:** 79-86.

Espin, J. C., J. van Leeuwen, *et al.* (1999). "Kinetic study of the activation process of a latent mushroom (*Agaricus bisporus*) tyrosinase by serine proteases." *J. Agric. Food Chem.* **47**(9): 3509-3517.

Espin, J. C., R. Varon, *et al.* (2000). "Kinetic characterization of the substrate specificity and mechanism of mushroom tyrosinase." *Eur. J. Biochem.* **267**(5): 1270-1279.

Espin, J. C. and H. J. Wichers (1999). "Slow-Binding Inhibition of Mushroom (Agaricus bisporus) Tyrosinase Isoforms by Tropolone." *J. Agric. Food Chem.* **47**(7): 2638-2644.

Espin, J. C. and H. J. Wichers (2000). Maturation and activation of latent tyrosinase from *Agaricus bisporus*. *Proceedings of the 15th international congress on the science and cultivation of edible fungi*. L. J. L. D. v. Griensven. Rotterdam, Balkema**:** 79-86.

Evans, P. (2006). "Scaling and assessment of data quality." *Acta Cryst.* **D62**: 72-82.

Fenoll, L. G., J. N. Rodriguez-Lopez, *et al.* (2002). "Unification for the expression of the monophenolase and diphenolase activities of tyrosinase." *IUBMB Life* **54**(3): 137-141.

Flurkey, A., J. Cooksey, *et al.* (2008). "Enzyme, protein, carbohydrate, and phenolic contaminants in commercial tyrosinase preparations: Potential problems affecting tyrosinase activity and inhibition studies." *J. Agric. Food Chem.* **56**(12): 4760-4768.

Flurkey, W. H. (1991). "Identification of tyrosinase in mushrooms by isoelectric-focusing." *J. Food Sci.* **56**(1): 93-95.

Flurkey, W. H. and J. K. Inlow (2008). "Proteolytic processing of polyphenol oxidase from plants and fungi." *J. Inorg. Biochem.* **102**(12): 2160-2170.

Gaykema, W. P. J., W. G. J. Hol, *et al.* (1984). "3.2 Å structure of the copper-containing, oxygen carrying protein *Palinurus interruptus* haemocyanin." *Nature* **309**: 23-29.

Gielens, C., N. Geest, *et al.* (1997). "Evidence for a cysteine-histidine thioether bridge in functional units of molluscan haemocyanins and location of the disulfide bridges in functional units *d* and *g* of the ß2c-Haemocyanin of *Helix Pomatia*." *Eur. J. Biochem.* **248**(3): 879-888.

Gouzi, H. and A. Benmansour (2007). "Partial purification and characterization of polyphenol oxidase extracted from Agaricus bisporus (JELange) Imbach." *Int. J. Chem. React. Eng.* **5**: 12.

Hazes, B., K. A. Magnus, *et al.* (1993). "Crystal structure of deoxygenated *Limulus polyphemus* subunit II haemocyanin at 2.18 Å resolution: clues for a mechanism for allosteric regulation." *Prot. Sci.* **2**: 597-619.

Holm, L., S. Kaariainen, *et al.* (2008). "Searching protein structure databases with DaliLite v.3." *Bioinformatics* **24**(23): 2780-2781.

Holm, R. H., P. Kennepohl, *et al.* (1996). "Structural and functional aspects of metal sites in biology." *Chem. Rev.* **96**(7): 2239-2314.

Ingebrigtsen, J., B. Kang, *et al.* (1989). "Tyrosinase activity and isozymes in developing mushrooms." *J. Food Sci.* **54**(1): 128-131.

Ismaya, W. T., H. J. Rozeboom, *et al.* (2011). "Crystallization and preliminary X-ray crystallographic analysis of mushroom *Agaricus bisporus* tyrosinase." *Acta Cryst.* **F67**: 575-578.

Ito, N., S. E. V. Phillips, *et al.* (1991). "Nover thioether bond revealed by a 1.7 Å crystal structure of galactosidase." *Nature* **350**: 87-90.

Jaroszewski, L., L. Rychlewski, *et al.* (2005). "FFAS03: a server for profile-profile sequence alignments." *Nucl. Acid Res.* **33**: W284-W288.

Jimenez, M., W. L. Maloy, *et al.* (1989). "Specific identification of an authentic clone for mammalian tyrosinase " *J. Biol. Chem.* **264**(6): 3397-3403.

Jolivet, S., N. Arpin, *et al.* (1998). "*Agaricus bisporus* browning: a review." *Mycol. Res.* **102**: 1459-1483.

Jolley, R. L., Jr., L. H. Evans, *et al.* (1974). "Oxytyrosinase." *J. Biol. Chem.* **249**(2): 335-345.

Jolley, R. L., R. M. Nelson, *et al.* (1969). "Multiple Forms of Mushroom Tyrosinase - Structural Studies on Isozymes." *J. Biol. Chem.* **244**(12): 3251-3257.

Jolley, R. L., D. A. Robb, *et al.* (1969). "Multiple Forms of Mushroom Tyrosinase - Association-Dissociation Phenomena." *J. Biol. Chem.* **244**(6): 1593-1598.

Kabsch, W. (1993). "Automatic Processing of Rotation Diffraction Data from Crystals of Initially Unknown Symmetry and Cell Constants." *J. Appl. Cryst.* **26**: 795-800.

Kahn, V. and A. Andrawis (1985). "Inhibition of mushroom tyrosinase by tropolone " *Phytochemistry* **24**: 905-908.

Karbassi, F., K. Haghbeen, *et al.* (2003). "Activity, structural and stability changes of mushroom tyrosinase by sodium dodecyl sulfate." *Colloid Surface B* **32**(2): 137-143.

Karlin, K. D. and Y. Gultneh (1987). "Binding and Activation of Molecular Oxygen by Copper Complexes." *Prog. Inorg. Chem.* **35**: 219-327.

Kawamura-Konishi, Y., M. Tsuji, *et al.* (2007). "Purification, characterization, and molecular cloning of tyrosinase from Pholiota nameko." *Biosci. Biotechnol. Biochem.* **71**(7): 1752-1760.

Keilin, D. and T. Mann (1938). "Polyphenol oxidase: purification, nature, and properties." *Proc. R. Soc. London Ser. B* **125**: 187-204.

Kertesz, D. and R. Zito (1957). "Polyphenoloxidase (tyrosinase): purification and molecular properties." *Nature* **179**: 1017-1018.

Kertesz, D. and R. Zito (1962). "Kinetic studies of polyphenol action - kinetics in presence of reducing agents " *Biochim. Biophys. Acta* **64**(1): 153-&.

Kim, Y.-J. and H. Uyama (2005). "Tyrosinase inhibitors from natural and synthetic sources: structure, inhibition mechanism and perspective for the future." *Cell. Mol. Life Sci.* **62**(15): 1707-1723.

Kitajima, N. (1992). "Synthetic Approach to the Structure and Function of Copper Proteins " *Adv. Inorg. Chem.* **39**: 1-77.

Klabunde, T., C. Eicken, *et al.* (1998). "Crystal structure of a plant catechol oxidase containing a dicopper center." *Nat. Struct. Biol.* **5**(12): 1084-1090.

Kohashi, P. Y., T. Kumagai, *et al.* (2004). "An efficient method for the overexpression and purification of active tyrosinase from Streptomyces castaneoglobisporus." *Prot. Express. Purif.* **34**(2): 202-207.

Kubo, I., I. Kinst-Hori, *et al.* (2000). "Molecular design of antibrowning agents." *J. Agric. Food Chem.* **48**(4): 1393-1399.

Kupper, U., D. M. Niedermann, *et al.* (1989). "Isolation and characterization of the tyrosinase gene from *Neurospora-crassa*." *J. Biol. Chem.* **264**(29): 17250-17258.

Lamzin, V. S., A. Perrakis, *et al.* (2001). The ARP/wARP suite for automated construction and refinement of protein models. International Tables for Crystallography. M. G. Rossmann and E. Arnold. Dordrecht, The Netherlands, Kluwer Academic Publishers. **F: Crystallography of biological macromolecules:** 720-722.

Land, E. J., C. A. Ramsden, *et al.* (2004). Quinone chemistry and melanogenesis. *Methods enzymol.* H. Sies and L. Packer. **378:** 88-109.

Lerch, K. (1982). "Primary structure of tyrosinase from *Neurospora crassa*. II. Complete amino acid sequence and chemical structure of a tripeptide containing an unusual thioether." *J. Biol. Chem.* **257**(11): 6414-6419.

Lerch, K. and L. Ettlinger (1972). "Purification and characterization of a tyrosinase from Streptomyces glaucescens." *Eur. J. Biochem* **31**: 427–437.

Leslie, A. G. W. (2006). "The integration of macromolecular diffraction data." *Acta Cryst.* **D62**: 48-57.

Ley, J. P. and H. J. Bertram (2001). "Hydroxy- or methoxy-substituted benzaldoximes and benzaldehyde-O-alkyloximes as tyrosinase inhibitors." *Bioorg. Med. Chem.* **9**(7): 1879-1885.

Li, Y. C., Y. Wang, *et al.* (2009). "Crystal structure of *Manduca sexta* prophenoloxidase provides insights into the mechanism of type 3 copper enzymes." *Proc. Natl Acad. Sci. USA* **106**(40): 17002-17006.

Lilie, H., E. Schwarz, *et al.* (1998). "Advances in refolding of proteins produced in E-coli." *Curr. Opin. Biotechnol.* **9**(5): 497-501.

Lind, T., P. E. M. Siegbahn, *et al.* (1999). "A quantum chemical study of the mechanism of tyrosinase." *J. Phys. Chem. B* **103**(7): 1193-1202.

Loomis, W. D. (1974). "Overcoming problems of phenolics and quinones in the isolation of plant enzymes and organelles." *Methods Enzymol.* **31**: 528-544.
Lovell, S. C., I. W. Davis, *et al.* (2003). "Structure validation by C-alpha geometry: phi, psi, and C-beta deviation." *Prot. Struct. Funct. Gen.* **50**: 437-450.
Macintyre, W. M., J. M. Robertson, *et al.* (1966). "Crystal structure of cupric tropolone - a refinement." *Proc. R. Soc. A* **289**(1417): 161-170.
Makino, N. and H. S. Mason (1973). "Reactivity of oxytyrosinase toward substrates." *J. Biol. Chem.* **248**(16): 5731-5735.
Mallette, M. F. and C. R. Dawson (1949). "On the Nature of Highly Purified Mushroom Tyrosinase Preparations." *Arch. Biochem.* **23**(1): 29-44.
Marusek, C. M., N. M. Trobaugh, *et al.* (2006). "Comparative analysis of polyphenol oxidase from plant and fungal species." *J. Inorg. Biochem.* **100**(1): 108-123.
Matoba, Y., T. Kumagai, *et al.* (2006). "Crystallographic evidence that the dinuclear copper center of tyrosinase is flexible during catalysis." *J. Biol. Chem.* **281**: 8981-8990.
Matthews, B. W. (1968). "Solvent content of protein crystals." *J. Mol. Biol.* **33**: 491-497.
McCoy, A. J., R. W. Grosse-Kunstleve, *et al.* (2005). "Likelihood-enhanced fast translation functions." *Acta Cryst.* **D61**: 458-464.
Menon, S., R. B. Fleck, *et al.* (1990). "Benzoic acid inhibition of the α, β and γ enzymes of *Agaricus bisporus* tyrosinase." *Arch. Biochem. Biophys.* **280**: 27-32.
Murshudov, G. N., A. A. Vagin, *et al.* (1997). "Refinement of macromolecular structures by the maximum-likelihood method." *Acta Cryst.* **D53**: 240-255.
Nelson, R. M. and H. S. Mason (1970). "Tyrosinase (mushroom)." *Methods Enzymol.* **17**: 626-632.
Park, Y.-D., S.-y. Kim, *et al.* (2005). "A new type of uncompetitive inhibition of tyrosinase induced by Cl- binding." *Biochimie* **87**(11): 931-937.
Perbandt, M., E. W. Guthöhrlein, *et al.* (2003). "The structure of a functional unit from the wall of a gastropod hemocyanin offers a possible mechanism for cooperativity." *Biochemistry* **42**(21): 6341-6346.
Reedijk, J. (2005). "Dioxygen surprises." *Science* **308**: 1876-1877.
Rescigno, A., P. Zucca, *et al.* (2007). "Identification and discrimination between some contaminant enzyme activities in commercial preparations of mushroom tyrosinase." *Enzym. Microb. Technol.* **41**(5): 620-627.
Robb, D. A. (1979). "Subunit differences among the multiple forms of mushroom tyrosinase." *Biochem. Soc. Trans.* **7**: 131-132.
Robb, D. A. (1984). Tyrosinase. *Copper proteins and copper enzymes*. R. Lontie. Florida, CRC Press, Inc. **2:** 207-240.
Robb, D. A. and S. Gutteridge (1981). "Polypeptide composition of two fungal tyrosinases." *Phytochemistry* **20**: 1481-1485.
Saller, M. J., F. Fusetti, *et al.* (2009). "*Bacillus subtilis* SpoIIIJ and YqjG function in membrane protein biogenesis." *J. Bacteriol.* **191**(21): 6749-6757.
Sanchez-Ferrer, A., J. N. Rodriguez-Lopez, *et al.* (1995). "Tyrosinase: a comprehensive review of its mechanism." *Biochim. Biophys. Acta* **1247**(1): 1-11.
Schoot-Uiterkamp, A. J. M. and H. S. Mason (1973). "Magnetic Dipole-Dipole Coupled Cu(II) Pairs in Nitric Oxide-Treated Tyrosinase: A Structural

Relationship Between the Active Sites of Tyrosinase and Hemocyanin." *Proc. Natl. Acad. Sci. USA* **70**: 993-996.

Schurink, M., W. J. H. van Berkel*, et al.* (2007). "Novel peptides with tyrosinase inhibitory activity." *Peptides* **28**: 485-495.

Schüttelkopf, A. W. and D. M. F. van Aalten (2004). "PRODRG: a tool for high-throughput crystallography of protein-ligand complexes." *Acta Cryst.* **D60**: 1355-1363.

Sendovski, M., M. Kanteev*, et al.* (2011). "First structures of an active bacterial tyrosinase reveal copper plasticity." *J. Mol. Biol.* **405**: 227–237.

Seo, S. Y., V. K. Sharma*, et al.* (2003). "Mushroom tyrosinase: Recent prospects." *J. Agric. Food Chem.* **51**(10): 2837-2853.

Sharma, R. C. and R. Ali (1981). "Hydrodynamic properties of mushroom tyrosinase." *Phytochemistry* **20**(3): 399-401.

Shimanouchi, H. and Y. Sasada (1973). "Crystal and Molecular Structure of Tropolone." *Acta Cryst.* **B29**: 81-90.

Smith, D. M. and M. W. Montgomery (1985). "Improved methods for the extraction of polyphenol oxidase from d'Anjou pears." *Phytochemistry* **24**(5): 901-904.

Smith, J. L. and R. C. Krüger (1962). "Separation and purification of the phenolase of common mushroom." *J. Biol. Chem.* **237**: 1121-1128.

Soler-Rivas, C., S. Jolivet*, et al.* (1999). "Biochemical and physiological aspects of brown blotch disease of *Agaricus bisporus*." *FEMS Microbiol. Rev.* **23**(5): 591-614.

Soler-Rivas, C., A. C. Moller*, et al.* (2001). "Induction of a tyrosinase mRNA in *Agaricus bisporus* upon treatment with a tolaasin preparation from *Pseudomonas tolaasii*." *Physiol. Mol. Plant Pathol.* **58**(2): 95-99.

Solna, R., S. Sapelnikova*, et al.* (2005). "Multienzyme electrochemical array sensor for determination of phenols and pesticides." *Talanta* **65**(2): 349-357.

Sreerama, N. and R. W. Woody (2000). "Analysis of protein CD spectra: Comparison of CONTIN, SELCON3, and CDSSTR methods in CDPro software." *Biophys. J.* **78**(1): 334A-334A.

Strothkamp, K. G., R. L. Jolley*, et al.* (1976). "Quarternary structure of mushroom tyrosinase." *Biochem. Biophys. Res. Commun.* **70**: 519-524.

Terwilliger, T. C. (2003). "Automated main-chain model building by template matching and interative fragment extension." *Acta Cryst.* **D59**: 38-44.

The UniProt Consortium (2007). "The universal protein resource (UniProt)." *Nucleic Acids Res.* **35**: D193-D197.

Vagin, A. A. and A. Teplyakov (1997). "MOLREP: an automated program for molecular replacement." *J. Appl. Cryst.* **30**: 1022-1025.

van Gelder, C. W. G., W. H. Flurkey*, et al.* (1997). "Sequence and structural features of plant and fungal tyrosinases." *Phytochemistry* **45**(7): 1309-1323.

van Holde, K. E. and K. I. Miller (1995). "Hemocyanins." *Advan. Protein Chem.* **47**: 1-81.

Van Leeuwen, J. and H. J. Wichers (1999). "Tyrosinase activity and isoform composition in separate tissues during development of Agaricus bisporus fruit bodies." *Mycol. Res.* **103**: 413-418.

Vanneste, V. H. and A. Zuberbühler (1974). Copper-containing oxygenases. *Molecular mechanism of oxygen activation*. O. Hayashi. New York, Academic Press**:** 371-404.

Whitaker, J. R. (1993). *Principles of enzymology for the food sciences*. New York, CRC Press.

Wichers, H. J., Y. A. M. Gerritsen, *et al.* (1996). "Tyrosinase isoforms from the fruitbodies of *Agaricus bisporus*." *Phytochemistry* **43**(2): 333-337.

Wichers, H. J., K. Recourt, *et al.* (2003). "Cloning, expression and characterisation of two tyrosinase cDNAs from *Agaricus bisporus*." *Appl. Microbiol. Biotechnol.* **61**(4): 336-341.

Wichers, H. J., T. van den Bosch, *et al.* (1995). Enzymology and molecular biology of *Agaricus bisporus* tyrosinase. Science and cultivation of edible fungi. Elliott. Rotterdam, Balkema. **14:** 723-728.

Winn, M., M. Isupov, *et al.* (2001). "Use of TLS parameters to model anisotropic displacements in macromolecular refinement." *Acta Cryst.* **D57**: 122-133.

Woerdenbag, H. J., N. Pras, *et al.* (1990). "Cyclodextrin-facilitated bioconversion of 17-β-estradiol by a phenoloxidase from *Mucuna pruriens* cell cultures." *Phytochemistry* **29**(5): 1551-1554.

Wu, J., H. Chen, *et al.* (2010). "Cloning, characterization and expression of two new polyphenol oxidase cDNAs from *Agaricus bisporus*." *Biotechnol. Lett.* **32**: 1439–1447.

Yamaguchi, M., P. M. Hwang, *et al.* (1970). "Latent *o*-diphenol oxidase in mushroom (*Agaricus bisporus*)." *Can. J. Biochem.* **48**: 198-202.

Yasunobu, K. T., E. W. Peterson, *et al.* (1959). "Oxidation of Tyrosine-Containing Peptides by Tyrosinase." *J. Biol. Chem.* **234**(12): 3291-3295.

Yoon, J., S. Fujii, *et al.* (2009). "Geometric and electronic structure differences between the type 3 copper sites of the multicopper oxidases and hemocyanin/tyrosinase." *Proc. Natl Acad. Sci. USA* **106**(16): 6585-6590.

Zhang, J. P., Q. X. Chen, *et al.* (2006). "Inhibitory effects of salicylic acid family compounds on the diphenolase activity of mushroom tyrosinase." *Food Chem.* **95**(4): 579-584.

Summary

This thesis discusses the elucidation of the three-dimensional structure of tyrosinase from the mushroom *Agaricus bisporus* (champignon, button mushroom) by means of X-ray crystallography. Tyrosinase is a copper-containing enzyme that catalyzes the conversion of monophenols to *ortho*-diphenols and their subsequent conversion to *ortho*-quinone derivatives. The final product is the main precursor in the biosynthesis of melanin, a pigment that is widely distributed in nature and that is present in various organisms from all phyla. Therefore, the enzyme is commonly associated with pigmentation and pigment-related diseases or disorders in humans and animals, such as melanoma, albinism and vitiligo. In fruits and vegetables, tyrosinase is associated with the browning process that causes depreciation of the value of agricultural produce. A potent inhibitor of the enzyme's activity is therefore highly desired to prevent this browning. Tyrosinase inhibition is also of interest for the cosmetics and pharmaceutical industry, i.e. for skin whitening and for treatment of post-inflammatory hyper-pigmentation due to burn or to other skin abrasion. The studies for these applications are mostly performed using the commercially available mushroom tyrosinase, which therefore has been studied extensively. However, the interpretation of the results is often hampered by the lack of knowledge of the enzyme's three-dimensional structure. Therefore, the elucidation of its structure has become highly desirable, and several groups in the world have already attempted to determine its three-dimensional structure. Moreover, the availability of a three-dimensional structure will also allow rational, structure-based design of inhibitors.

However, the elucidation of the enzyme's 3D-structure has been hampered by difficulties in obtaining pure enzyme because of contamination from melanin and because mushroom tyrosinase appears to be heterogeneous. The sources for this heterogeneity conceivably originated from protein polymerization by quinones, purification procedures, posttranslational modifications, or enzyme sources. Later, it was discovered that at least four genes exist that encode the expression of mushroom tyrosinase, namely *ppo*1, *ppo*2, *ppo*3, and *ppo*4. This indicates that the heterogeneity of the enzyme may also originate from the presence of isoforms. These facts show that obtaining a pure tyrosinase for structural study is very challenging.

The molecular mass of mushroom tyrosinase (from commercial preparation or directly isolated from mushroom fruit bodies) upon analysis with various methods is consistently found to be ~120 kDa. However, the view of its quaternary structure has evolved from a homo-tetramer with ~30 kDa subunits to a hetero-tetramer consisting of two ~45 kDa (heavy, H) and two ~14 kDa (light, L) subunits. Furthermore, a peptide mass-spectrometry fingerprinting (PMF) experiment using commercial mushroom tyrosinase revealed that the heavy subunit of the commercial preparation would probably be PPO2. The identity of the light subunit, on the other hand, is unclear. It could be part of tyrosinase or a completely other, unrelated protein, which was proposed to be a lectin occurring in the mushroom. Thus, the identity of commercial mushroom tyrosinase, which is widely used in research, is not unambiguously established.

Because several *ppo* genes are now available, each mushroom tyrosinase isoform can be produced independently, and thus the problem with heterogeneity may be overcome. This was achieved by cloning the *ppo*2 gene into a bacterial system for overexpression of recombinant protein (**chapter 2**). Recombinant PPO2 with a histidine tag was produced in *Escherichia coli* for convenient purification using a nickel affinity chromatography column. However, the enzyme was found to be insoluble, forming protein aggregates called inclusion bodies. The inclusion bodies were solubilized by denaturation of the protein, and the PPO2 was then recovered *via* a refolding procedure whilst bound to the nickel affinity column. The refolded PPO2 was monomeric in solution with a molecular mass of 64 kDa, which is the size of *ppo*2 gene product. Spectroscopic analysis showed that the copper centre was present in the refolded enzyme. However, the refolded enzyme had a very low activity in comparison to both the commercial preparation and the enzyme isolated directly from mushroom. Moreover, no protein crystals were obtained using the refolded PPO2.

Following an alternative route, mushroom tyrosinase was successfully purified directly from the commercial preparation. Using enzyme material from this purification procedure, we could obtain mushroom tyrosinase crystals (**chapter 3**). Mushroom tyrosinase could only be crystallized at low ionic strength conditions. The crystals were obtained at room temperature with 8% polyethylene glycol in 10 mM sodium acetate buffer, pH 4.6 as crystallizing agent. The protein crystals grew in competition with aggregation and precipitation, and suffered from browning; harvesting the protein crystals was therefore also challenging. From a thermal stability analysis, we discovered that the stability of the enzyme was increased in the presence of calcium ions. Therefore, 10 mM calcium chloride was included in the purification buffer, but the calcium was removed prior to the crystallization experiments. Interestingly, the quality

of the crystals was improved when the enzyme was crystallized in the presence of holmium chloride. Although holmium is a calcium analogue, no crystal was obtained in the presence of calcium chloride. For this reason, 5 mM holmium chloride was added to the crystallization solution. The crystals were then subjected to X-ray diffraction experiments and diffraction data were collected. The enzyme had crystallized in two different spacegroups, $P2_1$ (monoclinic) and $P2_12_12$ (orthorhombic). The analysis of the content of the protein crystals showed that both the heavy and light subunits were present in both crystal forms. Moreover, when a crystal that had been exposed to X-ray radiation was dissolved, significant tyrosinase activity was observed. This indicates that we crystallized active enzyme.

The success with obtaining X-ray diffraction data from the crystals allowed us to take the next step in the structure elucidation of the enzyme (**chapter 4**). An initial structural model was generated employing the PPO2 amino acid sequence and the conserved parts of structures of PPO2 homologs, which are the mollusc hemocyanins from *Octopus dofleini* (giant octopus) and *Rapana thaliana* (sea snails), catechol oxidase from *Ipomoea batatas* (sweet potato), and the tyrosinase from *Streptomyces castaneoglobisporus* (bacterial tyrosinase). This initial model contained only part of the heavy subunit of the enzyme. The tyrosinase structure was built using both automatic model building programs and by hand. The data set from orthorhombic crystal was employed, because its resolution was higher. The model was regularly transferred to the monoclinic crystal data set. This practice beneficially reduces the presence of model bias because of the independency of the two data sets. Nevertheless, the model building and refinement did not progress because the PPO2 amino acid sequence did not fit to the electron density map at various places. When a higher resolution data set was obtained, the automatic model-building program ARP/wARP was employed to extend the structural model. We found that modifications had to be introduced to the PPO2 sequence. This modified sequence matched perfectly with the N-terminal region of the PPO3 sequence. The N-terminal amino acid sequence of PPO2, identified by PMF analysis, was very similar to that of PPO3 (figure 1), and since at the start of the modelling the PPO3 sequence was not yet known, the enzyme had been misidentified as PPO2. The structural model for the heavy subunit was then completed using the PPO3 sequence. The amino acid sequence derived from structural model of the light subunit did not fit to the amino acid sequence of PPO1, PPO2, PPO3, PPO4, the proposed mushroom lectin, or even any other protein in the public databases. This sequence was then submitted to the mushroom *A. bisporus* genome database, which is recently published. One clear hit was found and the model could be completed with the amino acid sequence of this protein, assigned as ORF239342. Thus, the elucidation of the

crystal structure of mushroom tyrosinase revealed the true identities of the mushroom tyrosinase H and L subunits, which had been unclear until then.

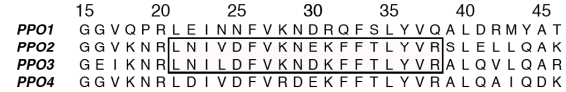

Figure 1. Alignment of the N – terminal regions of the PPO1 - PPO4 amino acid sequences. The box highlights the PPO2 fragment identified upon PFM analysis that is nearly identical to that of PPO3 and has the same mass. The numbering refers to the PPO3 sequence.

The overall structure of PPO3 is similar to the tyrosinase domain of mollusc hemocyanin, plant catechol oxidase, and bacterial tyrosinase. The tyrosinase domain is marked with an interaction between a strictly conserved arginine residue in the N–terminal region and a tyrosine or phenylalanine residue, part of the conserved Tyr/Phe-X-Tyr/Phe sequence motif, in the C–terminal domain. PPO3 structure, however, is 100-120 amino acid residues larger than the tyrosinase domain of its homologs. These additional residues reside mostly in the loops connecting the secondary structures. A binuclear copper centre resides in the heart of a bundle of four helices, which form the core of the enzyme. This copper centre is the catalytic centre of the enzyme; it is located in a spacious cavity on the surface of the protein, making it readily accessible from the solvent. The tyrosinase domain of PPO3 is followed by a 27 residues long extension that contains two α-helices, which are kept close to the core region *via* hydrogen bonds. This extension ends with a tyrosine–glycine sequence motif, which is highly conserved in fungal tyrosinases. Interestingly, in other fungal tyrosinases, the removal of the C–terminal part, *via* proteolytic cleavage upon maturation of the enzyme, has occurred at an amino acid residue immediately after this sequence motif. Unfortunately PPO3 structure provides no further information of amino acids beyond this sequence motif. Whether and where the cleavage upon maturation has occurred after this sequence motif can be explained when the structure of the full-length of PPO3 or its isoforms is elucidated.

One major question on the structure of tyrosinase has been the function of a thioether bond between Cys83 and His85 (PPO3 numbering) in the active site. His85 is one of the ligands that coordinate the first copper ion (Cu-A). This bond is conserved in hemocyanin and catechol oxidase (figure 2), with Cys-X-His and Cys-$(X)_{17}$-His sequence motif, respectively. Hemocyanin is an oxygen-carrier protein in molluscs and arthropods whilst catechol oxidase catalyzes the conversion of *ortho*-diphenols to *ortho*-quinones in plants. However, the thioether bond is absent in the structurally characterized bacterial tyrosinases from *S.*

castaneoglobisporus and *Bacillus megaterium*. Furthermore, the recently reported structures of these bacterial tyrosinases show that His85 is flexible. Therefore, in the current reaction mechanism based on their structures, the displacement of His85 is proposed in the *ortho*-hydroxylation step. However, the PPO3 structure shows that His85 displacement is unlikely because the thioether bond severely limits the rotational freedom of His85.

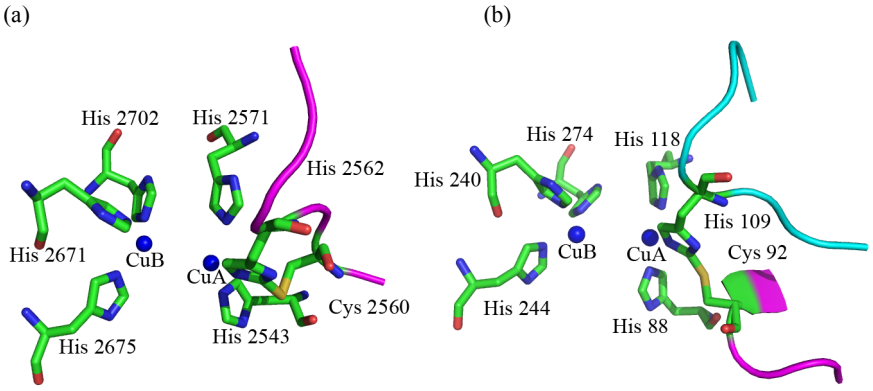

Figure 2. The thioether bond in (a) Octopus hemocyanin and (b) plant catechol oxidase. The ligands are colored according to atom type (green, blue, red, yellow for carbon, nitrogen, oxygen, sulfur, respectively). The blue spheres are the Cu-A and Cu-B copper ions. The ligands are numbered according to their amino acid sequence. The cyan and purple loops represent the polypeptide chains where the histidine and cysteine residues forming the thioether bond reside. Note that in catechol oxidase, the histidine and cysteine residues involved in the thioether bond originate from a different loop.

More insight into the reaction mechanism can be gained by studying the structure of tyrosinase in the presence of substrate or inhibitors. Unfortunately, the PPO3 as well as the PPO3–tropolone complex structures are in the *deoxy*-state, where the enzyme is not active. Furthermore, the tropolone inhibitor molecule is not bound specifically in the active site. Nevertheless, tropolone occupies a similar position as the phenylthiourea (PTU) inhibitor in catechol oxidase and the tyrosine side chain of the caddie protein in the *S. castaneoglobisporus* tyrosinase structure. The information on the steps in the reaction may be obtained by the elucidation of a structure of the *oxy*-state of PPO3, preferably in the presence of a substrate or substrate analogue.

The light subunit was identified as ORF 239342, which is a protein from mushroom with unknown function. Its architecture resembles proteins with agglutinating functionality but the carbohydrate binding is not conserved. Therefore, the function of this subunit as well as its

incorporation into the H_2L_2 tyrosinase tetramer remain questions because it is always found associated with the H subunit (tyrosinase). To find answers on these questions, new research can now be undertaken to studying the localization of this protein in mushroom and its regulation/expression in the cell, and to further characterize its biochemical characteristics.

Samenvatting

Dit proefschrift bespreekt de opheldering van de driedimensionale (3D) structuur van tyrosinase van de paddenstoel *Agaricus bisporus* (champignon) met Röntgenkristallografie. Tyrosinase is een koperhoudend enzym dat de omzetting van monofenolen naar *ortho*-difenolen en de latere omzetting tot *ortho*-chinonderivaten katalyseert. Het eindproduct is de voornaamste precursor in de biosynthese van melanine, een pigment dat op grote schaal wordt aangetroffen in de natuur en dat aanwezig is in verschillende organismen van allerlei phyla. Daarom wordt het enzym vaak geassocieerd met pigment en pigment-gerelateerde ziekten of aandoeningen bij mens en dier, zoals melanomen, albinisme en vitiligo. In groenten en fruit is tyrosinase verantwoordelijk voor het bruin worden van agrarische producten met als gevolg een waardevermindering. Een krachtige remmer van de activiteit van het enzym is dus zeer gewenst om deze bruinkleuring tegen te gaan. Tyrosinase remming is ook van belang voor de cosmetische en farmaceutische industrie, dat wil zeggen voor het bleken van de huid en voor de behandeling van post-inflammatoire hyperpigmentatie na brand- of schaafwonden. De studies naar deze toepassingen zijn meestal uitgevoerd met het commercieel verkrijgbare paddenstoelen tyrosinase, dat dus uitvoerig is bestudeerd. De interpretatie van de resultaten wordt echter vaak belemmerd door het gebrek aan kennis van de driedimensionale structuur van het enzym. Daarom is de opheldering van de structuur zeer wenselijk; diverse groepen in de wereld hebben al geprobeerd om deze driedimensionale structuur te bepalen. Bovendien zal de beschikbaarheid van een driedimensionale structuur het ook mogelijk maken remmers te fabriceren op een rationele, op de structuur gebaseerd ontwerp.

Het ophelderen van de 3D-structuur van het enzym wordt gehinderd door problemen bij het verkrijgen van zuiver enzym als gevolg van verontreiniging met melanine en omdat champignonstyrosinase heterogeen lijkt te zijn. De bron voor deze heterogeniteit is denkbaar eiwitpolymerisatie door chinonen, de gebruikte zuiveringprocedures, posttranslationele modificaties, of de bronnen van het enzym. Later is ontdekt dat er minstens vier genen bestaan die coderen voor de expressie van paddenstoelen-tyrosinase, namelijk *ppo*1, *ppo*2, *ppo*3 en *ppo*4. Dit geeft aan dat de heterogeniteit van het enzym ook afkomstig kan zijn van de aanwezigheid van isovormen. Dit toont aan dat het verkrijgen van een zuivere tyrosinase voor structuurstudie zeer uitdagend is.

De moleculaire massa van paddenstoelen-tyrosinase (uit commerciële preparaten of direct geïsoleerd uit paddenstoelvruchtlichamen) na analyse met verschillende methoden is consequent gerapporteerd als ~120 kDa. Het begrip van de quaternaire structuur is geëvolueerd van een homo-tetrameer met ~30 kDa subeenheden tot een hetero-tetrameer bestaande uit twee ~45 kDa (zware, H) en twee ~14 kDa (lichte, L) subeenheden. Bovendien is uit een peptide-massa-spectrometrisch-vingerafdruk (PMF) experiment met commerciële paddenstoel-tyrosinase gebleken dat de zware subeenheid van het commerciële preparaat waarschijnlijk PPO2 is. De identiteit van de lichte subeenheid is echter onduidelijk. Het zou deel kunnen uitmaken van tyrosinase of een volledig ander -niet verwant- eiwit, waarbij het om een lectine zou gaan dat in paddenstoelen aanwezig is. Zo is de identiteit van het commerciële paddenstoel-tyrosinase, dat op grote schaal wordt gebruikt in onderzoek, niet eenduidig vastgesteld.

Omdat een aantal *ppo*-genen nu beschikbaar is, kan elke paddenstoel-tyrosinase isovorm onafhankelijk van de andere worden geproduceerd, en zo kan het probleem met heterogeniteit worden overwonnen. Dit is bereikt door het klonen van het *ppo2*-gen in een bacterieel systeem voor de overexpressie van recombinant eiwit (**hoofdstuk 2**). Recombinant PPO2 met een histidine-tag wordt geproduceerd in *Escherichia coli* voor een gemakkelijke zuivering met behulp van een nikkel-affiniteitschromatografie kolom. Echter, het enzym bleek onoplosbaar te zijn en proteïneaggregaten te vormen, insluitingslichamen genoemd. De insluitingslichamen zijn opgelost door denaturatie van het eiwit; de PPO2 kan vervolgens hersteld worden met een hervouwprocedure terwijl het gebonden blijft aan de nikkel-affiniteitskolom. De gevouwen PPO2 is een monomeer in oplossing met een moleculaire massa van 64 kDa, dat is de grootte van het ppo2 genproduct. Spectroscopische analyse toont aan dat het kopercentrum aanwezig is in het hervouwen enzym. Het gevouwen enzym heeft echter een zeer lage activiteit in vergelijking met zowel het commerciële preparaat als met het direct uit paddenstoel geïsoleerde enzym. Er zijn ook geen eiwitkristallen verkregen van het hervouwen PPO2.

Via een alternatieve route is paddenstoel-tyrosinase met succes direct gezuiverd uit het commerciële preparaat. Met behulp van enzymmateriaal uit deze zuiveringsprocedure worden paddenstoel-tyrosinase-kristallen verkregen (**hoofdstuk 3**). Paddenstoel-tyrosinase kan alleen worden gekristalliseerd bij lage ionsterkte. Kristallen worden verkregen bij kamertemperatuur met 8% polyethyleenglycol in 10 mM natriumacetaat buffer, pH 4,6 als kristallisatiepunt agens. De eiwitkristallen groeien in concurrentie met samenklontering en neerslaan, en worden bruin: het oogsten van eiwitkristallen is daarom ook een uitdaging. Bij analyse van de

thermische stabiliteit ontdekken we dat de stabiliteit van het enzym wordt verhoogd in aanwezigheid van calciumionen. Daarom is 10 mM calciumchloride opgenomen in de zuiveringsbuffer; het calcium wordt verwijderd voorafgaand aan de kristallisatie. Interessant is dat de kwaliteit van de kristallen verbetert wanneer het enzym wordt gekristalliseerd in aanwezigheid van holmiumchloride. Hoewel holmium een calcium-analoog is, kunnen geen kristallen worden verkregen in aanwezigheid van calciumchloride. Daarom is 5 mM holmiumchloride toegevoegd aan de kristallisatieoplossing. De kristallen zijn vervolgens onderworpen aan Röntgendiffractie. Het enzym was uitgekristalliseerd in twee verschillende spacegroups, $P2_1$ (monoklien) en $P2_12_12$ (*ortho*-rhombisch). In de eiwitkristallen bleken zowel de zware als de lichte subeenheden aanwezig te zijn, in beide kristalvormen. Wanneer een kristal dat is blootgesteld aan röntgenstraling wordt opgelost, wordt significante tyrosinase activiteit waargenomen. Dit geeft aan dat we actief enzym hebben uitgekristalliseerd.

Het succes bij het verkrijgen van röntgendiffractiegegevens van de kristallen leidt ons naar de volgende stap in de structuurbepaling van het enzym (**hoofdstuk 4**). Een eerste structurele model is gegenereerd op grond van de PPO2-aminozuurvolgorde en de geconserveerde onderdelen van de structuren van PPO2-homologen, zoals de weekdier-hemocyanins van *Octopus dofleini* (reuzenoctopus) en *Rapana thaliana* (zeeslak), het catecholoxidase van *Ipomoea batatas* (zoete aardappel) en het tyrosinase van *Streptomyces castaneoglobisporus* (bacterieel tyrosinase). Dit eerste model bevat slechts een deel van de zware subeenheid van het enzym. Het bouwen van de tyrosinase-structuur is gedaan met zowel gecomputeriseerde modelbouw als met de hand. De dataset van het *ortho*-rhombische kristal is gebruikt, omdat de resolutie daarvan hoger is. Het model werd regelmatig overgezet naar de gegevens in de monoklien kristal set. Deze praktijk vermindert uiteindelijk de model bias als gevolg van de onafhankelijkheid van de twee datasets. Toch boekten we met de modelbouw en verfijning geen vooruitgang omdat de PPO2-aminozuursequentie op verschillende plaatsen niet paste op de elektronendichtheidskaart. Zodra een hogere resolutie dataset beschikbaar kwam, is het automatische model-programma voor het opbouwen ARP/Warp gebruikt om het structurele model uit te breiden. We vinden zo dat er wijzigingen moeten worden ingevoerd in de PPO2-sequentie. Deze gewijzigde volgorde past perfect op het N-terminale gebied van de PPO3-sequentie. De N-terminale aminozuursequentie van PPO2, geïdentificeerd door PMF analyse, is sterk vergelijkbaar met die van PPO3 (figuur 1), en omdat bij het begin van het modelleren van de PPO3-sequentie dit nog niet bekend was, werd het enzym ten onrechte aangemerkt als PPO2. Het structuurmodel voor de zware subeenheid is vervolgens afgemaakt met behulp van

de PPO3-sequentie. De aminozuurvolgorde, afgeleid van het structuurmodel van de lichte subeenheid, past niet op de aminozuurvolgorde van PPO1, PPO2, PPO3, PPO4, het eerder genoemde paddenstoellectine, of enig ander eiwit in de publieke databanken. Deze sequentie is vervolgens vergeleken met gegevens in de paddenstoel *A. bisporus* genoom-database die onlangs is gepubliceerd. Er is een duidelijke treffer gevonden en het model zou kunnen worden aangevuld met de aminozuursequentie van het eiwit ORF239342. De opheldering van de kristalstructuur van paddenstoeltyrosinase onthulde zo de ware identiteit van de H en L subeenheden, die tot dan toe onduidelijk was.

ZIE ENGELSE VERSIE

Figuur 1. Vergelijken van de N-terminale regio's van de PPO1-PPO4 aminozuurvolgordes. De rechthoek benadrukt het PPO2 fragment dat met de vingerafdruk analyse is geïdentificeerd als bijna gelijk aan het fragment in PPO3 en heeft dezelfde massa. De nummering is afkomstig van de PPO3 volgorde.

De overall structuur van PPO3 is vergelijkbaar met die in het tyrosinase domein van weekdier-hemocyanine, planten-catecholoxidase en bacteriële tyrosinases. Het tyrosinase domein wordt gemarkeerd door een interactie tussen een streng geconserveerd arginine-residu in de N-terminale regio en een tyrosine of fenylalanine residu, een deel van de geconserveerde Tyr/Phe-X-Tyr/Phe sequentiemotief, in het C-terminale domein. De PPO3-structuur is echter 100-120 aminozuurresiduen groter dan het tyrosinasedomein van de homologen. Deze extra residuen bevinden zich veelal in de lussen die de secundaire structuren verbinden. Een tweekernig kopercentrum ligt in het hart van een bundel van vier helices die de kern van het enzym vormen. Dit kopercentrum is het katalytische centrum van het enzym, het ligt in een ruime holte aan de oppervlakte van het eiwit, waardoor het gemakkelijk toegankelijk is vanuit de omgeving. Het tyrosinasedomein van PPO3 wordt gevolgd door een 27 residuen lange extensie, die twee α-helices bevat, die dicht bij de kernregio worden gehouden door waterstofbruggen. Deze extensie eindigt met een tyrosine-glycine sequentiemotief, dat sterk geconserveerd is in schimmeltyrosinases. Interessant is dat in andere schimmeltyrosinases, het verwijderen van het C-terminale deel -via proteolytische splitsing bij de rijping van het enzym- gebeurt aan een aminozuurresidu onmiddellijk na dit sequentiemotief. De PPO3-structuur biedt helaas geen verdere informatie over de aminozuren na dit sequentiemotief. Of en waar de splitsing bij de rijping heeft plaatsgevonden na dit sequentiemotief kan pas worden verklaard zodra de structuur van het volledig PPO3 of haar isovormen is opgehelderd.

Een belangrijke vraag over de structuur van de tyrosinase is de functie van een *thio*-etherbinding tussen Cys83 en His85 (PPO3 nummering) in het actieve centrum. His85 is een van de liganden die het eerste koperion (Cu-A) coördineert. Deze binding is geconserveerd in hemocyanine en catecholoxidase (figuur 2) met respectievelijk het Cys-X-His en het Cys-$(X)_{17}$-His sequentiemotief. Hemocyanine is een zuurstoftransport-eiwit in weekdieren en geleedpotigen, terwijl catecholoxidase in planten de omzetting katalyseert van *ortho*-difenolen tot *ortho*-chinonen. De *thio*-etherbinding is echter afwezig in de bacteriële tyrosinases van *S. castaneoglobisporus* en *Bacillus megaterium* waarvan de structuur bekend is. Uit recent gerapporteerde structuren van deze bacteriële tyrosinases blijkt dat His85 flexibel is. Daarom is in het huidige reactiemechanisme op basis van deze structuren, een verplaatsing van His85 voorgesteld in de *ortho*-hydroxylatie stap. De PPO3-structuur laat echter zien dat His85 verplaatsing onwaarschijnlijk is, omdat de *thio*-etherbinding de rotatievrijheid van His85 ernstig beperkt.

ZIE ENGELSE VERSIE

Figuur 2. De *thio*-etherbinding in (a) Octopus hemocyanine en (b) planten-catecholoxidase. De liganden zijn gekleurd naar atoomsoort (groen, blauw, rood, geel respectievelijk voor koolstof, stikstof, zuurstof en zwavel). De blauwe ballonnen zijn de Cu-A en Cu-B koperionen. De liganden zijn genummerd op grond van de aminozuurvolgorde. De cyaanblauwe en paarse lussen geven de polypeptide ketens aan waar de histidine en cysteïne residuen de *thio*-etherbinding maken. N.B. in catecholoxidase zijn de histidine en cysteïne residuen in de *thio*-etherbinding afkomstig uit een ander lus.

Meer inzicht in het reactiemechanisme kan worden verkregen door het bestuderen van de structuur van tyrosinase in de aanwezigheid van substraat of inhibitoren. Helaas zijn de complexstructuren van PPO3 evenals die van PPO3-tropolon in de deoxy-staat, waarbij het enzym niet actief is. Bovendien is het tropolon-remmermolecuul niet specifiek gebonden aan het actieve centrum. Toch neemt tropolon een vergelijkbare positie in als de fenylthioureum (PTU) remmer in catecholoxidase en de tyrosinezijketen van het eiwit in de *S. castaneoglobisporus* tyrosinase structuur. De informatie over de reactiestappen kan worden verkregen door de opheldering van de structuur van de oxy-stand van PPO3, bij voorkeur in aanwezigheid van een substraat of substraatanaloog.

De lichte subeenheid is geïdentificeerd als ORF 239342, dat is een eiwit uit paddenstoelen met onbekende functie. De architectuur lijkt op die van eiwitten met agglutinerende functionaliteit, maar de koolhydratenbinding is niet geconserveerd. Daarom blijft de functie van deze subeenheid onduidelijk evenals de inbouw in het H_2L_2 tyrosinase tetrameer, omdat het altijd gevonden wordt samen met de H-subeenheid (tyrosinase). Om antwoorden te vinden

op deze vragen, kan nu nieuw onderzoek worden ondernomen naar de lokalisatie van dit eiwit in paddenstoelen en de regulering/expressie in de cel, en om de biochemische eigenschappen verder te karakteriseren.

Ringkasan

Disertasi ini membahas penentuan struktur tiga dimensi (3D) tyrosinase dari jamur *Agaricus bisporus* (jamur kancing) dengan metode kristalografi sinar-X. Tyrosinase adalah enzim yang mengandung tembaga dan yang mengkatalisis pengubahan mono-orto-fenol menjadi diphenol dan pengubahan lebih lanjut menjadi orto-kuinon turunannya. Produk akhir dari reaksi tersebut adalah bahan baku utama dalam biosintesis melanin, pigmen yang banyak ditemukan di alam, yang dapat ditemukan pada bermacam organisme dari berbagai fila. Oleh karena itu, enzim ini sering dikaitkan dengan pigmen dan penyakit-penyakit atau gangguan yang terkait dengan pigmen, yang terjadi pada manusia dan hewan, seperti melanoma, albinisme dan vitiligo. Pada buah-buahan dan sayuran, tirosinase bertanggung jawab atas proses pencoklatan pada produk pertanian yang mengakibatkan penyusutan nilai produk-produk tersebut. Sebabnya, senyawaan yang dapat menghambat aktivitas enzim (inhibitor) sangat dicari untuk mencegah proses pencoklatan ini. Penghambatan aktivitas tirosinase juga penting bagi industri kosmetik dan farmasi, antara lain sebagai pemutih kulit dan pengobatan untuk hiperpigmentasi setelah terjadinya inflamasi akibat terbakar atau lecet. Penelaahan dengan tujuan untuk aplikasi-aplikasi ini biasanya dilakukan dengan tirosinase jamur yang tersedia secara komersial, yang dengan alasan tersebut telah dipelajari secara ekstensif. Namun demikian, interpretasi hasil-hasil penelaahan tersebut sering kurang tepat karena tidak adanya struktur tiga dimensi dari enzim tersebut. Oleh karena itu, struktur enzim ini menjadi sangat didambakan dan berbagai kelompok di seluruh dunia telah mencoba untuk menentukan struktur tiga dimensi enzim ini. Selain itu, ketersediaan struktur tiga dimensi enzim ini memungkinkan untuk perancangan senyawa inhibitor secara rasional dan berdasarkan pada struktur.

Penentuan struktur 3D enzim ini terhambat dengan kesulitan dalam memperoleh enzim murni akibat adanya kontaminasi oleh melamin dan karena tirosinase jamur tampaknya heterogen. Sumber-sumber heterogenitas ini diperkirakan berasal dari polimerisasi enzim oleh senyawa kuinon, perbedaan dalam prosedur pemurnian yang digunakan, modifikasi pasca-translasi, atau perbedaan sumber enzim. Baru-baru inilah diketahui bahwa terdapat setidaknya empat gen yang mengkode ekspresi tirosinase jamur, yaitu *ppo*1, *ppo*2, *ppo*3, dan *ppo*4. Hal ini menunjukkan bahwa heterogenitas enzim juga mungkin berasal dari adanya isoform. Fakta-

fakta ini menunjukkan bahwa mendapatkan tirosinase murni untuk tujuan penelaahan struktur adalah sangat menantang.

Massa molekul tirosinase jamur (yang diisolasi langsung dari bahan komersial maupun dari tubuh buah jamur) yang dilaporkan melalui analisis menggunakan berbagai macam metode adalah, secara konsisten, ~ 120 kDa. Disamping itu, konsep untuk struktur kuartenernya berkembang dari sebuah tetramer yang terdiri dari empat subunit dengan berat 30 kDa menjadi sebuat tetramer yang terdiri dari dari dua subunit dengan massa ~ 45 kDa (berat, H) dan dua subunit dengan massa ~ 14 kDa (ringan, L). Lebih lanjut lagi, percobaan dengan spektrometri-massa sidik-jari peptida (PMF) menggunakan tirosinase jamur yang berasal dari bahan komersial mengungkapkan bahwa subunit H mungkin adalah PPO2. Identitas subunit L masih belum diketahui. Ia boleh jadi merupakan bagian ujung dari tirosinase utuh atau boleh juga protein lain yang sama sekali tidak berkaitan dengan tirosinase, dalam hal ini diperkirakan adalah lektin dari jamur. Dengan demikian, identitas tirosinase jamur dari bahan komersial, yang banyak digunakan dalam berbagai penelitian, belum dapat dipastikan.

Karena sejumlah gen PPO sekarang tersedia, masing-masing isoform dari tirosinase jamur dapat diproduksi secara independen, dengan demikian permasalahan dalam heterogenitas dapat diatasi. Hal ini dicapai dengan mengkloning gen PPO2 ke dalam sistem bakteri untuk overekspresi protein rekombinan (**Bab 2**). PPO2 rekombinan yang diproduksi di *Escherichia coli* dilengkapi dengan histidin-penanda untuk kemudahan dalam pemurnian menggunakan kolom kromatografi afinitas nikel. Namun, enzim rekombinan ini ternyata tidak larut dan membentuk protein agregat, yang disebut badan inklusi. Badan inklusi ini dilarutkan dengan cara mendenaturasi protein agregatnya, dan PPO2 rekombinan didapatkan melalui proses pelipatan kembali sewaktu protein masih terikat pada kolom afinitas nikel. Dalam larutan, PPO2 hasil pelipatan ulang ditemukan dalam bentuk monomer dengan berat molekul 64 kDa, yang merupakan ukuran protein yang dihasilkan oleh gen *ppo*2. Analisis dengan spektroskopi menunjukkan bahwa pusat tembaga pada pusat aktif enzim telah terbentuk. Sayangnya, enzim hasil pelipatan ulang ini memiliki aktivitas yang jauh lebih rendah dibandingkan dengan enzim yang diisolasi dari bahan komersial maupun enzim yang diisolasi langsung dari jamur. Terlebih lagi, tidak ada kristal protein yang diperoleh menggunakan PPO2 hasil pelipatan ulang ini.

Melalui jalur alternatif, tirosinase jamur murni dari bahan komersial berhasil didapatkan. Dengan menggunakan prosedur yang dipakai untuk mendapatkan enzim murni dari bahan komersial ini, tirosinase kristal berhasil didapatkan (**Bab 3**). Tirosinase jamur hanya dapat mengkristal pada kekuatan ion yang rendah. Kristal diperoleh pada suhu kamar dengan

menggunakan 8% polietilen glikol dalam 10 mM larutan dapar natrium asetat, pH 4,6 sebagai bahan pengkristal. Kristal protein tumbuh bersaingan dengan agregasi dan pengendapan, dan pencoklatan: oleh sebab itu pemanenan kristal protein menjadi sangat menantang. Melalui analisis stabilitas termal, kami menemukan bahwa stabilitas enzim meningkat dengan adanya ion kalsium. Oleh karena itu, 10 mM kalsium klorida dihadirkan pada larutan dapar yang digunakan dalam pemurnian, tetapi ion kalsium ini dihilangkan sebelum eksperimen kristalisasi dilakukan. Menariknya, kualitas kristal meningkat ketika enzim dikristalkan dalam larutan yang mengandung holmium klorida. Meskipun holmium serupa dengan kalsium, tidak ada kristal diperoleh ketika kalsium klorida gunakan dalam kristalisasi. Oleh karena itu, 5 mM holmium klorida ditambahkan ke dalam larutan pengkristal. Kristal yang didapatkan kemudian ditembak dengan sinar-X dan data difraksinya dikumpulkan. Tirosinase mengkristal dalam dua bentuk kristal yang berbeda, yaitu $P2_1$ (monoklinik) dan $P2_12_12$ (ortorombik). Kristal protein dengan kedua bentuk kristal tersebut mengandung subunit H dan L. Ketika kristal yang sudah ditembaki dengan sinar-X dilarutkan kembali, aktivitas tirosinase teramati dalam jumlah yang sginifikan. Hal ini menunjukkan bahwa kami telah mengkristalkan enzim aktif.

Keberhasilan dalam memperoleh data difraksi sinar-X dari kristal membawa kita ke langkah berikutnya dalam menentukan struktur enzim (**Bab 4**). Model struktur terawal dihasilkan berdasarkan urutan asam amino PPO2 dan bagian daerah terlestarikan pada struktur protein homolog dari PPO2, seperti hemosianin moluska dari *Octopus dofleini* (gurita raksasa) dan *Rapana thaliana* (siput laut), katekol oksidase dari *Ipomoea batatas* (ubi manis), dan tirosinase dari *Streptomyces castaneoglobisporus* (tirosinase bakteri). Model awal ini hanya mencakup sebagian dari subunit H dari tirosinase jamur. Pemodelan struktur tirosinase dilakukan dengan cara komputasi dan manual. Data set dari kristal ortorombik digunakan karena resolusinya lebih tinggi. Model secara berkala dipindahkan ke data set dari kristal monoklinik. Praktek ini mengurangi bias dari model karena kedua data set bersifat independen. Namun, pemodelan tidak dapat dilanjutkan karena urutan asam amino PPO2 tidak cocok dengan peta kerapatan electron diberbagai posisi. Baru setelah data set dengan resolusi yang lebih tinggi tersedia, pemodelan dapat dilanjutkan dengan menggunakan program otomatik ARP/wARP. Kami menemukan bahwa perlu dilakukan perubahan terhadap urutan asam amino PPO2. Urutan asam amino yang sudah diubah ini ternyata cocok dengan urutan asam amino di daerah N-terminal dari PPO3. Urutan asam amino di daerah N-terminal dari PPO2 yang diidentifikasi dengan analisis PMF hampir sama dengan kepunyaan PPO3 (Gambar 1). Karena pada awal pemodelan urutan asam amino PPO3 belum diketahui, enzim

tersebut disalahartikan sebagai PPO2. Model untuk struktur subunit H kemudian diselesaikan dengan menggunakan urutan asam amino PPO3. Sementara itu, urutan asam amino yang didapatkan dari model struktur subunit L tidak cocok dengan urutan asam amino dari PPO1, PPO2, PPO3, PPO4, lektin dari jamur, maupun protein lain yang ada di data base publik. Urutan asam amino dari subunit L ini kemudian dibandingkan dengan data base genomik di jamur *A. bisporus* yang baru saja diterbitkan. Suatu kecocokan urutan asam amino ditemukan dimana protein tersebut diidentifikasi sebagai ORF239342, dan model struktur protein ini diselesaikan dengan menggunakan urutan asam aminonya. Penentuan struktur kristal tirosinase jamur dengan demikian telah berhasil mengungkapkan identitas yang sesungguhnya daripada subunit H dan L, yang hingga saat itu belum diketahui.

LIHAT VERSI BAHASA INGGRIS

Gambar 1. Perbandingan urutan asam amino di daerah N-terminal dari PPO1-PPO4. Daerah yang ditandai dengan kotak menunjukkan fragmen yang ditemukan pada analisis dengan spektrometri mass sidik jari peptida, yang diidentifikasi sebagai PPO2, yang hampir sama dengan fragmen dari PPO3 dan memiliki massa yang sama. Penomoran berdasarkan dari urutan asam amino PPO3.

Struktur keseluruhan dari PPO3 mirip dengan domain tirosinase pada hemosianin dari moluska, katekol oksidase dari tanaman, dan tirosinase-tirosinase dari bakteri. Tirosinase domain ditandai dengan sebuah interaksi antara residu arginin yang terlestarikan secara pasti di daerah N-terminal dan residu tirosin atau fenilalanin, yang merupakan bagian motif tirosin/fenilalanin-X-tirosin/fenilalanin yang juga terlestarikan di daerah C-terminal. Struktur PPO3 namun demikian 100-120 residu asam amino lebih besar daripada tirosinase domain dari homolog-homolognya. Residu tambahan ini sebagian besar terletak di untaian yang menghubungkan struktur sekunder. Sebuah pusat dua-tembaga terletak di tengah-tengah dari kelompok empat heliks yang membentuk inti dari enzim. Pusat tembaga ini merupakan pusat katalitik dari enzim, yang berada pada suatu rongga besar pada permukaan protein, sehingga mudah dimasuki dari luar. Tirosinase domain pada PPO3 diikuti oleh sebuah perpanjangan sebanyak 27 residu, yang memiliki dua alfa-heliks, yang dijaga agar tetap dekat dengan domain pusat melalui ikatan-ikatan hidrogen. Perpanjangan urutan asam amino ini berakhir dengan sebuah motif tirosin-glisin yang sangat terlestarikan di semua tirosinase dari jamur. Menariknya, pada tirosinase dari jamur-jamur lain, penghilangan bagian C-terminal melalui pemotongan secara proteolitik, yang terjadi pada proses pematangan enzim, juga terjadi pada residu asam amino tepat setelah motif tirosin-glisin ini. Sayangnya, struktur PPO3 tidak memberikan informasi lebih lanjut tentang asam-asam amino setelah motif ini. Apakah terjadi

dan dimana terjadinya pemotongan dalam proses pematangan, yang terjadi setelah motif tirosin-glisin ini, hanya dapat dipastikan jikalau struktur PPO3 atau isoformnya yang utuh berhasil ditentukan.

Satu tanda Tanya besar dalam struktur tirosinase adalah fungsi ikatan tio-eter antara sistein-83 dan hisitidin-85 (penomoran PPO3) yang ada di pusat aktif. Histidin-85 adalah salah satu ligan pengkoordinase ion tembaga yang pertama (Cu-A). Ikatan ini ditemukan juga pada hemosianin dan katekol oksidase (Gambar 2), masing-masing dengan motif urutan asam amino sistein-X-histidin dan sistein-$(X)_{17}$-histidin. Hemosianin adalah pembawa oksigen protein pada moluska dan arthropoda sedangkan katekol oksidasi adalah yang mengkatalisis perubahan orto-diphenol menjadi orto-kuinon pada tanaman. Tapi, ikatan tio-eter ini tidak ditemukan pada tirosinase-tirosinase dari bakteri-bakteri *S. castaneoglobisporus* dan *Bacillus megaterium* yang strukturnya sudah diketahui. Struktur-sturktur tyrosinase bakteri ini menunjukkan bahwa histidine-85 ini fleksibel. Oleh sebab itu, dalam mekanisme reaksi yang berdasarkan struktur-struktur mereka, pergerakan histidin-85 pada langkah orto-hidroksilasi diperkirakan terjadi. Struktur PPO3 menunjukkan bahwa pergerakan histidin-85 tidak mungkin terjadi karena kemampuan rotasi histidin-85 sangat terbatas dengan adanya ikatan tio-eter ini.

LIHAT VERSI BAHASA INGGRIS

Gambar 2. Ikatan tio-eter pada (a) dan hemosianin dari gurita (b) katekol oksidase dari tanaman. Ligan diwarnai sesuai dengan jenis atomnya (hijau, biru, merah, kuning masing-masing untuk karbon, nitrogen, oksigen dan belerang). Bola biru adalah untuk ion-ion tembaga A dan B. Ligan dinomori sesuai dengan urutan asam amino masing-masing protein. Untaian warna biru muda dan ungu menunjukkan rantai poli peptida dimana residu histidin dan sistein yang membentuk ikatan tio-eter berada. Perlu diperhatikan bahwa residu histidin dan sistein yang membentuk ikatan tio-eter di katekol oksidase berasal dari untaian yang berbeda.

Wawasan lebih mendalam tentang mekanisme reaksi dapat diperoleh dengan mempelajari struktur tirosinase yang mengandung substrat atau inhibitor. Sayangnya, struktur PPO3 dan kompleks dari PPO3 dengan tropolon adalah struktur dalam keadaan deoksi, dimana enzim tidak dalam keadaan aktif. Selain itu, molekul inhibitor tropolon tidak terikat secara spesifik di pusat aktif. Namun demikian, posisi tropolon serupa dengan posisi feniltiourea (PTU) dalam struktur katekol oksidase dari ubi manis dan rantai samping tirosin pada protein penyerta dalam struktur tirosinase dari *S. castaneoglobisporus*. Informasi mengenai tahapan dalam reaksi dapat diperoleh dari struktur PPO3 dalam keadaan oksi, baik tanpa maupun dengan keberadaan substrat atau substrat analog.

Subunit L diidentifikasi sebagai ORF 239342, yang merupakan protein dari jamur dengan fungsi yang tidak diketahui. Arsitekturnya menyerupai protein dengan fungsi menggumpalkan, tetapi daerah pengikatan karbohidrat yang terlestarikan pada protein tersebut tidak ditemukan. Oleh karena itu, fungsi subunit ini tidak jelas walaupun pada tetramer H_2L_2 tirosinase, protein ini selalu ditemukan bersama-sama dengan subunit-H (tirosinase). Untuk menemukan jawaban atas pertanyaan-pertanyaan ini, penelitian baru dapat dilakukan dengan mempelajari lokalisasi protein ini dalam jamur, regulasi/ekspresinya dalam sel, dan lebih lanjut karakterisasi sifat biokimianya.

Acknowledgements

It is the time for the fat lady to sing. An epilogue that may sounds clinical but still worth to see. The final moment before the audience go away with their laugh and tears. And while the curtain downs slowly, words are now out with dear.

Foremost, I would like to thank Bauke for tirelessly guiding me through out my study. So much I have learned about science and life in the past nine years, would not be possible without the opportunity you have given to me to come and be in Groningen. I truly thank pak Bein for your full support, pumping my spirit, and being so thoughtful. You have made my study bearable and brought me comfort. I thank Harry for your support and keeping me alert to move forward in my study. I dearly thank Henriëtte, because without your significant contribution in elucidating the structure, there would be no light at the end of the tunnel of my PhD study. I am also deeply indebted to pak Yos, long time patron in my scientific endeavor.

My sincere thanks to Tjaard, Cor, Andy, Jaap, and Anke for sharing your valuable knowledge and experiences in protein crystallography. Specially for Jan Drenth, you are one of the people who inspires me. I learned a lot from you all. Also for my workmates from X-ray and EM groups: Niels, Marcel, Jan Ties, Avi, Andre, Andreja, Pramod, Guntur, mas Ali, Cyril, Gjalt, Hiromi, Fabrizia, Milena, Sami, Anna, Jelle, Roman, Wilma, Egbert, Michaela, Kasia …. Thank you all for the time we spent together: on synchrotron trips, group discussion, and most certainly social events. I want to also thank Lubbert, Madeleine, and Tim for joyous and fruitful occasions we had. Not to forget, my sincere thanks to Tamara Korr and Hilda for all the help. Because of you all, I find Groningen as a place I call home.

I would also like to thank Bernd and Coos from Utrecht University, who have given me trust to work as a postdoct although I have not yet earned my degree. Being fully understanding and considerate to allow me working on my thesis. I truly believe that this postdoc appointment has salvaged my PhD degree. Here I would also like to appreciate my colleagues at department of biochemistry and cell biology, veterinary medicine of Utrecht University, for providing good atmosphere, scientifically and socially, upon the completion of my thesis.

For Ans, thanks for your sweet motivation cards. I put them around my desk to cheer me up when I feel down. The time in our warm and homey house in Saturnuslaan will never be

forgotten. I also want to thank Hans, for all your never ending support and care. You both stood by me in good and bad times, provide me strength and courage.

For papi dan mami, thank you for countless prayers and never ending love and care. Also for Dede, Hery, uwak Ating, dan uwak istri for being at my side throughout my life. Your contribution cannot be measured for return, so I can only name you all in my prayer. Last but not least, I thank Yeni, who nevertheless was once part of my life, for providing a piece in the life lesson curve of mine.

For the Indonesian families in Groningen and Nederland: bude Nannie, wak Asiyah en oom Meno te Delfzijl, Aas en Benny, pak Wid dan bu Indah, tante Arminie en oom Iyan te Delft, tante Hana, tante Pantja, tante Wilhelmina, and many others. Thank you very much for your warmth reception. And last but not least, my big Indonesian family: de Gromiest and PPI-Groningen, with too many names to mention. You have made my stay in Groningen useful and colorful, with so many precious and memorable moments.

Wangsa